Solar Charging Station for Light Electric Vehicles

A Design and Feasibility Study

Nishant S. Narayan

Master of Science Thesis

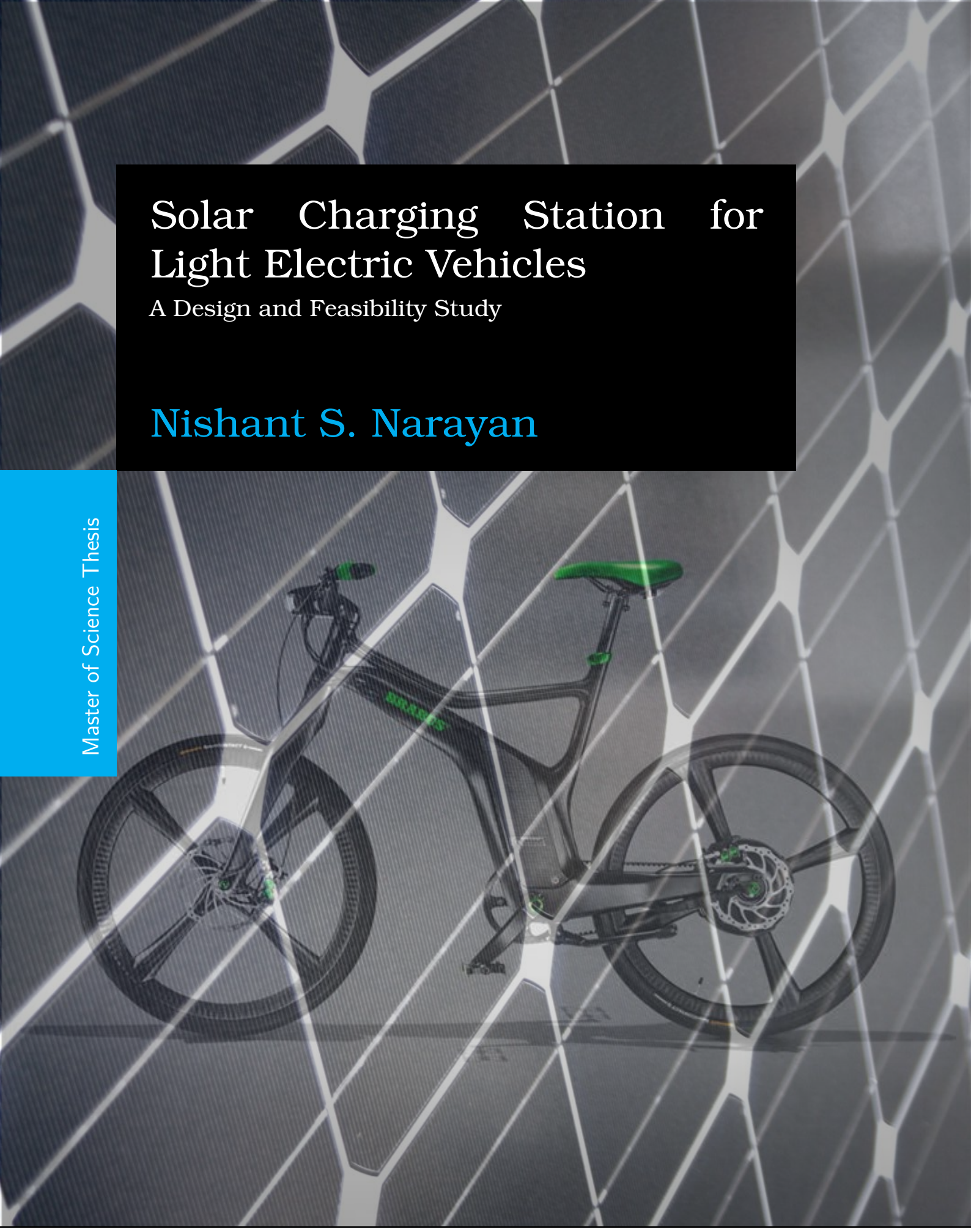

TU Delft Delft University of Technology

Photovoltaic Materials and Devices

Solar Charging Station for Light Electric Vehicles

A Design and Feasibility Study

Master of Science Thesis

For the degree of Master of Science in Sustainable Energy Technology at Delft University of Technology

Nishant S. Narayan

July 30, 2013

Faculty of Applied Sciences · Delft University of Technology

Cover picture: ASP monocrystalline panel and Smart Brabus e-bike.

Delft University of Technology
Department of
Photovoltaic Materials and Devices (pvmd)

The undersigned hereby certify that they have read and recommend to the Faculty of Applied Sciences for acceptance a thesis entitled

Solar Charging Station for Light Electric Vehicles

by

Nishant S. Narayan

in partial fulfillment of the requirements for the degree of

Master of Science Sustainable Energy Technology

Dated: July 30, 2013

Supervisor(s):

Dr. A. H. M. Smets

Prof. dr. M. Zeman

Reader(s):

Dr. P. Bauer

Abstract

The growth in technology and increased public interest has brought about a rapid evolution in the realm of e-mobiilty. While generally viewed as non-polluting and environmentally friendly, the Electrical Vehicles (EVs) could still contribute significantly towards indirect emissions, depending on the source of their energy. The only way they can be made truly emission free is if they are charged from renewable energy sources.

This thesis aims at designing such a charging station powered by solar energy. The charging station would cater to the most popular type of Light Electric Vehicles (LEVs) - the e-bikes, and would be located at Delft in the Netherlands. Given that the Netherlands is estimated to have close to a million e-bikes already in use, the design of such a charging station would undoubtedly heighten the positive impact of LEVs.

Firstly, the amount of solar energy that can be harnessed in the Netherlands is accurately found out. A photovoltaic (PV) model is developed to predict the PV module yields based on minimal weather parameters. The PV model gives a Module Ideality Factor that is indicative of the drop in PV yield due to temperature and irradiance effects.

Two main system topologies are analyzed - an autonomous charging station and a grid-connected charging station - under two different load profiles. While the system reliability is of primary concern in an autonomous charging station, the electrical autarky and the Effective Autarky Ratio are optimized for sizing the grid-connected system.

Lifetime estimation models are developed to predict the PV module and battery lifetimes. A basic economical analysis is performed to determine the financial viability of such a project. At large scales (several kW), the system is shown to have a Levelized Cost of Electricity (LCOE) that is grid competitive. Finally, the environmental impact of the system is studied.

It is concluded that the implementation of such a charging station is not only technically feasible, but is also environmentally friendly and economically viable, especially at large scales.

Contents

List of Figures

List of Tables

न चोरहार्यं न च राजहार्यं न भ्रातृभ्राज्यं न च भारकारि ।

व्यये कृते वर्धत एव नित्यं विद्याधनं सर्वधनप्रधानम् ।।

"It cannot be stolen by a thief. It cannot taken away by a King.
It cannot be divided among brothers. It does not cause burden.
It always increases when spent.
The wealth of knowledge is the greatest of all wealths."

— *An old Sanskrit quote.*

Chapter 1

Introduction

1-1 Energy Crisis

"The Stone Age did not end for lack of stone, and the Oil Age will end long before the world runs out of oil."

- Sheikh Zaki Yamani, Minister of Oil and Mineral Resources (1962-86)

Decades after the Saudi oil minister expressed these words, technology has evolved at a rapid pace and has given the world a fighting chance to speed up the end of the oil-age. But the modern world still remains heavily addicted to the Middle Eastern oil[1].

Energy security is the key to future growth and progress of mankind. It has been established beyond doubt, that nations that are 'energy secure' have the best economic growth prospects, while those which rely on external energy sources are vulnerable to energy supply, fuel price and currency fluctuations. However, conventional sources of energy are rapidly running out. To make matters worse, existing users of fossil fuels dump huge amounts of carbon-dioxide (CO_2) and other Green House Gases (GHGs) into the atmosphere, thus jeopardizing the climate of the earth, reducing the quality of air and causing weather anomalies(refer Figure 1-1).

It is important to realize that energy security and climate change mitigation go hand in hand. In such a scenario where energy requirements are growing multi-fold and conventional energy sources are dwindling, it is imperative that we look for solutions that decrease our dependence on 'dirty fuels' like coal and petroleum.

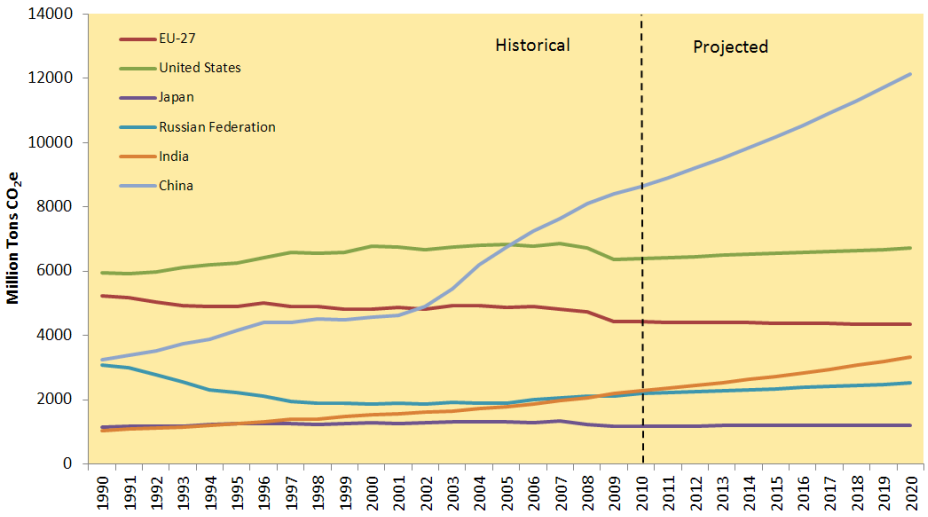

Figure 1-1: GHG emissions for Major economies (illustration from [2])

According to International Energy Agency (IEA) [3], *"the integrated use of key existing technologies would make it possible to reduce dependency on imported fossil fuels or on limited domestic resources, de-carbonize electricity, enhance energy efficiency and reduce emissions in the industry, transport and buildings sectors. This would dampen the surging energy demand, reduce imports, strengthen domestic economies, and over time dramatically reduce GHG emissions."*

Indeed, there is no single renewable energy technology that can serve as a solution to all the energy problems of the world. An integrated and multi-pronged approach is required. There are plenty of energy technologies that would serve as vital pieces in the sustainable future jigsaw.

1-2 Significance of E-mobility

The International Energy Agency states that in 2009, transportation accounted for approximately 20% of the world's primary energy use and 25% of all energy-based CO_2 emissions. Approximately 50% of these CO_2 emissions are said to have originated from passenger vehicles alone.

For a planet that is reeling under the impact of climate change, the above statistics are very disturbing. The IEA talks about how vehicle inventory and fuel consumption are set to rise steadily, and are likely to double by 2050 if the policy and incentives remain unchanged. Further analysis reveals that this would not only end up increasing CO_2 emissions but also lead to a spike in oil demand [3].

Today, there are many clean energy technologies and alternate fuels that are being explored as possible sustainable transport solutions. However, if we take oil usage and

CO_2 emission reduction per mile as the main priority, then Electrical Vehicles (EVs) seem to hold the most promise. The EV City Casebook by IEA[4], highlights an important statistic - *"With a moderately clean electric grid, EVs can achieve 50 grams of CO_2 per kilometer, which is much lower than emissions by the most efficient of hydrocarbon driven cars, which emit between 100 and 150 grams of CO_2 per kilometer. Even hybrid electric vehicles (HEVs) achieve only around 90 grams of CO_2 per kilometer."* The difference is too significant to ignore, and clearly, EVs can make a huge impact on overall GHG reduction.

However, introducing electric vehicles is just the first step in tackling the problem of emissions. Additionally, an elaborate and appropriate eco-system needs to be developed to support the deployment of EVs. This includes building infrastructure for charging, improving the electricity distribution grid, and ensuring that the requisite policies are in place to enable a "smart" charging system. Evolution of the Electrical Vehicle (EV) market will not only help alleviate CO_2 woes, but also provide an important economic stimulation for technology innovation[5].

1-2-1 Indirect Emission Conundrum

While manufacturers of fully electric vehicles or Battery Electric Vehicles (BEVs) claim to be completely emission free, this is often not true. Indeed, the direct emissions are minimal in EVs, but depending on the source of their everyday charging, they could add significant indirect emissions. For instance, if the EVs are charged from the grid, and majority of the national grid is fossil powered like in the Netherlands (refer Figure 1-2), then this means that the emissions have just shifted to the source. The GHG emissions from EVs can vary from 0 g/km for a renewable-powered EV to 155 g/km for an EV charged with electricity from a coal-based plant [6].

Thus, for the EVs to be truly free of emissions, they should be powered in the cleanest way possible. For instance, there are already a number of Renewable Energy (RE) powered charging stations for vehicles in many countries. Figure 1-3 shows the largest solar charging station of Washington at the time.

1-2-2 Light Electric Vehicles (LEVs)

A Light Electric Vehicle (LEV) is typically a land driven vehicle chiefly propelled by an electric motor using an energy storage device such as battery. LEVs usually weigh below 100 kg. Most LEVs are either two or three wheeled. Today, most LEVs are electric bikes (e-bikes), and this is to be so for a long time to come [8]. E-bikes, or pedelecs, as they are sometimes referred to, are bikes with electric assist that can supply electrical energy on demand. Figure 1-4 shows the recently launched e-bike from Smart.

Today the LEV industry is largely dominated by major bike manufacturers who have in recent past started manufacturing e-bikes. They enjoy a much larger access to distribution. Also, e-bikes have gained tremendous popularity over the years.

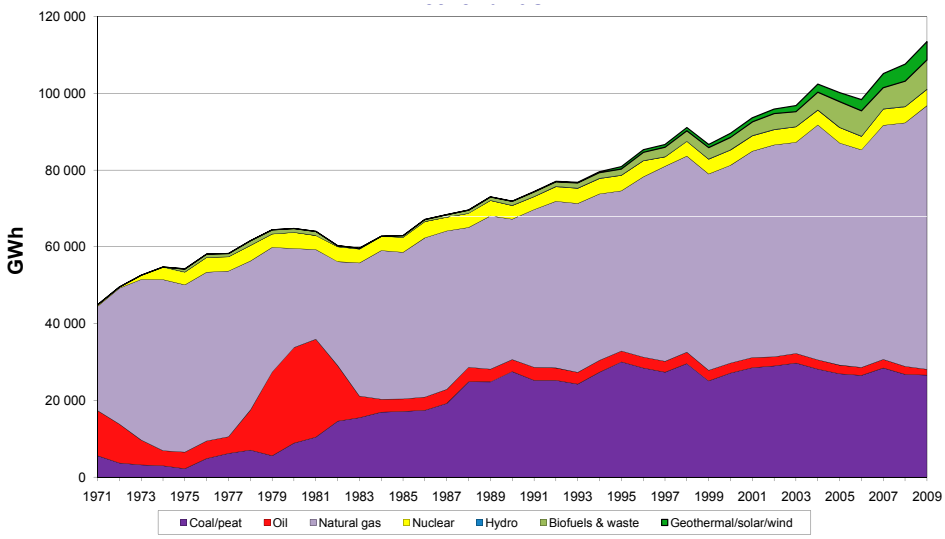

Figure 1-2: Electricity production by fuel in the Netherlands (*source: IEA*).

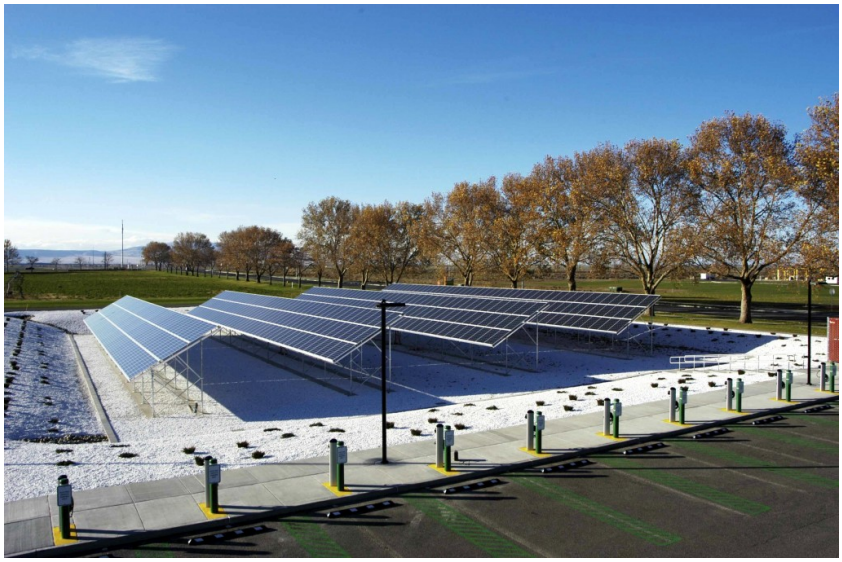

Figure 1-3: Solar charging station in the city of Richland, Washington (reprinted from [7]).

Figure 1-4: The Smart e-bike.

E-bikes or LEVs in general differ from conventional EVs in a lot of ways. The most significant difference is the electrical storage size. While a Battery Electric Vehicle (BEV) like **Tesla Roadster** (2008) carries a **53 kWh** of battery pack [9], a typical e-bike in comparison has a **250 Wh battery**. On the other hand, while the Tesla roadster consumes **15 kWh** of electrical energy per **100 km** traveled [9], a standard Gazelle e-bike consumes around **400 to 450 Wh** of electrical energy per **100 km** [10].

E-bikes in the Netherlands

It has been long established that the Netherlands is the bike capital of the world. In fact, the Dutch enjoy a total of **35000 km** of bike paths [11], the highest in the world. E-bikes have recently become the most popular category of bikes in this bike-friendly nation. In 2012 alone, around **171000** new e-bikes were added in the Netherlands, accounting for up to **42%** of the revenues in the bike market [12]. It was estimated that the total e-bike fleet size in the Netherlands touched one million by the start of 2013. In general, today **one** out of every **five** bikes sold in this country is an e-bike [13]. Most of the e-bikes in Netherlands, however, are currently being charged from the grid, adding to the indirect emissions (1-2-1).

1-3 Motivation of the thesis

The author has had a growing interest in the field of renewable energy as well as LEVs. This thesis was motivated by the fact that the Netherlands has one of the largest growing fleets of LEVs but has a predominantly fossil-based grid (refer Figure 1-2). Thus, designing a solar powered charging station for LEVs perfectly fits into the '*clean energy* -

e-transport' paradigm of the Netherlands. This project is a confluence of a multitude of technologies coming together.

The design of such a charging station could be carried out in two different ways. One type of setup is an autonomous system, completely independent from the public electric grid. This could be useful if such charging stations are setup in remote countryside where grid connectivity may not be an option. But this would entail extra costs for storage. A storage system is indispensable to meet the load requirements for the times when there is not enough sunlight.

The other kind of setup is a grid-connected charging system. In this case, whenever the PV modules produce insufficient power, the grid proves to be a reliable backup. On the other hand, when the PV modules are producing excess power, the grid can absorb the surplus.

Although it is well intentioned to design a charging station based on solar power, it needs to be technically and financially viable. Thus, to design such a system and determine its feasibility, a comprehensive set of research questions needs to be defined.

1-3-1 Research questions

In order to design a solar charging station, a variety of questions need to be answered. These questions have formed the basis of the research covered in this thesis. The following form the set of research questions:

1. How much of solar energy can be harnessed through existing photovoltaic (PV) technologies for a LEV charging station based in the Netherlands?
   (a) How much of solar energy is available throughout the year in the Netherlands?
   (b) Given the intermittent nature of the weather conditions, how much of electrical power can be generated by a PV module throughout the year?
2. Is it possible to rely entirely on the solar power through the year to meet the daily charging requirements?
   (a) How does an autonomous PV system fare in terms of meeting the energy demand for LEV charging throughout the year? How can the performance of an autonomous PV system be reliably measured?
   (b) Can the reliance on the utility grid be minimized for a grid-connected charging station? How can the performance of a grid-connected system be reliably measured?
3. Does it make economical and environmental sense to move to a solar based solution for charging LEVs?

(a) Is it financially viable to invest in a solar based charging station, as opposed to simply charging the LEVs from the grid?

(b) Does a solar charging station payback the energy it used up in its production?

1-3-2 Scope of the thesis project

As the chosen topic for the thesis is very broad in nature, a scope has to be defined that limits the breadth and depth of this project.

The charging station design does not take into account the State of Health (SOH) of the LEVs that are plugged into the station. It is assumed the chargers of the all the LEVs plugged into the charging station consume the same power, which is a simplification, albeit the majority of the e-bikes currently in use have similarly rated chargers.

Although the thesis estimates the calendar effects in the lifetime of the PV module and the storage system, it does not take them into account during the system modeling that spans one year of operation.

The power electronics in use in the system are assumed to be working at rated efficiencies, although in reality the efficiency is a function of the connected load. However, as all the system components used in the system model are taken from commercially available sources, some of the properties like the efficiency as a function of load, etc are proprietary and hence unavailable.

All the system models, components and their attributes covered in the various chapters have an associated scope discussed alongside them, which would talk about the individual extent of their applicability.

1-4 Thesis outline

This thesis report is divided into 7 chapters. Figure 1-5 illustrates the organization of the thesis report.

Chapter 1 - Introduction This chapter provides an overview of the motivation and defines the research questions.

Chapter 2 - Estimating Energy Resources This chapter aims at accurately determining the amount of solar energy annually available for use in the Netherlands. The total amount of raw solar energy incident per area in Delft, Netherlands is estimated in this chapter.

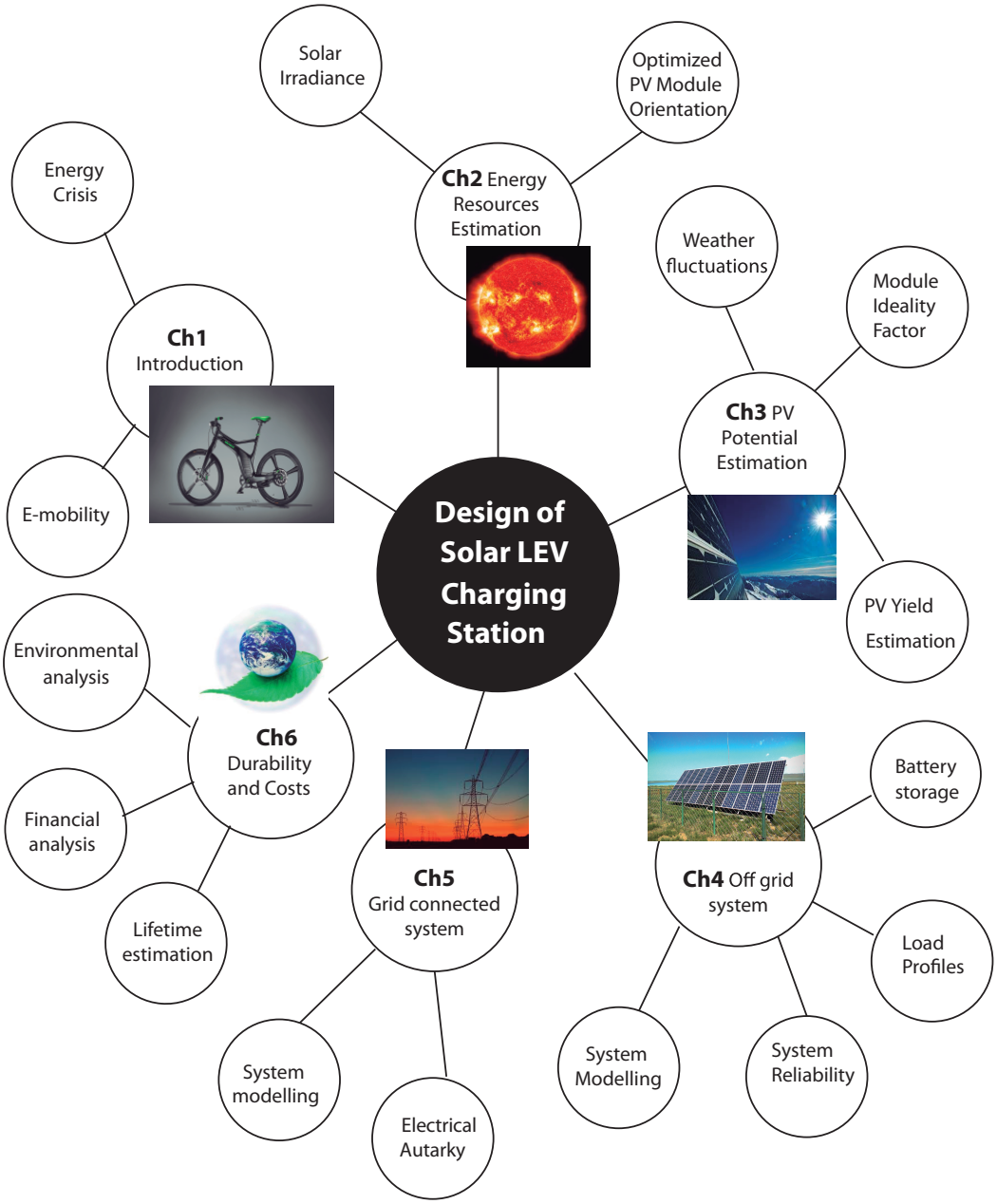

Figure 1-5: Outline of the thesis.

Chapter 3 - Estimating the PV Potential This chapter discusses a methodology to accurately determine the energy yield of a PV module under varying conditions. The PV model described in this chapter will take into account the irradiance and temperature effects on the output of a PV module.

Chapter 4 - Storage and System Modeling This chapter analyzes the reliability of an autonomous charging station throughout the year for certain load profiles. Extensive modeling is carried out and the storage behavior is analyzed under varying conditions.

Chapter 5 - Grid Connected System This chapter explores the technical feasibility of a grid connected charging station with an on-site storage to reduce grid reliance. An optimal system sizing is arrived at to maximize the electrical autarky of the charging system.

Chapter 6 - Lifetime, Costs, and Environmental Impact This chapter determines the economical feasibility and the environmental impact of building such a charging station for LEVs. Some algorithms are also developed to estimate the lifetime and calendar effects on the system components of the grid connected and autonomous system configurations.

Chapter 7 - Conclusions This chapter summarizes the key results of this project, and also lists some recommendations for further studies into the topic.

Chapter 2

Estimating Energy Resources

The first step in designing a Renewable Energy (RE) based system is determining the potential of the RE involved. While there is a plethora of RE sources and their accompanying technologies currently being used around the world, the scope of this thesis report is limited to photovoltaic (PV) energy. This chapter deals with estimating the availability of usable solar energy on Earth, specifically in the city of Delft in Netherlands.

2-1 Solar Radiation components

The Earth receives energy from the sun in the form of solar radiation. As the solar radiation travels through the Earth's atmosphere, it interacts with various components in the atmospheric layers. While some of these components like ozone, carbon dioxide, oxygen and water-vapour contribute to notable absorption of radiation at various spectral bands, others like water droplets and dust also contribute to scattering. Clouds tend to reflect most of the radiation falling on them.

Scattering, reflection and absorption of light in the atmospheric layers leads to a distinct decomposition of solar radiation incident on the Earth's surface into different components [14].

Direct radiation This component of radiation streams through the atmosphere unaltered, reaching the Earth's surface in a straight line from the sun. It is denoted as B.

Diffused radiation This component is composed of all the radiation that is scattered from the atmosphere to the Earth's surface and not coming directly from the sun. It is denoted as D.

Albedo radiation This is the radiation reflected from the ground. It depends on a variety of factors like nature of the soil, vegetation, etc. It is denoted as R.

Global radiation This is the total radiation falling on the surface of the earth, and is the sum of direct + diffused + albedo radiation. It is denoted as G. In general, $G = B + D + R$. Figure 2-1 shows the different components of radiation.

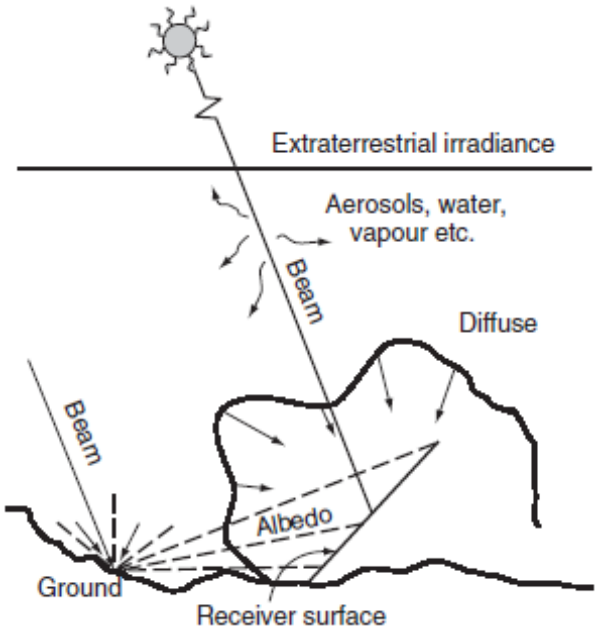

Figure 2-1: Different components of solar radiation(illustration from [15])

Radiation, irradiance and irradiation Radiation is used in this chapter, as well as the rest of the thesis as a generic term. To distinguish between power and energy, the terms irradiance and irradiation are used. Irradiance is the power density incident per unit surface, measured in W/m^2. Irradiation is the incident energy intensity falling over a period of time, measured in Wh/m^2.

2-2 Solar irradiance on The Netherlands

All the analysis and estimations in this thesis report stem from the solar irradiance data for the Netherlands. Hence it was important to have used a reliable source for the data. In this report, the global irradiance data has been sourced from the Dutch Meteorological Institute called Koninklijk Nederlands Meteorologisch Instituut (KNMI).

2-2-1 Scope of the irradiance data from KNMI

The irradiance data plays a big role in the overall system design task at hand, and the scope of the irradiance data is discussed in this section.

Resolution of the data The data has been recorded by KNMI at intervals of 1 minute. Thus the resolution of the data analysis, as well as the system modeling (refer section 4-5) is 1 minute. This is also the highest resolution offered by most Meteorological stations around the world.

Geographical location of the source As per the Baseline Surface Radiation Network (BSRN) dataset obtained from KNMI, the data has been recorded at the weather station location shown in Figure 2-2 as Loc B,which lies in Utrecht. It is assumed without loss of generality that the global irradiance does not differ too much across the Netherlands. So the system, proposed to be located in the city of Delft in the Netherlands (Loc A in Figure 2-2), is designed based on this irradiance data.

Figure 2-2: Location of the irradiance data source - KNMI

Time span of the data A total of 4 years (2009 to 2012) are considered for analyzing the irradiance data.

Global horizontal irradiance G_H The irradiance data from KNMI is for the global horizontal irradiance, which is the irradiance that is received by a solar panel when kept completely horizontal on flat ground. The effective irradiance will, however, change when the solar panel is fixed at a particular orientation. The irradiance is converted for an optimized orientation of the PV module in section 2-3.

2-2-2 Irradiance profiles

In this section, the global horizontal irradiance data and its trends over the years 2009 - 2012 are discussed.

Annual trends Firstly, the annual trends in the solar irradiance as measured on the ground in the Netherlands are examined. A common thread can be seen in figures 2-3 through 2-6. The irradiance peaks around the middle of the year, corresponding to summer, and falls to almost a third of the summer value towards the winter months. It can be concluded that the annual trends in irradiance over the years are very similar.

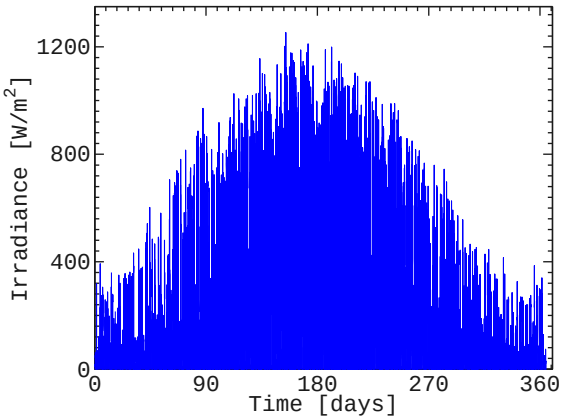

Figure 2-3: Annual irradiance - 2009

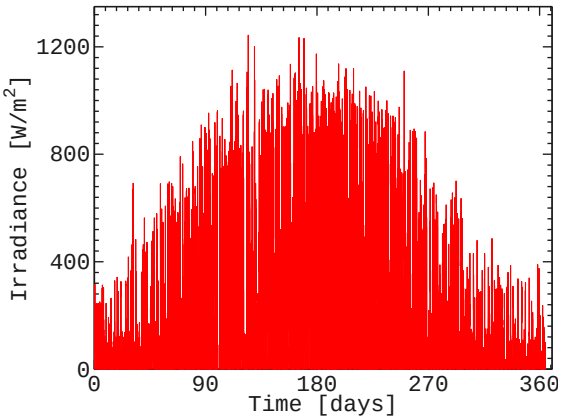

Figure 2-4: Annual irradiance - 2010

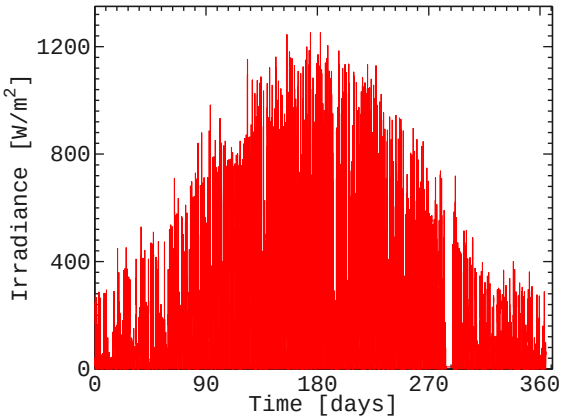

Figure 2-5: Annual irradiance - 2011

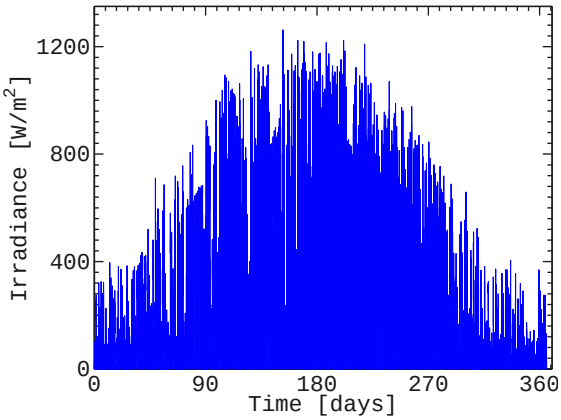

Figure 2-6: Annual irradiance - 2012

Seasonal trends To look a little more closely at the seasonal trends, sample months of summer and winter over the time span of the data are examined. Figures 2-7 through 2-10 depict the irradiance in typical summer and winter months. As seen in these figures, the summer irradiance in the sunny month of June falls by almost two-thirds in the winter month of December. There are significant fluctuations in daily irradiance as well. For instance, in Figure 2-10, there are days with around 300 W/m^2 of irradiance suddenly followed by a few days with only 100 W/m^2.
These seasonal and daily fluctuations in the irradiance can prove to be a big hurdle in

the design of an autonomous PV system, as seen later in chapter 4.

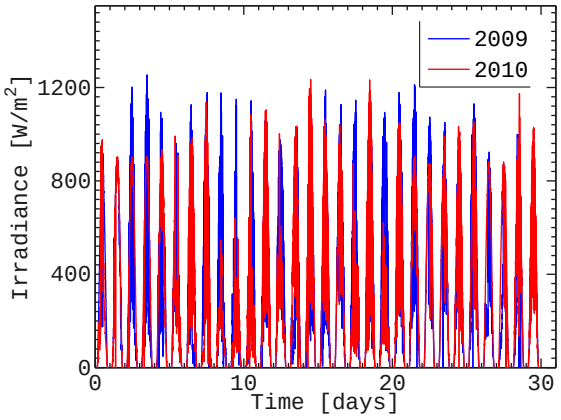

Figure 2-7: Summer trends - June 2009 and 2010

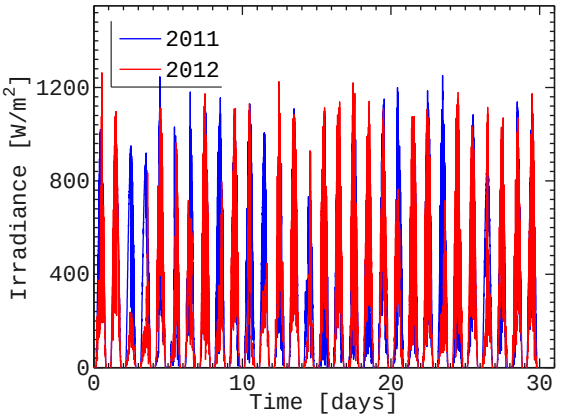

Figure 2-8: Summer trends - June 2011 and 2012

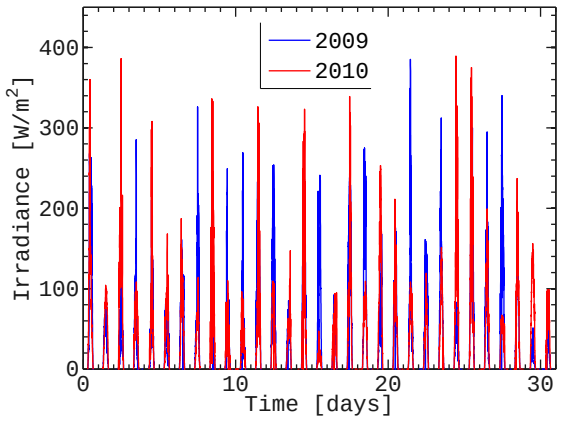

Figure 2-9: Winter trends - December 2009 and 2010

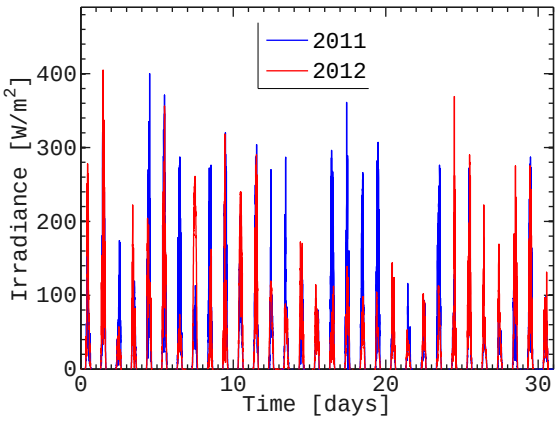

Figure 2-10: Winter trends - December 2011 and 2012

Diurnal trends Now let us move on to a smaller span of time, wherein we can witness the effect of rotation of the earth on the quantity of irradiance falling on it. The irradiance over a single representative day of the year is analyzed here. This diurnal data is obtained by taking the average of all the irradiance points in the corresponding time of the day in the rest of the year. Thus, the irradiance at noon is the average irradiance at noon throughout the year, and so on.

As shown in Figure 2-11, there is a sharp peak observed in the middle of the day. This coincides with the maximal sunlight in the form of direct radiation present at those times. On the other hand, the diffused sunlight is contributing to the irradiance at times closer

to sunrise and sunset. Thus the irradiance levels are also lower.
The average diurnal irradiance for these 4 years also show a remarkable correlation, which is also represented in the calculated energy intensity in section 2-4. These curves would of course be taller or smaller if the representative days of summer and winter are observed respectively, instead of the whole year. It should be noted that these curves represent the global horizontal irradiance, which is the sum of all the radiation components(refer section 2-1) falling on the horizontal surface of the earth.
The diurnal fluctuations are relatively easier to handle in an autonomous PV system with the use of popular storage solutions like batteries.

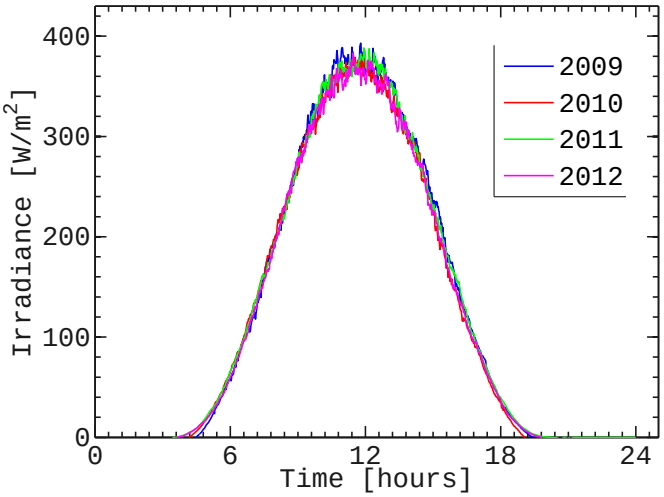

Figure 2-11: Diurnal irradiance trends - 2009 to 2012

A summary of trends - 3D plot A 3D plot that captures both the seasonal and diurnal trends is shown in Figure 2-12. The daily bell curves of irradiance can be clearly seen to increase towards the middle of the year with the peaks getting taller. Also, the daily curves seem to move closer to the Time(daily) axis in the middle of the year signifying earlier sunrises.

2-2-3 Computing available energy

As the entire data is in terms of irradiance (W/m^2), it needs to be converted to irradiation (Wh/m^2). The estimated available energy (as shown in section 2-4) has been calculated as follows:

$$E_s = \int_{t_0}^{t} G(t).dt \tag{2-1}$$

where
E_s = Solar irradiation or energy per unit area over the period t_0 to t,

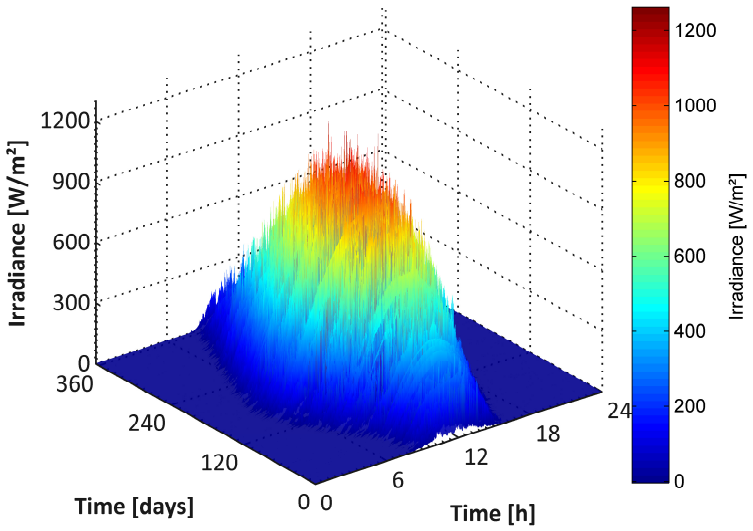

Figure 2-12: Irradiance: daily Vs diurnal - 2012

$G(t)$ = Solar irradiance at time t.

Since irradiance data is discrete having 1 minute intervals, a more appropriate relation would be:

$$E_s = \sum_{i=1}^{n} G.\Delta t \tag{2-2}$$

where
$\Delta t = t_i - t_{i-1}$,
E_s = Solar irradiation or the energy per unit area in Wh/m^2 over the interval Δt,
G_i = Solar irradiance measured at minute i in W/m^2.

Sun hours or peak sun hours is a term defined as the average amount of time per day that the surface in question receives a peak irradiance of $1000 W/m^2$. So the average sun hours are calculated as follows:

$$Sun\ hours\,(h/day) = \sum_{i=1}^{3600*24*365} \frac{G_i\,(W/m^2)}{60\,h^{-1} * 365\,days * 1000\,W/m^2} \tag{2-3}$$

where
G_i = Solar irradiance measured at minute i in W/m^2.

Equations (2-2) and (2-3) have been used extensively in arriving at the results shown in section 2-4.

2-3 Optimizing for tilt and azimuth

As discussed before, the global horizontal irradiance G_H needs to be translated to equivalent irradiance incident on the Plane of Array (POA)[1] of the PV module. First, the fixed orientation requirements of the PV module must be decided to define the POA. The PV module position is defined by fixing two main parameters, tilt and azimuth.

Tilt This is the angle of elevation of the PV module with respect to the horizontal. The further away a PV module is from the equator, the higher is the tilt angle. For the system discussed in this chapter, as the proposed location is in the Netherlands, a positive tilt angle would help in facing the sun compared to a tilt angle of 0°.

Azimuth This is the horizontal angle of deviation measured from a base meridian. The reference meridian varies in different fields of study. In this case, the azimuth is defined with respect to true south. For example, an azimuth of 0° implies facing South, while an azimuth of 90° means facing West.

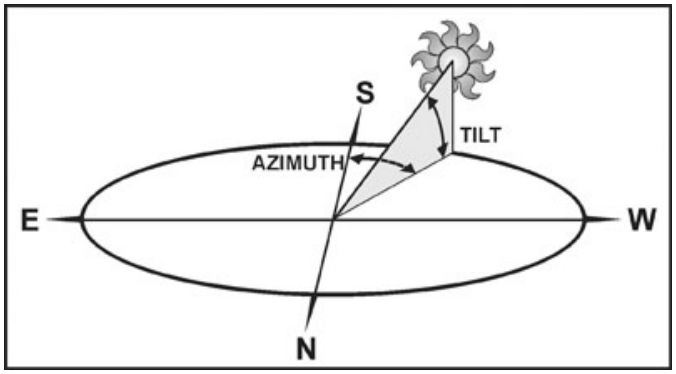

Figure 2-13: Tilt and Azimuth.
(*Credit:e-education course EGEE 401, Pennsylvania State University*)

Optimal position for Delft

It is tricky to optimize the fixed position of a PV module, because of the change in relative position of the sun during the day and throughout the year. For instance, a lower tilt angle optimizes the POA irradiance for winter, while a higher tilt angle maximizes the PV yield for summer. Ideally, a position that is optimal for both winter and summer is preferred.
The Solar Electricity Handbook [16] helped in optimizing the position of the PV module placed in Delft (Loc A in Figure 2-2). The position for optimized yield throughout the

[1] POA is the plane containing the entire PV module.

year is defined by an azimuth of 0° and a tilt of 38°.

The global horizontal irradiance from the irradiance data was translated for the above fixed PV position using a complex model [17] that evaluates a transposition factor[2] for the minutely G_H data and estimates the global irradiance incident on the POA. The results have been captured in section 2-4. The modified irradiance data for the optimized PV position is referred to as G_{opt}.

2-4 Results

Analysis on the solar irradiance data for the Netherlands over the last 4 years gave the results as summarized in Table 2-1.

Table 2-1: Solar irradiance available per m^2 and the sun hours for years 2009-2012

	2009	**2010**	**2011**	**2012**
Sun hours per day (h/day)	2.89	2.8	2.94	2.86
Total energy (kWh/m^2) **under** G_H	1053	1023	1072	1045
Total energy (kWh/m^2) **under** G_{opt}	1210	1179	1232	1203
Percent increase due to G_{opt}**(%)**	14.91	15.25	14.93	15.12
Average daily energy (Wh/m^2) **under** G_H	2886	2802	2938	2863
Average daily energy (Wh/m^2) **under** G_{opt}	3316	3232	3375	3296

2-4-1 Conclusions

Diurnal and seasonal trends As expected, the irradiance data over the days, months and year clearly shows the increase in irradiance in the middle of the day, and in the middle of the year (summer), both resulting from the direct sunlight incident on earth.

Consistency of irradiance data It appears that the available annual solar energy does not vary much over the years. This fortifies our initial assumption and justifies choosing only one representative data set to model the whole system on.

Optimal PV orientation Up to 15% energy increase is achieved by optimizing the PV position. Going for a higher tilt might help in increasing the yield in summer, at the cost of impacting the winter yield. There could be multiple fixed positions throughout the year to maximize the yield per season, but that case is not considered in this report.

[2]Transposition factor is the ratio of the global incident irradiation to the global horizontal irradiation.

An abundance of solar energy There is over $1MWh/m^2$ of energy available over a calendar year, even in a place like the Netherlands that lacks abundant sunshine throughout the year. This further boosts our faith in designing a system based on solar energy.

Approximate PV yield It might be tempting to estimate the annual PV yield by simply mutiplying it with the manufacturer's claimed nominal efficiency. However, the answer would differ significantly from a more realistic estimate, as shown in chapter 3. This is because other effects come into play, like temperature and irradiance and their impact on the PV output parameters.

These learnings provide the foundation of the next chapter, which deals with estimating the exact PV yield while taking several factors into account.

Implications of the results on the load

As the system to be designed is a charging station for Light Electric Vehicles (LEVs), some crude estimates are discussed to determine the feasibility of a PV based project.

Let us take the most common type of Light Electric Vehicle (LEV) on the road in the Netherlands - an e-bike. A typical e-bike has a battery of around 250 Wh (refer section 4-4). Let us assume a 20% efficient PV module (an optimistic number, but fine for an approximate estimate). Approximate average PV yield per day = 3.2 $kWh/m^2 \times 20\% =$ 640 Wh/m^2. This means that over 2 e-bikes can be charged from 0 to 100% per m^2 of PV module per day. This is just a very crude estimate.

Chapter 4 discusses with great detail how a full fledged PV system fares against these numbers under real life factors.

Chapter 3

Estimating the PV Potential

This chapter shows a simple way of estimating the output of a photovoltaic (PV) module, which varies greatly with surrounding conditions of temperature and irradiance. A few of the most standard PV modules and their electrical throughput are analyzed over a period of time, as a function of temperature and irradiance.

The estimated PV output will thus give a more realistic estimate of the energy yield possible throughout the year than what is expected if a constant efficiency is assumed for the PV module over a period of time.

3-1 Introduction

Let us first look at the way in which the elements of weather like irradiance and temperature vary throughout the year. As the PV output depends on these elements, we will also get a good measure of how the operating conditions of the PV module are affected with time. The PV modeling in this chapter is limited to module level only. Other inefficiencies occurring at systems level are looked at in detail in chapter 4.

3-2 The dynamic Dutch weather

For the purpose of an in-depth analysis of the diurnal and seasonal variations in temperature and irradiance, an extensive range of data was obtained from the Koninklijk Nederlands Meteorologisch Instituut (KNMI) database. The weather data from KNMI is largely a realistic representation of the average weather conditions across the Netherlands.

Time frame of analysis Throughout this chapter, we shall look at these variations and the corresponding PV response over 2011. However, without any loss of generality, the model used in this chapter can be extended to study the PV outputs for the weather data of any year and any place.

Tools used The software Matrix Laboratory (MATLAB) has been extensively used for modeling, simulation, and plotting of graphs.

3-2-1 Irradiance fluctuations

This has already been covered in great detail in chapter 2. It was seen how the diurnal irradiance peaks in the middle of the day, and the daily irradiance has a seasonal pattern such that it reaches its maximum in the summer and minimum in the winter.

3-2-2 Temperature fluctuations

Similar to the irradiance data, it has been observed that the annual temperature profiles also are quite comparable. Hence a representative year (2011) has been chosen as the standard time-frame to analyze the PV module in this chapter, and the system in general against all the irradiance and temperature variations.

The temperature fluctuation over the year has been analyzed and plotted in Figure 3-1. The x-axis represents the diurnal changes in temperature, while the y-axis represents the daily changes in the temperature throughout the year. The z-axis shows the temperature value at various points of time.

Diurnal fluctuations Figure 3-1 clearly shows how the intra-day temperature peaks around the middle of the solar day. Also, these curves grow taller in summer as compared to winter, showing how the days are longer and warmer in summer and shorter and colder in winter.

Seasonal fluctuations It can also be seen from the figure that the highest peaks of temperature are achieved in the June-August time frame, which coincides well with the apparent seasonal changes in the country. This is more discernible in Figure 3-2. The temperature across the seasons varies from subzero temperatures in January to over $30^{\circ}C$ in June. The system thus has to be designed taking into account this range of temperature.

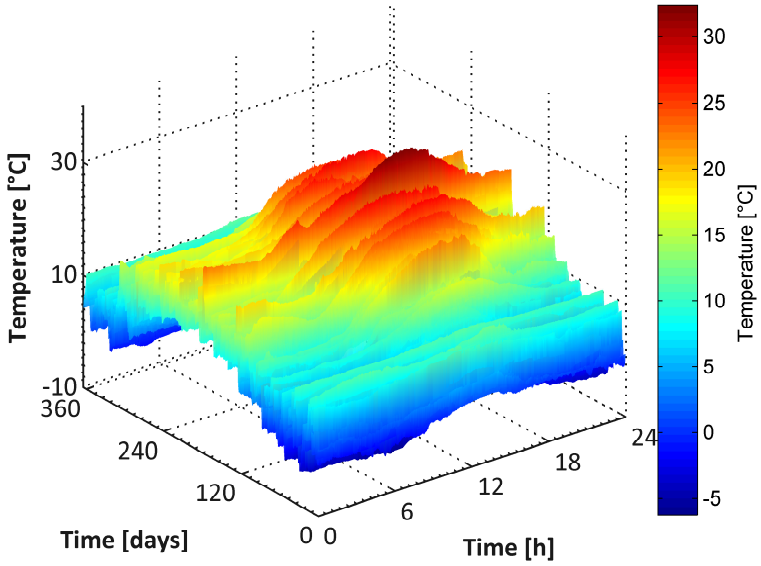

Figure 3-1: Temperature: daily Vs diurnal - 2011

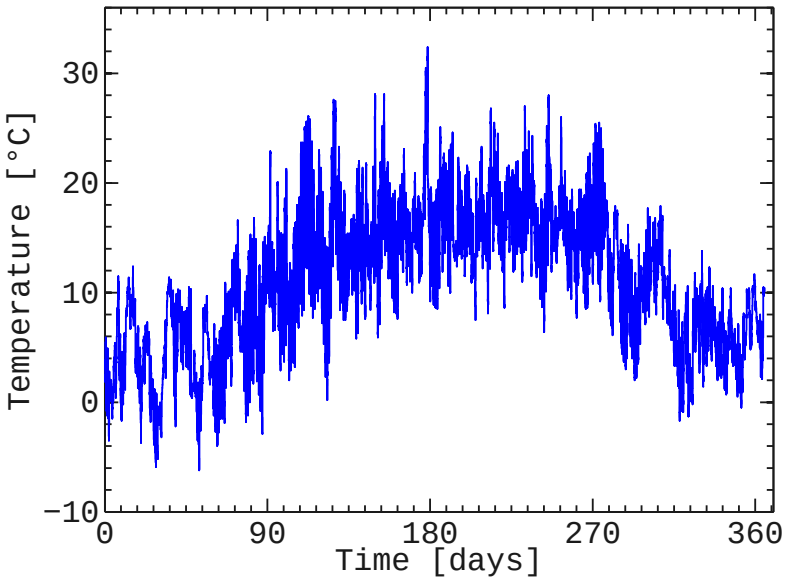

Figure 3-2: Annual Temperature - 2011

Monthly plots

To validate these observations, a comparative plot has been drawn here for two representative months in Figure 3-3. The months of July and December have been chosen as the representative summer and winter months respectively. The peak Dutch summer temperatures are seen in the month of July. These high temperatures can have an adverse effect on the PV output, as discussed later in section 3-3. The typical Dutch winter can be seen in the temperature plot of December. It can be seen how even the daily temperatures can fluctuate greatly in the same month. The temperature fluctuations in December seem to be around $10°C$ between consecutive days, while the temperature fluctuations in July seem to be much higher, with some days differing in temperature up to 15 $°C$.

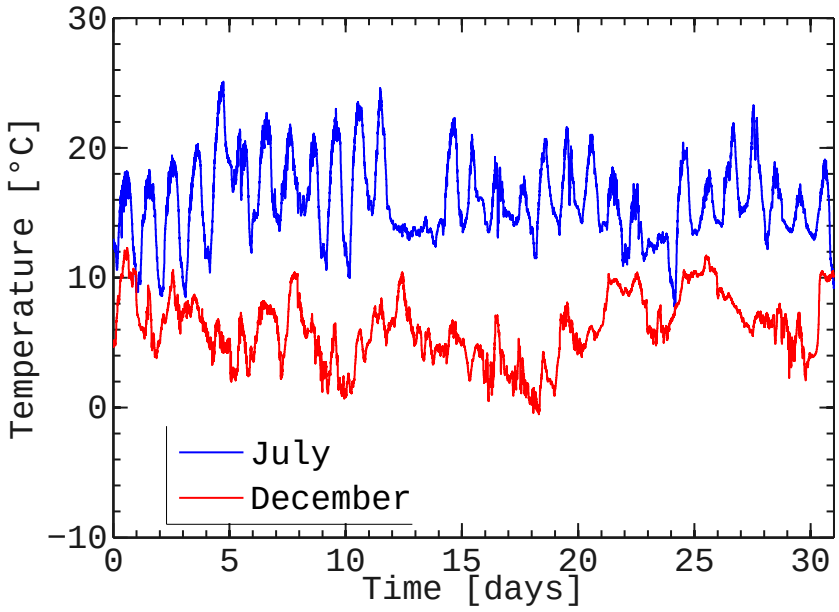

Figure 3-3: Temperature: July and December 2011

Now let us examine how the PV output varies as a function of these weather parameters.

3-3 PV output variations

In this section we shall look at how the different output parameters of the PV module like power, voltage and current vary with temperature, irradiance and time. The results have been obtained through extensive modeling of these parameters by the author.

Why PV datasheets are insufficient in exact yield estimation

Irradiance and temperature have a major impact on the output of a PV module. Manufacturers of PV module typically provide the output parameters only under limited test conditions. However, the everyday conditions under which most PV modules are used in the field vary greatly from the Standard Testing Conditions (STC)[1]. This is a big handicap for most PV system designers and installers, who need to estimate the actual PV output over the year to weigh the PV system's usefulness for a desired application.

Lack of a unified model Moreover, the parameters specified in a typical PVdatasheet do not consider the combined effect of temperature and irradiance. For instance, the temperature coefficient of the electrical output parameters are specified at a constant irradiance of $1000 W/m^2$.

3-3-1 Scope of the PV model

The PV model discussed in this chapter is a simple model that determines the output parameters of a PV module over time. It takes in the rated parameters of the module (like P_{max}, I_{sc} and V_{oc}), the temperature and irradiance profiles along with the temperature and irradiance coefficients defined for the module at STC or Nominal Operating Cell Temperature (NOCT)[2] conditions by the manufacturer. The model analyzes these inputs and gives an estimate of the operational parameters of the module as a function of time (including performance metrics like Fill Factor and efficiency), under varying conditions of temperature and irradiance. An illustration can be seen in Figure 3-4.
The model has a certain scope under which it performs accurately. The scope of the model is discussed in this section.

Resolution of the data The resolution of the weather data is 1 minute. It is assumed that the value of the parameter in the duration of the 1 minute interval is constant. Thus this model assumes a steady-state within this interval.

Temperature and irradiance latency Latency is the delay of the PV parameter in responding to the ambient parameters like temperature and irradiance. The latency in the temperature response has been considered(section 3-3-3). The irradiance latency is difficult to estimate and has been ignored. It can be argued that for the resolution of the data at hand, 1 minute is ample time for the irradiance to stabilize to the steady-state value. Thus ignoring the latency in irradiance is justified while aiming for reasonable accuracies.

[1] STC is defined by an ambient temperature of $25^\circ C$ and an irradiance of $1000\ W/m^2$.

[2] NOCT condition is defined by an ambient temperature of $20\ ^\circ C$, an irradiance of $800\ W/m^2$ and a wind speed of $1\ m/s$ with the back of the solar panel open to the breeze.

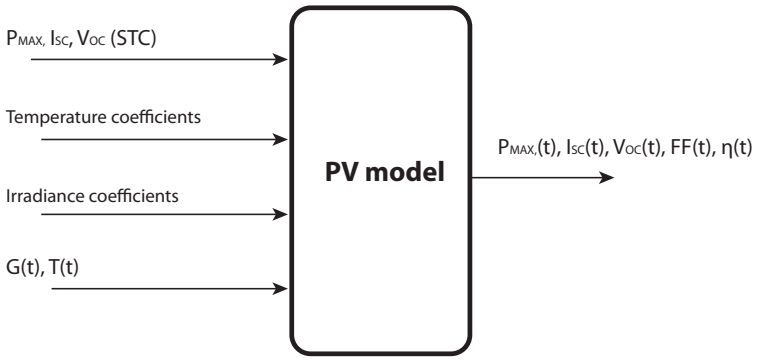

Figure 3-4: An illustration of the PV model.

Minimal parameters The model stands out amongst most of the PV models in literature for needing just a few basic parameters (temperature, irradiance, temperature coefficients). Even though the model excludes the effects of sporadic weather phenomena like gusts, hail, etc. it gives fairly accurate estimates of the PV output, taking into account the two most significant parameters of temperature and irradiance.

3-3-2 PV modules

A total of 12 different PV modules(11 crystalline silicon (c-Si) and one Heterojunction with Intrinsic Thin-layer (HIT)) have been looked at from 6 different manufacturers, namely: ET Solar, Luxor, Suntech, Sun Power, Sanyo and Conergy. For this report, only monocrystalline[3] and polycrystalline[4] silicon modules have been considered.

Table 3-1 shows the mapping of the Module number to the commercially available product, while Table 3-2 captures a summary of the key module parameters. Although the various parameters have been evaluated for all the 12 modules in Table 3-1, for the sake of simplicity, the various results obtained through the model have been reported for one module only, viz. Sun Power E19 240 W_p (Module 12). Nonetheless the rest of the modules have also been analyzed similarly through the model, and the final module yields are shown in section 3-4.

[3] A monocrystalline solar cell is produced from a single crystal of silicon.
[4] A polycrystalline solar cell is produced from a piece of silicon having many silicon crystals.

Table 3-1: PV module brand and W_p

Module No.	Module Name
1	Conergy Powerplus Poly 210Wp
2	Conergy Powerplus Poly 250Wp
3	ET solar Mono 210Wp
4	ET solar Mono 260Wp
5	ET solar Poly 200Wp
6	ET solar Poly 250Wp
7	LuxorPV Ecoline Poly 250Wp
8	LuxorPV Ecoline Poly 290Wp
9	Suntech Pluto HiPerforma 255Wp
10	Suntech Pluto Poly STP 255Wp
11	Sanyo HIT N240SE10 240Wp
12	Sun Power E19 Mono 240Wp

Table 3-2: PV modules - key parameters

Module No.	P_{max} STC(W)	NOCT ($^{\circ}C$)	Area (m^2)	Efficiency nom STC (%)	V_{oc} STC (V)	I_sc STC (A)	Temp coeff P_{max} (%/$^{\circ}C$)	Temp coeff V_oc (%/$^{\circ}C$)	Temp coeff I_{sc} (%/$^{\circ}C$)
1	210	48	1.32	15.95	30.59	8.73	-0.44	-0.33	0.059
2	250	48	1.63	15.36	37.12	8.81	-0.44	-0.33	0.059
3	210	44.4	1.28	16.45	46.82	5.86	-0.44	-0.31	0.02
4	260	44.4	1.63	15.98	37.86	8.96	-0.44	-0.31	0.02
5	200	45.3	1.31	15.23	29.98	8.76	-0.44	-0.34	0.04
6	250	45.3	1.63	15.37	37.47	8.76	-0.44	-0.34	0.04
7	250	47	1.63	15.46	37.41	8.61	-0.45	-0.32	0.05
8	290	47	1.94	15.03	45.23	848	-0.45	-0.32	0.05
9	255	45	1.63	15.7	37.7	8.72	-0.4	-0.31	0.051
10	255	45	1.63	15.7	37.6	8.76	-0.44	-0.33	0.055
11	240	44	1.26	19	52.4	5.85	-0.30	-0.25	0.030
12	240	45	1.24	19.3	48.6	6.3	-0.38	-0.27	0.055

3-3-3 Estimating cell temperature

The PV module output greatly varies with the temperature, or more accurately, the cell temperature T_{cell}. As the PV module is comprised of several smaller solar cells, the temperature dependence of the solar cell output is evident from the diode equation: [18]

$$I = I_{ph} - I_0(\exp(\frac{qV}{kT}) - 1) \tag{3-1}$$

When the open circuit voltage (V_{oc}) is considered, the net current = I = 0. Thus equation (3-1) transforms as follows:

$$V_{oc} = \frac{kT}{q}\log(\frac{I_{ph}}{I_0} + 1) \tag{3-2}$$

where:
I = The net current flowing through the diode,
I_0 = Diode saturation current,
I_{ph} = Photogenerated current,
V = Applied voltage across the terminals of the diode,
V_{oc} = Open circuit voltage,
q = Absolute value of electron charge,
k = Boltzmann's constant, and
T = Absolute temperature of the cell.

The diode current I_0 is heavily dependent on the cell temperature. In general, higher the temperature, greater the diode current I_0 (stems from the fact that semi-conductors exhibit a higher conductance with increase in temperature). Therefore, it is clear from equation (3-2) that the open circuit voltage also depends on temperature, but exhibits an inverse relation.

First we shall determine the apparent ambient temperature as perceived by the body of the PV module.

Temperature latency modeling Though the ambient temperature fluctuates greatly (Figure 3-2), the PV module body cannot keep up with the temperature changes of the surroundings. Due to the thermal inertia of the PV module, there is always a delay in the module's bulk temperature trying to respond to the ambient temperature. While the PV module tries to respond to the ambient temperature, the ambient temperature might well have moved to a different value. This temperature latency is included in the storage model. A first order maximum rate that limits the rate of change of temperature is defined. In this case, it is $L_T = 2°\text{C}/min$. Given below is an example and a plot that explains the significance of L_T.

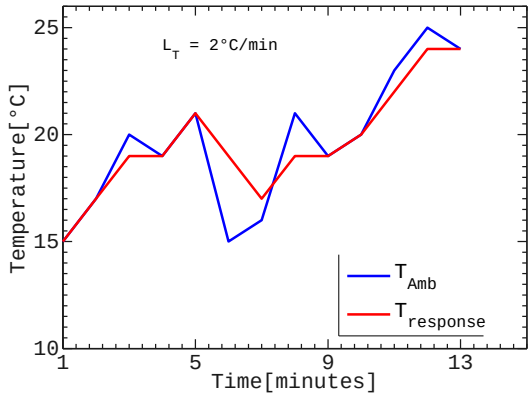

Figure 3-5: Temperature latency of the PV module.

Example of latency in temperature response of PV module

- PV module body responds sluggishly to ambient temperature changes at a rate $> L_T = 2°\text{C/min}$
- With ambient fluctuations within the temperature latency limits, the PV body temperature responds well and follows suit.

It must be noted that the PV body temperature referred to here is the apparent ambient temperature perceived by the PV module. This should not be confused with the cell temperature[5]. The cell temperature is a function of the irradiance and the apparent ambient temperature (body temperature).

To determine T_{cell}, we shall use the NOCT model [19], according to which:

$$T_{cell} = T_{amb} + (NOCT - 20°C) * \frac{G}{G_{NOCT}} \tag{3-3}$$

where:
T_{cell} = Cell Temperature ($°C$) ;
T_{amb} = Ambient Temperature ($°C$) ;
$NOCT$ = Nominal Operating Cell Temperature ($°C$) ;
G = Irradiance incident on the PV module (W/m^2) ;
G_{NOCT} = Irradiance under NOCT conditions = 800 W/m^2 ;

Since we have also approximately estimated the temperature latency of the PV module, we shall factor in this apparent ambient temperature in the above model in place of T_{amb}. Now let us look at the cell temperature as a function of the ambient temperature.

As can be seen from Figure 3-6, both irradiance and temperature have a simultaneous role to play in affecting the T_{cell}[6].
The cell temperature, is in general always greater than the ambient temperature, as shown by equation 3-3. In winter, this disparity is lower due to lower irradiance levels. In summer, the cell temperature is much higher than the ambient temperature due to

[5] Although the cell temperature is defined at cell level, it is assumed that the all the cells in the module respond similarly to temperature and irradiance effects

[6] All the graphs shown in this section pertain to the Sun Power module from Table 3-2.

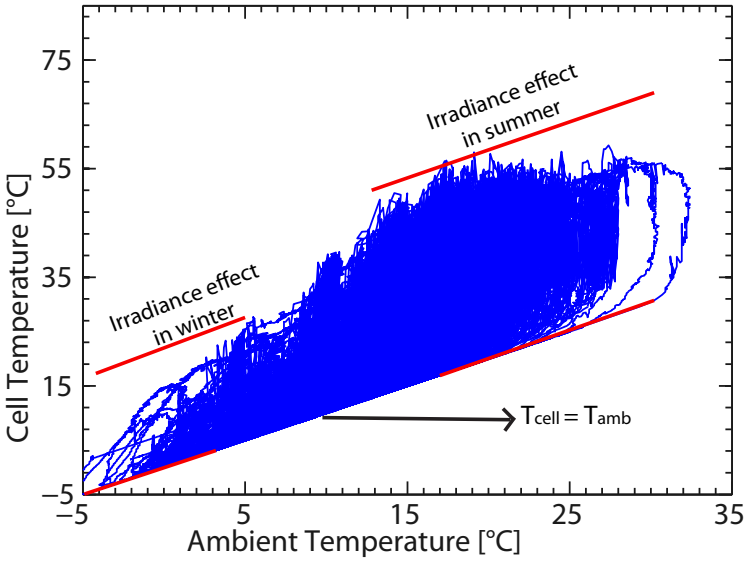

Figure 3-6: T_{cell} variation against T_{amb} - 2011

higher levels of irradiance. The only time when it is equal to the ambient temperature is when the irradiance is zero(at night).

Next, the cell temperature is compared with the ambient temperature as a function of time in Figure 3-7. The nature of the cell temperature is not purely a shadow of the ambient temperature. It is an amalgamation of both ambient temperature and irradiance variations, as seen in equation (3-3).

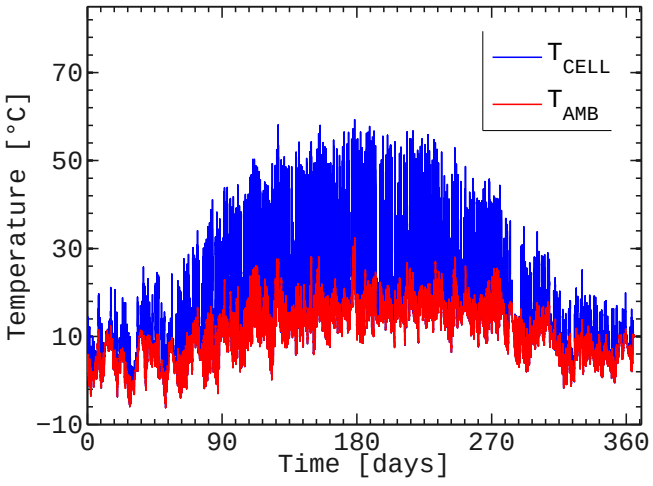

Figure 3-7: Annual T_{cell} variation - 2011

3-3-4 PV output parameters

Now that the cell temperature is determined throughout the year, we can go on to estimate the various PV parameters like voltage, current, power, fill factor, efficiency that depend on the cell temperature and irradiance.

Temperature coefficients

The PV manufacturer provides temperature coefficients for the output parameters like maximum power, open circuit voltage and short circuit current (P_{max}, V_{oc} and I_{sc}). Refer Table 3-2 for all the values. These temperature coefficients capture the first order behavior of the PV output.

For instance, a temperature coefficient of power of -0.44%/$^{\circ}C$ for a $250W_p$ rated module is a measure of how much the power varies with change in temperature. The nominal value of $250W$ is measured at STC conditions, i.e. $1000W/m^2$ and $25^{\circ}C$. So a cell temperature of $30^{\circ}C$ would signify a power output of $250W - 0.44 * (30 - 25) * 250W/100 = 244.5W$, all other conditions remaining constant. Similarly the other temperature coefficients have been defined for (V_{oc} and I_{sc}).

Thus, taking a $1000W/m^2$ irradiance as base, the temperature effects of the cell temperature throughout the year is calculated for the PV output parameters as shown above. The temperature effects on the output power of the PV module is depicted in Figure 3-8.

The temperature effects are similarly modeled for the V_{oc} and I_{sc} of the PV module.

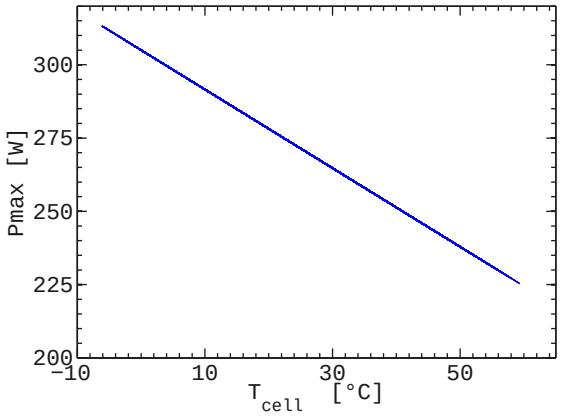

Figure 3-8: Dependence of P_{max} on temperature under constant irradiance.

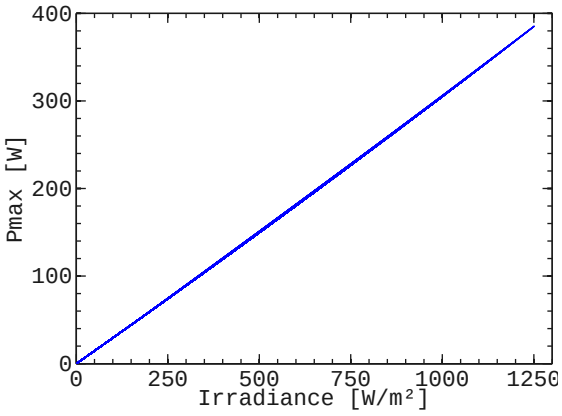

Figure 3-9: Dependence of P_{max} on irradiance under constant temperature.

Irradiance effects

One would expect that the PV module exhibits a constant efficiency across various irradiance levels[7]. But this is inaccurate. The efficiency of the modules at an irradiance of $200W/m^2$, as stated by the manufacturer, drops by around 3% of its value at STC. This is translated to very similar irradiance behavior for the I_{sc} and P_{max} of the module, while the V_{oc} undergoes almost negligible changes. In general, the effect of irradiance on the output power has been captured in Figure 3-9. Refer to Figure 3-10 for the manufacturer's data on the irradiance effects.

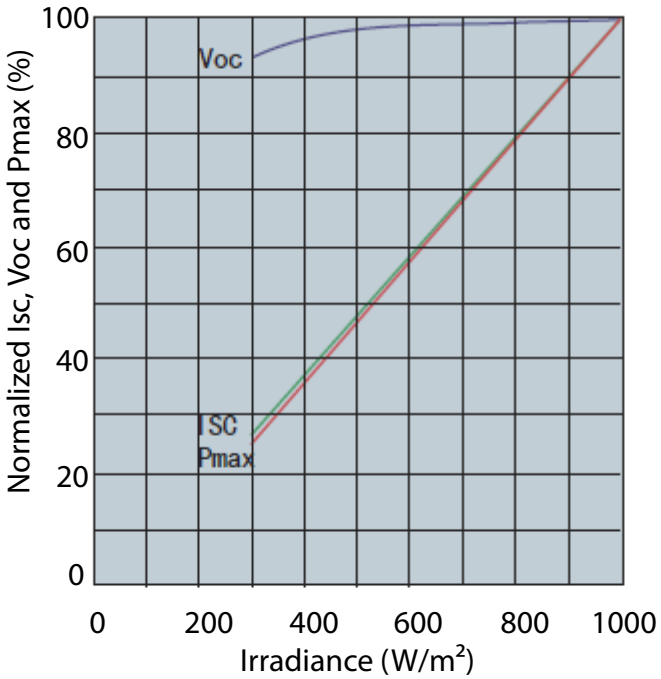

Figure 3-10: Irradiance dependence of I_{sc}, V_{oc} and P_{max}

Thus, the temperature dependent output parameters of the PV module are now processed through the range of irradiance values that the year 2011 experienced every minute.

3-3-5 Function of time

Now that the effects of both irradiance and temperature are established, the model can estimate the various PV parameters as a function of time, as the irradiance and temperature profiles over time are already known. The various output parameters have been plotted in the following figures.

[7]The irradiance shown in these graphs are the global irrradiance values, as might be experienced by PV module for a given inclination.

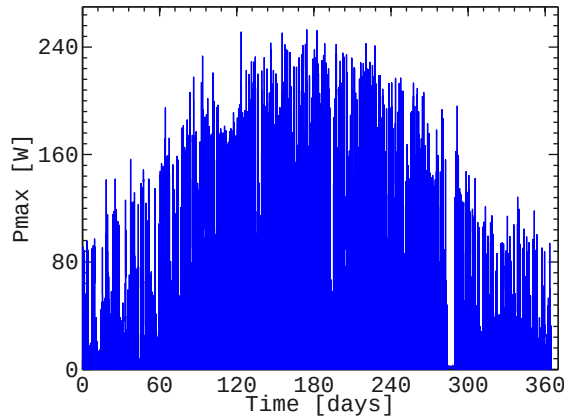

Figure 3-11: P_{max} variation over the year

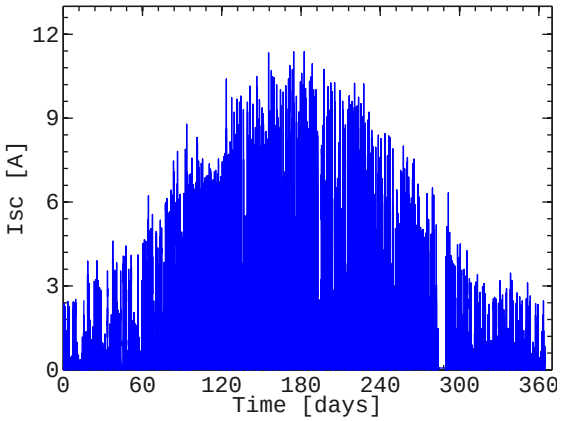

Figure 3-12: I_{sc} variation over the year

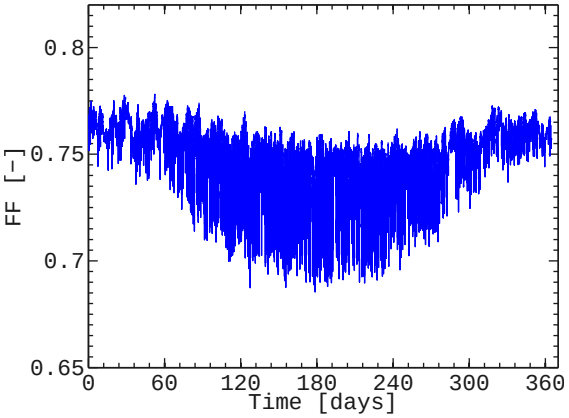

Figure 3-13: FF variation over the year

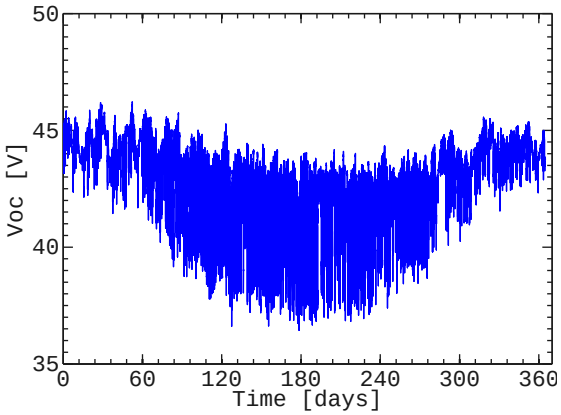

Figure 3-14: V_{oc} variation over the year

There is a strong correlation seen in these figures between power and the current on one hand, and voltage and FF on the other. The voltage behavior also strongly correlates with the annual temperature trends(refer Figure 3-2). This means that the effect that dominates the most in shaping PV outputs is the temperature effect for voltage.

The correlation in these graphs can be explained in the following manner. For a PV module, current is affected more by irradiance than by temperature while voltage is affected more by temperature. Considering minutely variation, the irradiance changes are greater in magnitude compared to temperature. Thus the output power = voltage $\times$ current follows the trend shown by the electric current, which tends to fluctuate more than the voltage. Similarly, FF is defined by equation (3-4).

$$FF = \frac{P_{max}}{V_{oc} \times I_{sc}} \tag{3-4}$$

As P_{max} is known to follow I_{sc} trends, this means that FF is dictated by similar trends as seen in V_{oc}.

And finally, the efficiency is plotted as a function of time in Figure 3-15. The efficiency trend can again be explained by examining the temperature and irradiance effects on the individual components that make up the parameter.

$$\eta_{PV} = \frac{P_{out}}{P_{in}} \tag{3-5}$$

where
P_{out} = Total output power of the PV module,
P_{in} = Total input incident irradiance on the module.

Equation (3-5) defines the efficiency η_{PV} of the module. The output power of the module is an amalgamation of both the irradiance and temperature effects. Thus the ratio of output power to input irradiance for the PV module has temperature as the dominant effect.

Similar estimations for all the modules yield results as shown in section 3-4.

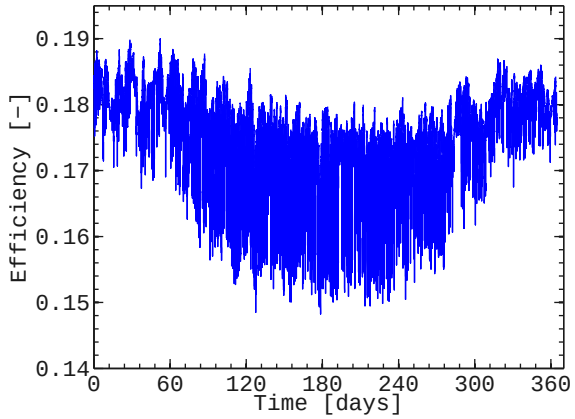

Figure 3-15: Module efficiency (η) variation over the year

3-4 Results

We know from chapter 2 about the amount of potential solar energy available. With the help of the PV model discussed in this chapter, the various PV modules from Table 3-1 are compared for their energy yields. Equation 2-2 has been used to translate the power estimations of the PV model into energy yields.

It is noticed in Table 3-3 that the model estimates a reduced energy throughput, as opposed to the 'without model' scenario, which simply assumes the PV module is generating power at a constant efficiency throughout the year. The constant efficiency assumed in the 'without model' scenario is the one that is described by the manufacturer under STC conditions.

Table 3-3: Estimated energy yield with and without the model

	Annual yield without model (kWh)	**Annual yield with model (kWh)**	**Yield per area with model (kWh/m^2)**	**MIF* (%)**
Module 1	258.64	215.47	163.69	83.31
Module 2	308.03	256.52	157.57	83.28
Module 3	258.71	218.19	170.90	84.34
Module 4	320.27	270.14	166.04	84.35
Module 5	246.42	207.16	157.72	84.07
Module 6	308.04	258.94	159.16	84.06
Module 7	309.85	256.38	157.58	82.74
Module 8	359.27	297.41	153.27	82.78
Module 9	314.66	268.42	164.99	85.30
Module 10	314.66	264.4	162.51	84.03
Module 11	295.12	262.7	208.36	89.01
Module 12	295.79	254.53	204.59	86.05

***Module Ideality Factor (MIF)**

Consequently, a module ideality factor is found out, which gives a more accurate estimate of the energy yield. MIF can be defined as *the factor that indicates the proportion of expected PV yield actually available, as estimated by the model for a given PV module.* This is also expressed in equation 3-6.

$$\text{MIF} = \frac{\text{PV } Yield_{model}}{\text{PV } Yield_{nomodel}} \tag{3-6}$$

where
PV $Yield_{model}$ = The PV yield estimated by the model taking into account the temperature and irradiance effects,
PV $Yield_{nomodel}$ = The PV yield assuming a constant module efficiency throughout the duration of interest.

A higher MIF indicates that the module fares better in the face of adverse temperature and irradiance effects throughout the year. In this case, Module 11 turns out to have the highest MIF and also the yield per unit area, and hence is the module of choice for system simulations in Chapter 4. The reason for a discernibly higher MIF shown by Module 11 is because of the HIT technology, which guarantees a much better temperature response of the module.

Correlation with temperature coefficient As it is evident that the output of the PV module is most heavily impacted by temperature, a correlation between MIF and the

temperature coefficient of power of the PV module was sought. Figure 3-16 shows the MIF values for the various modules analyzed through the PV model. It can be clearly seen that modules with a lower temperature coefficient fare much better with a higher MIF. This also translates to a much higher yield per area as seen before in Table 3-3.

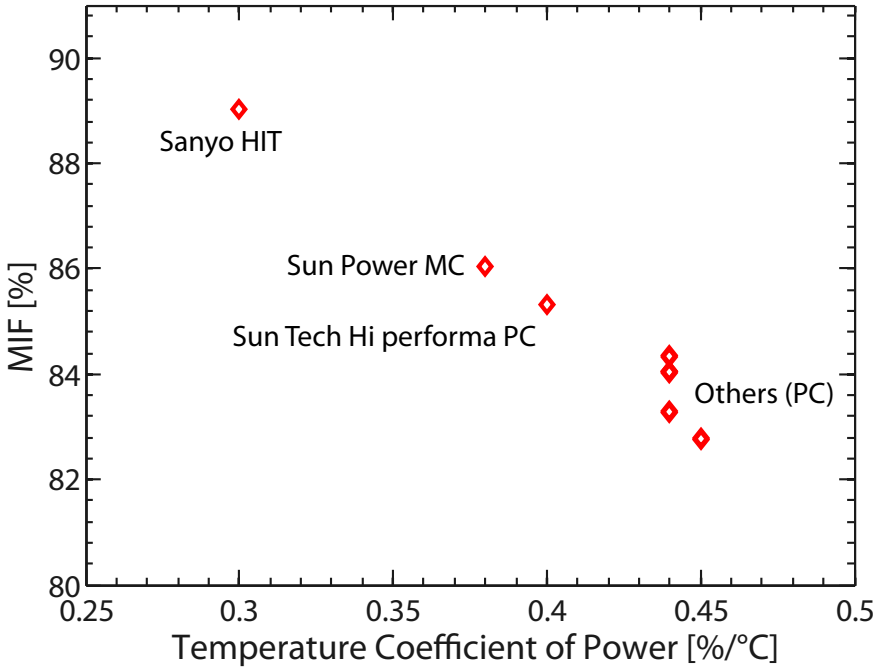

Figure 3-16: MIF correlation with temperature coefficient of power (absolute value). *MC: Monocrystalline, PC: Polycrystalline.*

It should be noted that the MIF value for the same PV technology can vary depending on the geographical location of the PV module. The MIF values reported in this chapter are for a PV module in Delft, The Netherlands.

As more technologies are analyzed through the PV model mentioned in this chapter, a plot like Figure 3-16 can serve as a handy reference to estimate the drop in expected yield across technologies. Thus, the use of this factor (MIF) can help engineers and system architects to size and optimize their designs to a higher degree of accuracy.

3-5 Conclusion

Cell temperature The cell temperature can differ significantly from the ambient temperature. The actual cell temperature is a function of both the ambient temperature and the irradiance.

Irradiance and temperature Different PV output parameters are affected to different levels due to irradiance and temperature fluctuations. The extent of this effect depends on the technology as well as the quality of the module.

Yield The PV yield increases with increasing irradiance and decreases with increasing temperature. The temperature effect plays a big role in dictating the annual yield of the PV module.

Module Ideality Factor (MIF) A more accurate PV yield is estimated by the PV model discussed in this chapter, and a measure of this is given by the MIF value for a given PV module.

Chapter 4

Storage and Autonomous System Modeling

In this chapter, we shall first examine the feasibility of a standalone photovoltaic (PV) system with a storage element for powering the Light Electric Vehicle (LEV) charging station. Several aspects in the modeling, optimizing and sizing of an off-grid PV system are considered in significant detail in this chapter.

4-1 System topology

A standalone PV system is not connected to the public utility grid, and usually relies solely on PV power to meet its load requirements. When coming up with a new solution for an energy need, it is always desirable to be as independent of the conventional grid as possible. Therefore, we shall examine an autonomous PV system to power the charging station.

4-1-1 Application

The application of this system will be to power the load, and in this case the load will be Light Electric Vehicles (LEVs), or to be precise, the batteries of the LEVs. Most LEVs that are in the market today come with their own alternating current (AC) chargers(refer to section 4-4 for more details on the load). Thus the system needs to provide AC power to the load. This would dictate the exact system components to be used.

4-1-2 System components

Various components are required to put together a standalone PV system[1]. The most common components used are discussed below. They have also been implemented in the system model discussed in section 4-5.

PV modules

An array of PV modules is required for powering the system. The work covered in chapters 2 and 3 have led us to choose one particular PV module for the system implementation, namely the Sanyo Heterojunction with Intrinsic Thin-layer (HIT) SE10 $240W_p$ solar panel. The module characteristics have already been captured in Table 3-2.

Storage

Storage forms the backbone of the autonomous PV system. Storage is an exhaustive topic, and is covered in much greater detail in section 4-2.

Charge controller

A charge controller is a very useful power electronic device that performs multiple functions. Some of the most common functions performed by a modern day charge controller are:

- to prevent the battery from getting overcharged.
- to prevent the battery from getting over discharged.
- to prevent backward discharge of the battery.
- to provide optimum charge to the battery.
- to provide information on the State of Charge (SOC) of the battery.
- to perform Maximum Power Point Tracking (MPPT) on the PV array output.

With advances in power electronics, more useful functionalities are being added in the charge controller than ever before.

[1]The terms standalone, off-grid and autonomous are synonymous when referring to this class of PV systems, and are used interchangeably throughout this chapter.

Inverter

An inverter is used to convert the direct current (DC) output of the PV array and the battery into usable AC power for an AC load. Inverters come in a variety of sizes, and the exact type and size of the inverter will be discussed in the appendix A-4.

Load

In this case the load will be LEVs that charge at different points of time during the day. These are discussed in greater depth in section 4-4.

Cables, connectors, mounting systems and DC disconnectors

As the size of the system grows, so do the losses arising from the cables. Therefore, these need to be modeled in the system too.
While implementing PV arrays having several modules, it is always a safe practice to use DC disconnectors, or junction boxes. In the system model, the cable losses are considered to be 2% of the PV production at all points of time.

The system modeling in section 4-5 will aim at sizing the above listed system components so as to optimize the system reliability. Figure 4-1 shows how the various system components are interconnected.

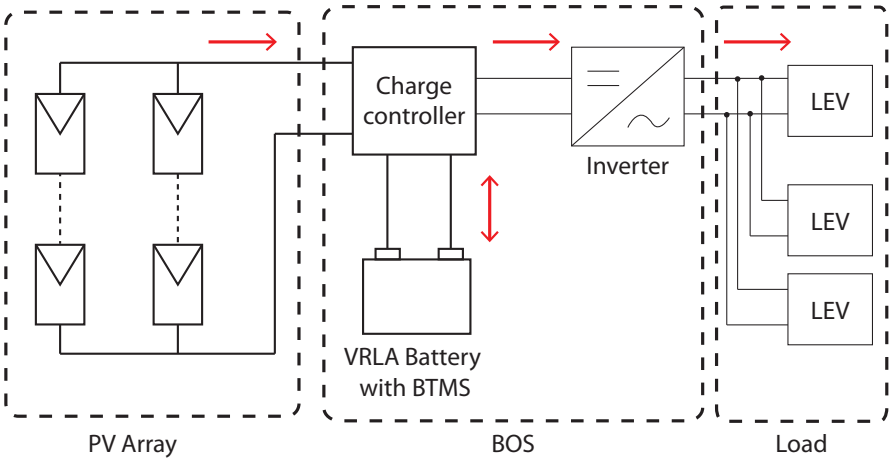

Figure 4-1: System schematic for a typical standalone PV system.

4-2 Battery storage

Due to the intermittent nature of solar energy, a storage system is indispensable in standalone systems. Of the various storage technologies available in the current day and

age, batteries are still the preferred storage option for system architects. Some of the traditional battery technologies like Lead Acid are low cost and mature enough to be a popular choice for short-term storage applications.
For the off-grid PV system modeling in this chapter, the so-called solar batteries are considered. These are usually lead-acid grid plate batteries with fluid electrolyte[20].

4-2-1 Solar battery

A commercial solar battery is chosen for the purpose of modeling. The product specifications of a typical Valve Regulated Lead Acid (VRLA) battery from Hoppecke[2] are tabulated below.

Table 4-1: Battery specs of VRLA from Hoppecke

Capacity (Ah)	Voltage (V)
92	12
170	12

For the optimized storage modeling scenario, a constant battery capacity is assumed with similar technical characteristics as the above battery. For all other cases, a range of battery capacities are considered with similar technical characteristics. This is to determine the optimal capacity of storage that can be achieved for a given PV size and load profile.
Also, the datasheet for the above battery in most cases serves as a good reference for optimal ranges of operation, temperature behavior and life-cycles.

4-2-2 Battery efficiencies

Like every other component of the PV system, the battery also has an inherent efficiency associated with it. As was the case with the PV module, this efficiency is not constant, and changes with time. Therefore, an analysis of the battery efficiency is required so as to appropriately build the system model.

Types of efficiencies

There are two main types of battery efficiencies generally discussed: voltaic efficiency and coulombic efficiency. These two efficiencies encompass all the electrical and chemical non-idealities occurring inside a secondary cell.
In simple terms, these efficiencies are defined as follows:

$$\eta_V = \frac{\text{Average discharging voltage (V)}}{\text{Average charging voltage (V)}} \tag{4-1}$$

[2]Hoppecke is a battery manufacturer.

where η_V = Voltaic efficiency of the battery.

$$\eta_C = \frac{\text{Total charge out of the battery (Ah)}}{\text{Total charge into the battery (Ah)}} \text{ over one full cycle} \tag{4-2}$$

where η_C = Coulombic efficiency of the battery.

$$\eta_{Batt} = \eta_V \times \eta_C \tag{4-3}$$

where η_{Batt} = total battery efficiency.

The voltaic efficiency is an indicator of the electrical non-ideality of the battery that can be modeled as the battery's internal resistance. This internal resistance is itself a function of temperature and SOC [21, 22]. This is talked about in a greater detail in section 4-2-5.

The coulombic efficiency or Faraday efficiency is indicative of the charge that is lost in chemical inefficiencies like side reactions. This efficiency directly impairs the effective capacity of the battery. The following section deals with a way to model the coulombic efficiency of the battery.

These efficiencies, including the internal resistance and other parameters are fundamentally defined for an electrochemical cell. The term battery in this case refers to the entire storage system, which comprises of several such electrochemical cells. When talking about the cell parameters, the term battery will be used interchangeably with cell, as the battery is being modeled as one big homogeneous storage system(refer 4-2-3: Bulk modeling for more details).

Modeling coulombic efficiency

The battery efficiency is itself a function of the SOC [23]. Given below is the approximate coulombic efficiency as a function of SOC, derived from a look-up table for VRLA batteries provided in [20]

The function plotted in Figure 4-2 is approximate, and generally valid for the nominal temperature and a given discharge rate. It can be seen that the coulombic efficiency drops with increasing SOC. This is because of unwanted processes that take up the useful energy being supplied to charge the battery. For instance, as charging proceeds the battery voltage increases, and at some point electrolysis of water occurs leading to gas formation. This leads to a drop in the efficiency as the charge being supplied is poorly utilized by the battery.

As the operating temperature range and discharge rate have been bound by the model, Figure 4-2 is taken as a reference to estimate the efficiency of the battery at every instant. Additionally, as the SOC has been normalized in the model for every step to compensate for temperature effects, it can be said that the graph serves as a good approximation of the coulombic efficiency of the battery.

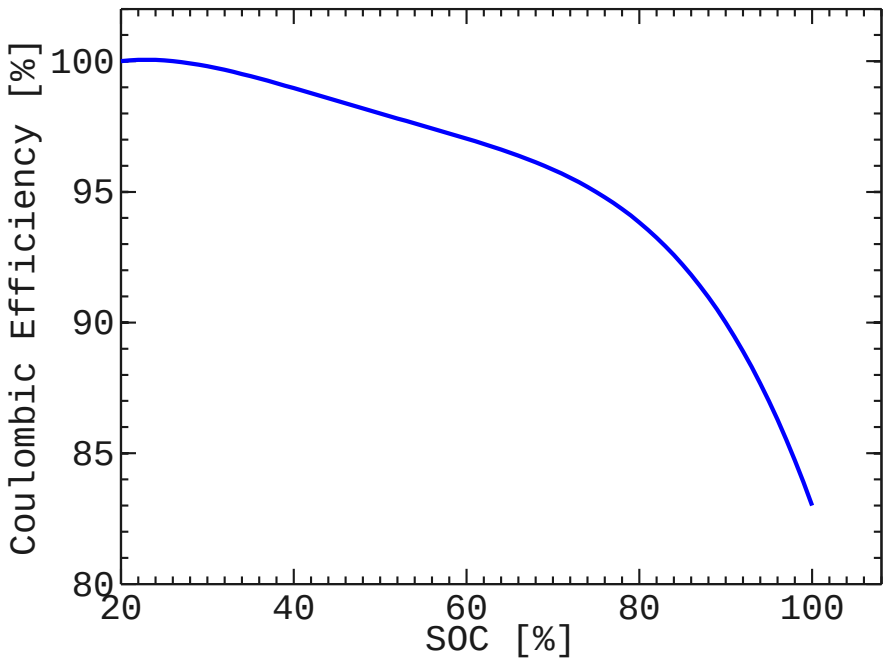

Figure 4-2: Coulombic efficiency as a function of SOC

4-2-3 Scope of the storage model

Battery modeling itself is an extremely vast topic with several branches of research within. Hence it is important to define a scope for the storage[3] model.

Model resolution While all the data being used in the simulation have been either actual observed values (e.g. from Koninklijk Nederlands Meteorologisch Instituut (KNMI)) or commercial datasheets and white-papers(e.g. [24]), the resolution of the model is limited to steps of 1 minute interval. This is because all the weather data that has been obtained from KNMI are with a resolution of 1 minute.

Initial conditions Most of the storage behavior, including heat generation depends a lot on the initial conditions like SOC, temperature, and C-rates for charge and discharge. It is assumed in the system modeling that the storage is put together in the system, fresh off the shelf with 100% SOC at 00:00 hours on 01.01.2011. The simulation of the model spans an entire calendar year with the resolution of 1 minute.

Transients To limit the scope of the storage model(it being just one of the several design blocks of interest in this thesis project), transient analysis on the battery parameters like

[3]Specifically in the context of modeling, the terms storage and battery will be used interchangeably henceforth in this thesis report.

voltage and current have not been taken into account. It is assumed that the parameters 'stabilize' by the beginning of each sample time(1 minute). On the other hand, the temperature latency is being taken into account(refer 4-2-4). Though there is some loss of precision in using steady state values, it can be said that given the low step size of simulation, the results derived are within reasonable engineering accuracies.

Bulk modeling The storage is taken as one big, homogeneous mass while dealing with its thermal aspects. Although the actual implementation might consist of several cells in various topologies, the control volume for the thermodynamic analysis is taken as the entire bulk of the storage. This also means that the temperature distribution within the structure of individual cells has been ignored. It is assumed that the entire mass of the storage is at the same temperature at the same time.

From literature it is seen that temperature distribution within individual modules/cells depends on their structural design, and that thermal imaging systems can provide more insights into the temperature distribution within the cells. [25] For the storage model presented in this thesis, however, we will adhere to bulk modeling only.

4-2-4 Temperature effects on the Battery

Like the PV module, temperature has a major impact on the battery performance too. In this section, an attempt is made to study the various effects of temperature on the battery behavior and the steps that can be taken at the system level to ensure an optimal performance from the battery in the light of these effects.

Effect on capacity

Battery performance is largely dictated by temperature, and the following plot (Figure 4-3) shows the variation of overall battery capacity with temperature. It is observed that a increase in temperature increases the capacity of the battery. However, this is also accompanied by loss of water and reduced number of cycles in the battery life.

Figure 4-4 shows the variation of the battery capacity throughout the year of 2011. The KNMI temperature data has been used in the model.

Effect on lifetime

While the increase in temperature has a positive effect on the battery capacity, it has a negative impact on the lifetime. Figure 4-5 captures the impact of temperature on lifetime. Thus temperature swings on either extremes are bad for the battery operation. Hence we need to limit the operating temperature range of the battery. The storage model handles the implementation of such a scenario, described in greater detail below.

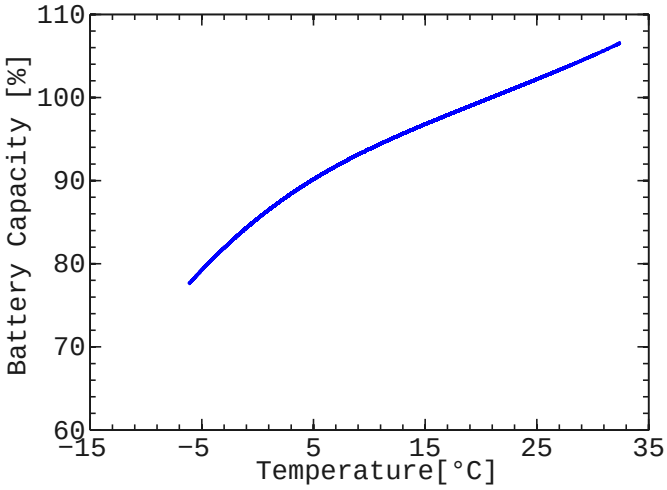

Figure 4-3: Battery capacity variations with temperature

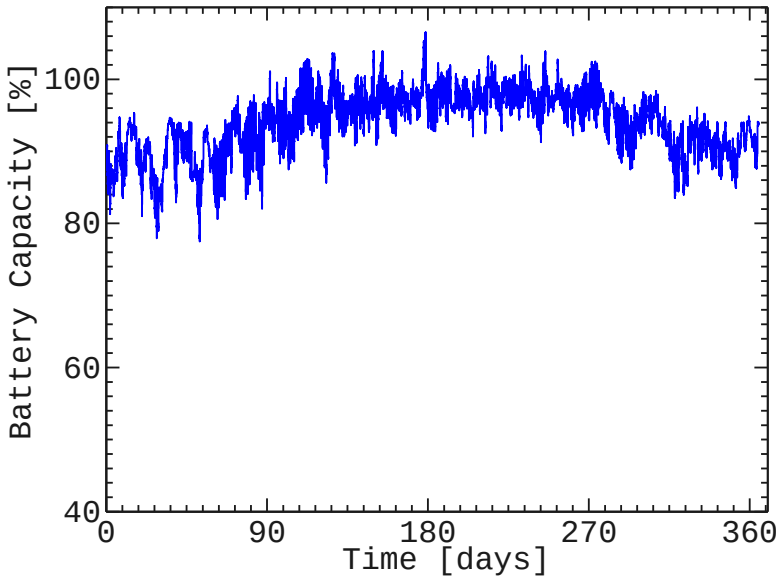

Figure 4-4: Battery capacity over 2011

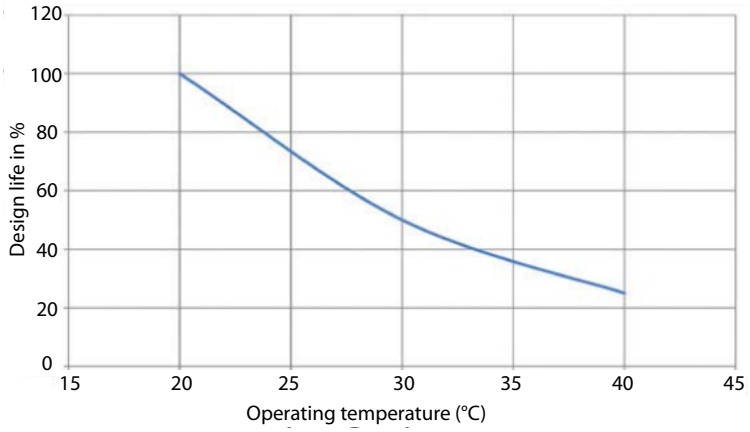

Figure 4-5: Temperature impacts on the design lifetime of VRLA battery. [24]

Temperature latency modeling

Though the ambient temperature fluctuates greatly (Figure 3-2), the battery material cannot keep up with the temperature changes of the surroundings. Due to the thermal inertia of the battery storage, there is always a delay in the battery temperature trying to reach towards the ambient temperature. While the battery temperature tries to reach the ambient temperature, the ambient temperature might well have moved to a different value.
This temperature latency is included in the storage model. A first order maximum rate is defined that limits the rate of change of temperature. In this case, it is $L_T\,^{\circ}\mathrm{C}/min$, which will be a function of irradiance. Given below is an example and a plot that explains the significance of L_T.

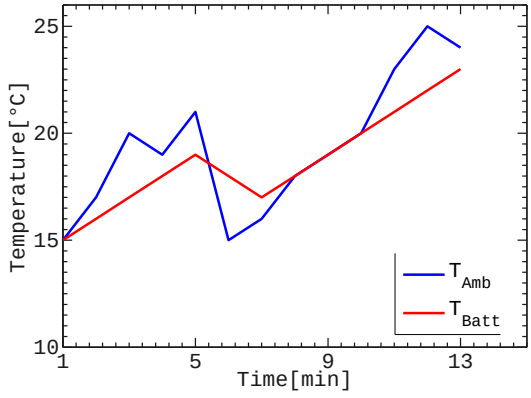

Example of temperature latency of storage system

- Storage system responds sluggishly to ambient temperature changes at a rate $> L_T\,^{\circ}\mathrm{C}/min$
- With ambient fluctuations within the temperature latency limits, the storage system responds well and follows suit.

Temperature limits - optimal range of operation

As per the battery manufacturer, the recommended range of operation for the VRLA battery system is between 10°C and 30°C, while the optimal operating temperature is

20°C [24].
While it would be too exacting on the Battery Thermal Management System (BTMS) to constantly maintain the operational temperature at 20°C, it is easier to maintain the recommended operating range specified by the manufacturer. The storage model tries to limit the operational range of the battery, irrespective of the ambient temperature.

It is important for the battery to operate in the recommended temperature range because both the battery capacity and the lifetime are a function of operating temperature, as seen previously in Figure 4-3 and Figure 4-5.

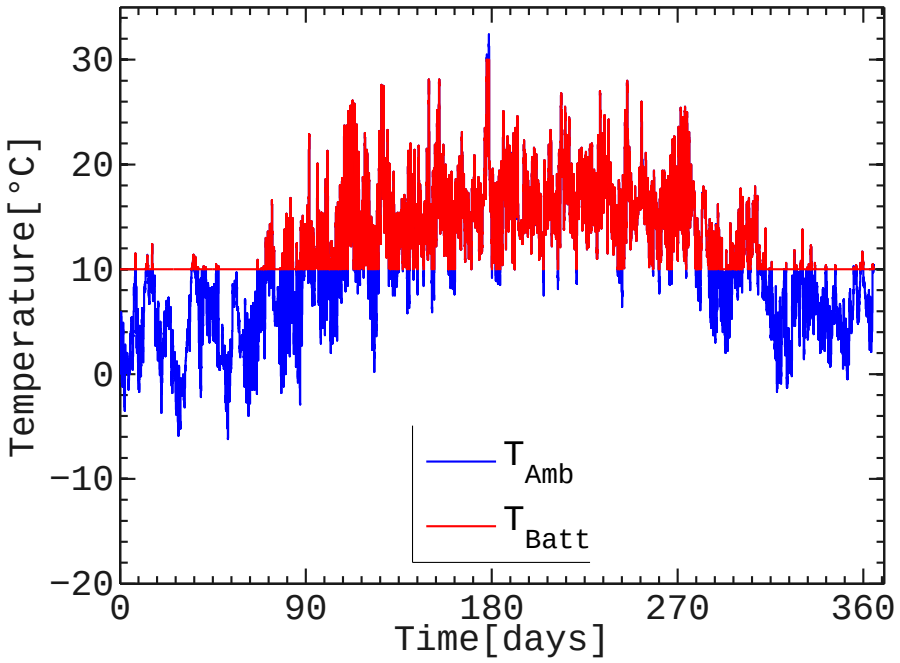

Figure 4-6: Battery operating temperature restricted to recommended range

Figure 4-6 shows clearly how the operating temperature range of the storage system has been restricted in the model between 10°C and 30°C. The model also takes into account the temperature latency of the battery storage system as discussed in the previous section. It seems for the Dutch weather, the lower bound of the operating temperature is mostly encountered.

4-2-5 Battery Thermal Management System (BTMS)

While it is good to have temperature regulation to optimize the performance and longevity of the storage device, it comes at a price. The price is the extra energy required by the storage so that the temperature is maintained within recommended limits.
In case of autonomous system, this extra energy is of-course ultimately powered by the

PV modules. Thus this should also be factored in the calculation. There are two aspects of BTMS: active and passive thermal regulation.

Active thermal regulation This is the process through which an external heating or cooling is achieved by expending energy. It is assumed that this energy is supplied from a heating element powered electrically. This would effect the effective yield of the system.

Passive thermal regulation This is the process through which the heat loss from the system is minimized without spending active energy. An example of this could be a very effective thermal insulation layer.

Energy Balance

A rudimentary steady-state energy balance of the storage system gives us an estimate of the heat energy required in implementing the BTMS.

$$H_{\mathrm{BTMS}} = M_S * C_P * \Delta T \tag{4-4}$$

where: H_{BTMS} = Heat energy required by the BTMS,
M_S = Mass of the storage system,
C_P = Specific heat of the storage system = 660 J/kg/°C[25],
$\Delta T = T_s - T_{ambient}$ = Temperature difference between the storage system and the surroundings,
T_s = Storage temperature,
$T_{ambient}$ = Ambient temperature.

The mass of the storage system can be estimated based on the gravimetric energy density of VRLA, known to be anywhere between 30 Wh/kg and 44 Wh/kg, depending on the C-rate[22]. The dependence on C-rate follows the popular axiom in the class of battery devices - lower the C-rate, higher the energy density[26]. More details on the C-rate can be found in section 4-2-6 (Power regulation).

For the battery being used in the system model here, an energy density of 40 Wh/kg is assumed. This is justified by the fact that the system model has power limits imposed on the storage device, as explained later in section 4-2-6. The C-rate for the storage system is also discussed more in section 4-2-6.

Most of the BTMS efforts will go into keeping the battery warmer than the ambiance in the winter, while in peak summer, it is assumed that the temperature regulation occurs through the use of a coolant as is the case with most standard battery systems. Battery system housed safely in the shade of the charging station would further save the battery from excessive summer heat. It is also assumed that the battery system will have a thermal insulation to passively tackle the thermal regulation.

Opportunity in adversity

The BTMS finds a silver lining in the electrical non-ideality of the battery. The voltaic inefficiency is used to the advantage of BTMS.

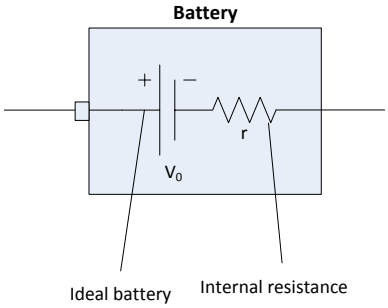

From electrical loss to thermal gain:

- Voltage drop across the internal resistor.
- Heat loss in the internal resistor given by i^2r.
- This power 'loss', albeit less, essentially aids the thermal regulation efforts of the BTMS.

Thus, the energy balance of Eq. (4-4) now develops as:

$$H_{\text{BTMS}} + i^2 r = M_S * C_P * \Delta T \tag{4-5}$$

Another favorable phenomenon is that the internal resistance of the battery increases with decreasing temperature and SOC[21], thus helping the BTMS even more. The BTMS is also implemented in the overall system model described in section 4-5. This is also how the voltaic efficiency is factored into the system model.

Active-passive thermal regulation

The system described in this chapter employs an active-passive combination for thermal regulation. The battery is said to have a high-insulation material around it that minimizes heat loss. When the battery is operational during the day, i.e. when charging or discharging, the heat generated by the internal resistor of the battery is assumed to keep the battery at the right temperature by using an insulating layer. When the battery is not operational, this heat is assumed to gradually go down, when the active regulation kicks in and supplies heat to the battery in gradual steps. This makes the entire BTMS system as implemented in the system model.

4-2-6 Regulation of battery's electrical parameters

To ensure the optimal operation and longevity of the battery, various regulations have to be ensured.

Charge regulation

Both overcharge and over-discharge are detrimental to the battery system. Cycle lifetime is defined as the number of charging and discharging cycles until the actual remaining battery capacity drops below 80% of the nominal capacity [24]. As shown in Figure 4-7, the cycle life decreases non-linearly with increase in Depth of Discharge (DOD). In the physical implementation of the system, the charge-controller handles both the requirements of preventing over-charge and over-discharge of the battery.

In the system model, when the battery is fully charged and there is no load demand, the excess production is simply 'dumped'(refer section 4-5-2). Also the maximum DOD is limited to 80% in the model.

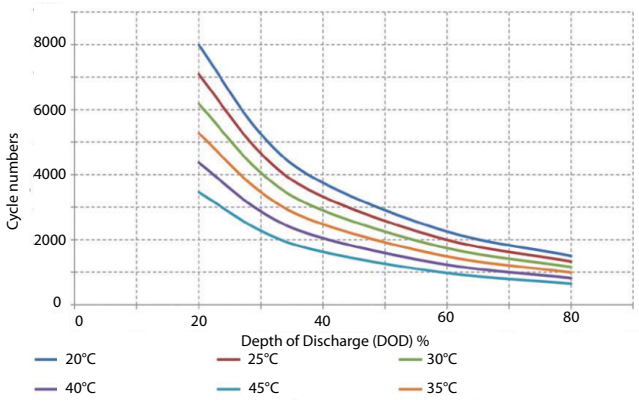

Figure 4-7: Cycle life Vs DOD at different temperatures (*source: [24]*).

Voltage regulation

There are two main voltage limits that the charging process should adhere to: the charge cut-off voltage and the discharge cut-off voltage. The charge controller is tasked with ensuring the voltage limits are abode by the manufacturer's requirements.

Current regulation

Although ideally the battery is able to provide limitless current for longer periods, in reality high currents limit the energy capacity of the battery. Again, the charge controller is the saviour and has a current cut-off limit. This is discussed in greater detail in chapter 5.

Power regulation

A byproduct of the voltage and current regulation is the power regulation. In the system model, the power delivered to and from the load is also limited to correspond to a C-rate

of $C_{1/5}$. C-rate is a measure of the rate of discharge of a battery relative to its capacity. A C-rate of 1C corresponds to a discharge time of 1 hour. A C-rate of 3C will discharge the battery in 20 minutes, while a C-rate of $C_{1/2}$ will discharge the battery in 2 hours.

4-3 PV modules and Balance of System (BOS)

In this section, the PV modules and the BOS[4] constituents of the system are discussed.

4-3-1 PV module

From the PV modeling in the chapter 3, we know of the performance of various panels under irradiance and temperature. For the purpose of system modeling, the $240W_p$ Sanyo HIT PV modules are used. The important specifications at Standard Testing Conditions (STC) or Nominal Operating Cell Temperature (NOCT) of the PV module have been re-tabulated below.

Table 4-2: Characteristics of Sanyo HIT 240 W_p PV module

Name	Sanyo HIT N240 SE10
Brand	Sanyo
Type	HIT
Pmax STC(W)	240
NOCT ($^\circ C$)	44
Width (m)	1.58
Height (m)	0.798
Area (m^2)	1.26084
Efficiency nom STC (%)	19
Voc STC (V)	52.4
Isc STC (A)	5.85
Temp coeff Pmmp (%/$^\circ C$)	-0.3
Temp coeff Voc (%/$^\circ C$)	-0.25
Temp coeff Isc (%/$^\circ C$)	0.0301

In the model itself, the performance of the PV module takes into account the various effects of temperature and irradiance. The PV model from the previous chapter has been used to feed the system model.

[4]Balance of system comprises of all the other PV system components apart from PV modules.

4-3-2 Power electronic components

These have been briefly discussed already in section 4-1-2. While the power flow in the system model is discussed in this chapter, the detailed behavior of the various power electronic devices are discussed in the appendix A-4.

4-3-3 Scope of the PV model

The PV model implemented as part of the larger system model covers several aspects that reflect the module level behavior discussed in chapter 3. However, the array level effects like mismatch losses are not considered. It is assumed that all the PV modules that make up the arrays are similar in all technical aspects. Array level issues are discussed in greater detail in the appendix A-4 that delves more into the electrical implementation.

4-4 Load Profile

For modeling the energy balance, we need a load profile that approximately simulates the load behavior, i.e. the charging of a certain number of LEVs. For the case of our simulation, we will look at two simple load profiles A and B.

4-4-1 Charging e-bikes

For the purpose of modeling the load, the e-bikes are assumed to be Gazelle Orange plus Innergy model, which was a top-selling e-bike in Holland in 2012. The e-bike comes with 3 types of battery packs: Bronze, Silver and Gold[10]. The characteristics of these battery packs have been summarized in table 4-3

Table 4-3: Different battery configurations for Gazelle e-bike Innergy series

	Bronze	**Silver**	**Gold**
Capacity (Wh)	252	324	396
Current (A)	7	9	11
Voltage (V)	36	36	36
Nominal Range (km)	40 - 60	50 - 80	90 - 120
Normal charging time (h)	5	7	9
Fast charging time(h)	< 2	2	3

4-4-2 Load profile A

In Load profile A, it is assumed that a maximum of 5 e-bikes can be catered to at the charging station, and that over an entire day, there are a total of 10 e-bikes charging, at

two different times. The load profile has been plotted in Figure 4-8 below.

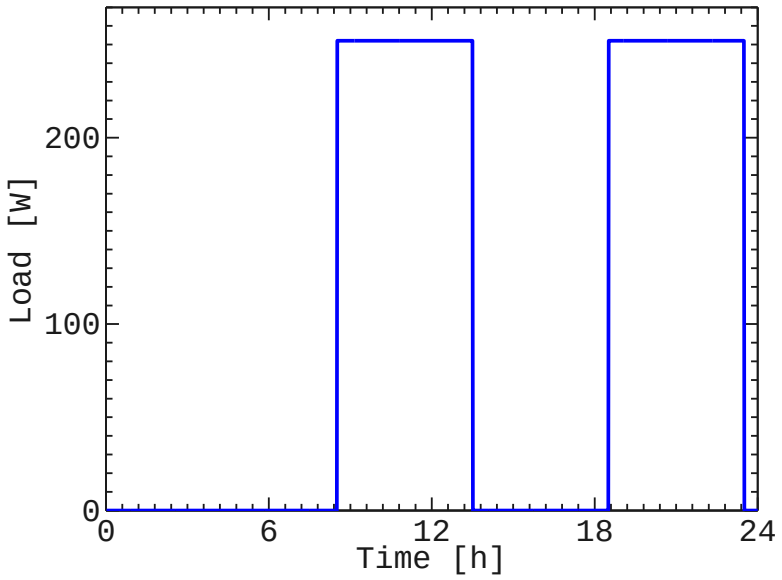

Figure 4-8: Load profile A in Watts over 24 hours

This is an over-simplified load profile. In reality, it is unlikely that the e-bikes are always being charged from 0 to 100 %. But the system modeling with this load Profile indeed gives some keen insights, as described later in this chapter.

4-4-3 Load Profile B

This load profile takes the daily bike usage statistics into account. The charging times for the e-bikes are chosen so as to correlate with the bike usage statistics of the Dutch biking population. As seen in Figure 4-9 the three most important purposes for using bikes are commuting for education, work and shopping. Thus, it is reasonable to choose the location for the charging station in a public place, like a university or an industrial complex as opposed to private residential space, like a house.

Figure 4-10 shows the popular biking times over the day in the Netherlands. Load profile B assumes that the charging station is located in one such public space where there is a higher demand for charging in the early part of the day. It tries to emulate the trends shown in Figure 4-10.

In this load profile, there are a total of **30 e-bikes** that are being charged at different points of time in the day. Compared to load profile A, profile B has the e-bikes not charging 0 to 100%, but charging by an amount of one-third their standard battery size. It is estimated that this would take around **100 minutes** of charging time. The charge times shown in profile B are approximately correlated to the expected bike traffic at the public places at different times. The load profile has been plotted in Figure 4-11.

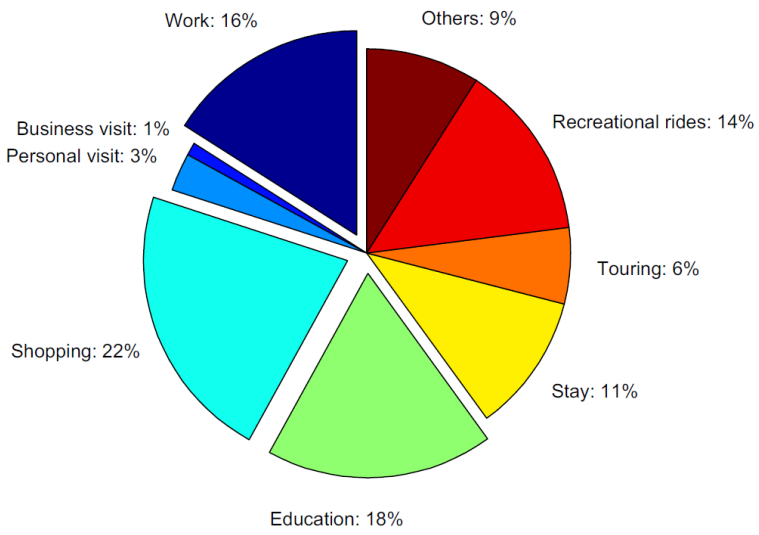

Figure 4-9: Purpose of using bike as a means of transport. *Data for the graph from [11]*

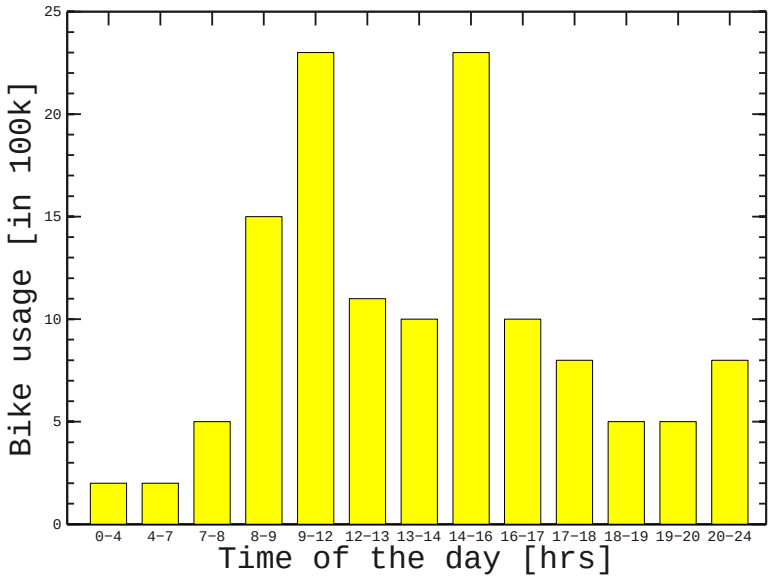

Figure 4-10: Transport use over the day in the Netherlands. *Data source [11]*

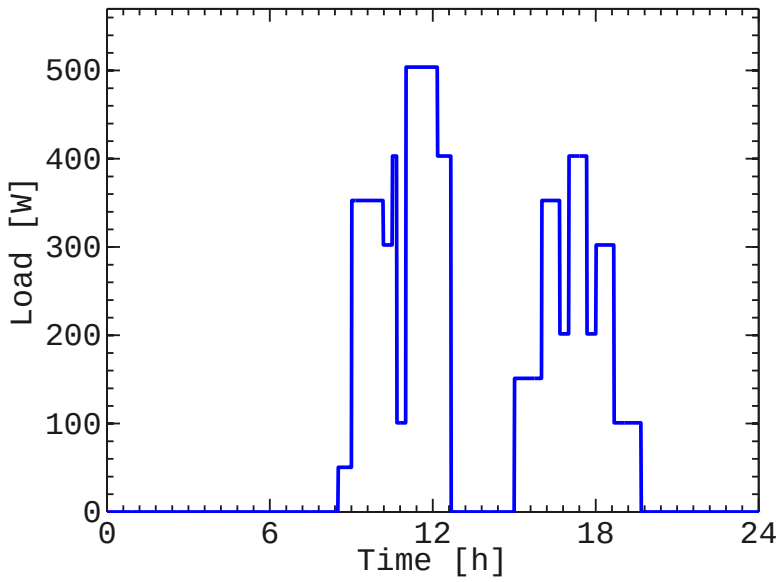

Figure 4-11: Daily load profile B. A higher demand can be seen earlier in the day.

4-4-4 Scope of the load profiles

The load profile is basically a prediction of the kind of load the system expects to face on a daily basis. Thus the scope of such a model for the load needs to be discussed.

Accurate load profiles The load profiles (especially profile B) are based on statistics that are nationwide averages that may not reflect the true nature of the load at such a charging station. A more realistic load profile may be obtained from statistics of a more focused region, like a municipality. Also, true load profiles will differ on the demand in the weekdays and weekends, depending on the exact location of the charging station. These are beyond the scope of the current work discussed in this thesis.

Predicting the future It is difficult to estimate how the load at a particular charging station would change over the months and years, because the LEV segment is an extremely popular segment, as discussed in Chapter 1. But in the author's opinion, catering to the loads at any scale using renewable energy is a positive step from being 100% reliant on a fossil fuels based grid.

4-5 System Modeling

4-5-1 Energy Balance

The entire system modeling is based on the premise of energy balance. Equation (4-6) to (4-9) capture the essence of energy balance happening in the system. In general, the system model samples the load at intervals of 1 minute, and follows an algorithm to control the power flow in the system. This explained in greater detail in section (4-5-3). Equation (4-6) considers the case of a surplus of PV power production when the excess power is used to charge the battery storage, while equation (4-7) represents the scenario of deficit in PV power where the battery covers the load.

$$\begin{gathered} E_{Load} = E_{PV} - E_{Battery} - E_{Losses} \\ (\text{if } E_{PV} \text{ - } E_{Losses} > E_{Load}, \text{ Battery SOC} \leq 100\%) \end{gathered} \tag{4-6}$$

$$E_{Load} = E_{PV} + E_{Battery} - E_{Losses} \quad (\text{if } E_{PV} - E_{Losses} < E_{Load}) \tag{4-7}$$

$$E_{Load} = E_{PV} - E_{Losses} \quad (\text{if } E_{PV} - E_{Losses} = E_{Load}) \tag{4-8}$$

$$\begin{gathered} E_{Load} = E_{PV} - E_{Battery} - E_{Losses} - E_{Dump} \\ (\text{if } E_{PV} - E_{Losses} > E_{Load} \text{ and Battery SOC} = 100\%) \end{gathered} \tag{4-9}$$

where
E_{Load} = Energy supplied to the load,
E_{PV} = Energy generated by the PV array,
$\pm\ E_{Battery}$ = The energy flowing from or to the battery,
E_{Losses} = All the losses happening in the system bundled together, like cable losses and component inefficiencies,
E_{Dump} = The energy being dumped when there is a surplus production and the battery is full.

4-5-2 Energy Dump

As the total energy in sunny days might exceed the demand and the storage capacity, this excess of energy has to be dumped somewhere. In the model, 'energy dump' quantifies the energy dumped every minute over the year 2011. This happens whenever the demand is lesser than supply, and the battery is already full. The energy dump is a measure of the oversizing of the system in summer. It is desirable to have a very low amount of energy dumped throughout the year.

4-5-3 Control strategy

The control strategy for the has been outlined in Figure 4-12. The system shown in the flow chart does not implement an on-site BTMS. The control algorithm for the case with an on-site BTMS will be similar, the only difference being that there's a basal load in the form of active thermal regulation of the storage when the ambient temperature is much lower than the battery temperature. A combination of active and passive thermal regulation is used to keep the battery temperature within optimal limits.

There are two main cases that the control algorithm considers.

surplus energy ≥ 0 In this case the system is able to fulfill the load requirements completely. The excess energy after meeting load requirements is sent to the battery. If the battery gets full, the excess energy is dumped.

surplus energy < 0 In this case the system first checks if the battery can supply energy within allowed limits. If yes, then the battery supplies the energy to the load till the load needs are met fully, or the battery runs out of allowed deliverable energy, whichever is sooner. In the worst case scenario, the load is left unfed.

4-5-4 Reliability Analysis

One of the major yardsticks while designing a system is reliability. Translated to the present case of the charging station design, it simply means how reliable the system is in meeting the load requirements over the year. The author defines 4 new metrics that serve as points of comparison across various system sizing options. The four new metric correspond to four levels of reliability as follows:

- Reliability25: Number of days at least 25% of load demanded is delivered.
- Reliability50: Number of days at least 50% of load demanded is delivered.
- Reliability75: Number of days at least 75% of load demanded is delivered.
- Reliability100: Number of days 100% of load demanded is delivered.

This means that as the number of days that meet at least 25% load requirement increase through the year, the system performs better across the Reliability25 metric. The same is true of the other metrics. This concept is illustrated in Figure 4-13. There are 4 load levels drawn that correspond to 25%, 50%, 75% and 100% of the total load requisites. The reliability metrics are also drawn which are cumulative and increase throughout the year as the system meets the load requirements at various levels.

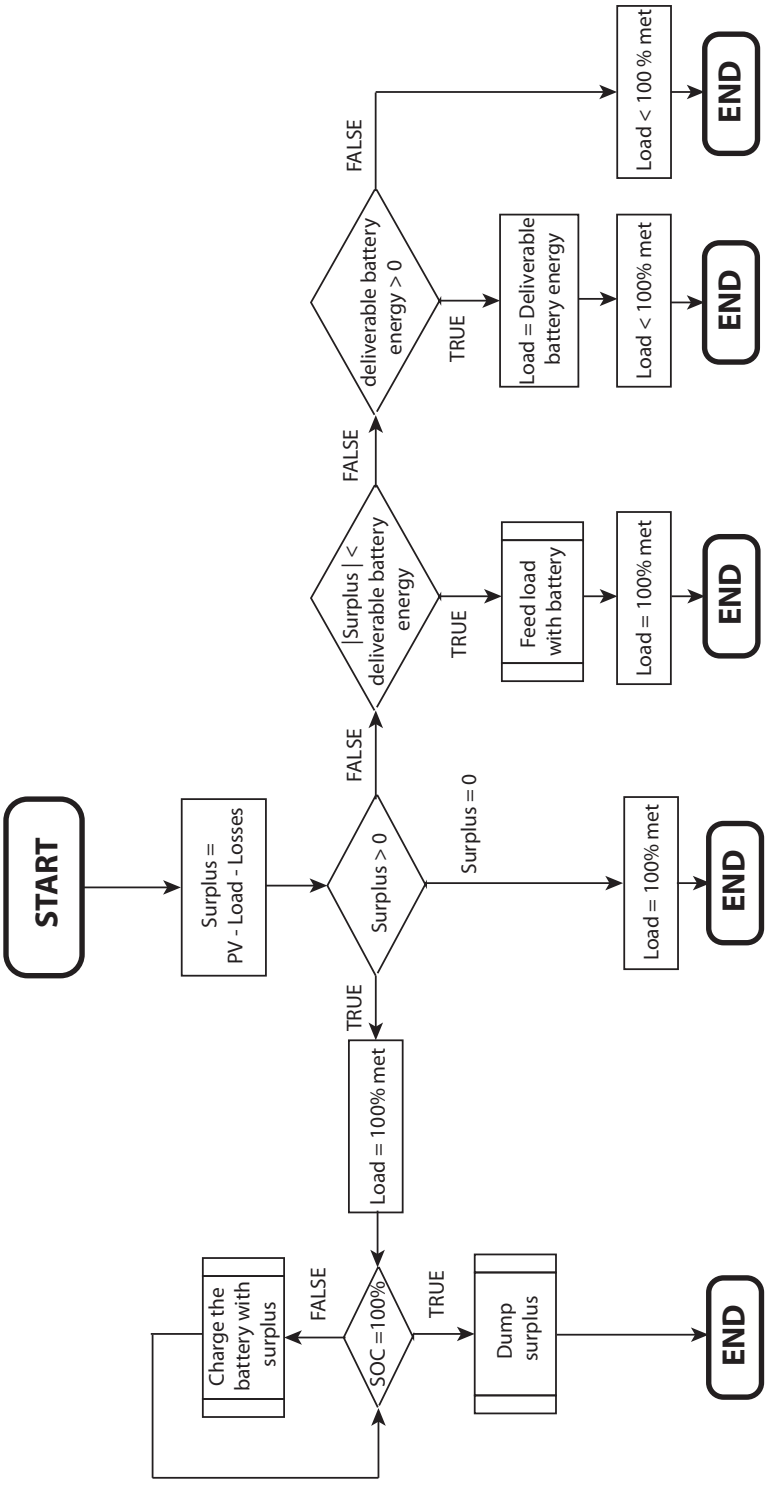

Figure 4-12: Control strategy for the system model. (No active BTMS.)

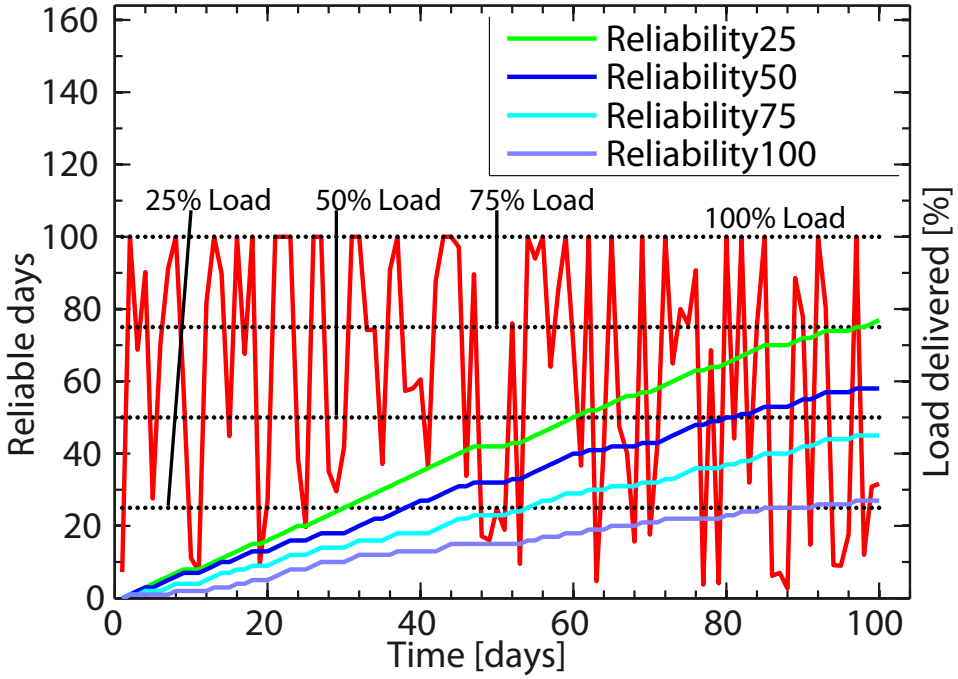

Figure 4-13: An illustration of the system performance under the reliability metrics

.

These metrics have been regularly used in the following sections in validating the usefulness of various system sizing options. The results of optimizations performed with the standalone system model are discussed in the following sections. The optimizations done on a system without active BTMS are discussed first. That is, the thermal regulation is mainly passive with thermal insulation material around the battery body. Active BTMS is considered for the optimized model purely to look at the effects of the energy appendage required due to its addition.

Storage Variation with a constant PV sizing

For a constant PV sizing (12 modules of Sanyo HIT, listed in Table 4-2 as Module 11) and the load profiles A (Figure 4-8) and B(Figure 4-11), the system reliability is evaluated against the reliability metrics.

From Figure 4-14 it seems that the reliability metric saturates beyond a particular storage value in each case, with Reliability25 saturating earliest, and Reliability100 the last. To be more accurate, the curve only saturates temporarily, as for a given PV sizing, moderate storage sizes would eventually drain out in winter, especially with consecutive days of minimal illumination.
On the other hand, it is obvious that extremely large storage sizes will eventually be

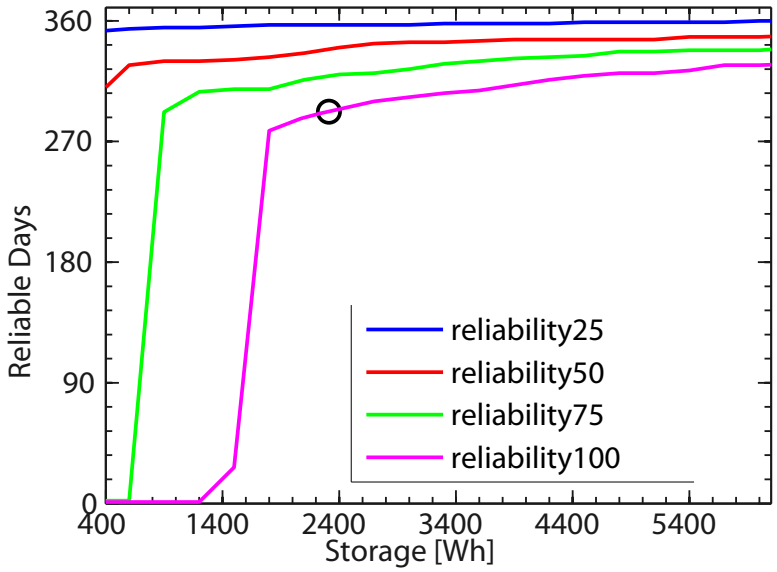

Figure 4-14: Reliability with storage variation under load A

able to cover all the deficits. But such a sizing would not only be too expensive, but also very wasteful. Therefore, an optimal storage size of 2400 Wh is considered for the model. This storage size is in the saturation range of Reliability100 for both load profiles.

Optimization for maximum reliability

Now, the reliability can of course be increased, but there is a very high price to pay. If the fundamental requirement of 100% grid autonomy is enforced, then a 100% reliability would mean that the system is being sized for the extremes. However, this would mean that the system is overly wasteful in summer. Also the costs of the system will spiral upward.

Therefore, the effect of varying storage and PV sizes on the different reliability metrics is examined. It can be seen in Figure 4-16 and Figure 4-17 how reaching maximum reliability is too demanding, and inadvisable due to the extreme and wasteful sizes the system will assume.

Optimizing for maximum reliability - Load A

Again, the same behavior is seen as in the figures 4-14 and 4-15. The storage size tends to saturate beyond a point for a fixed PV size.

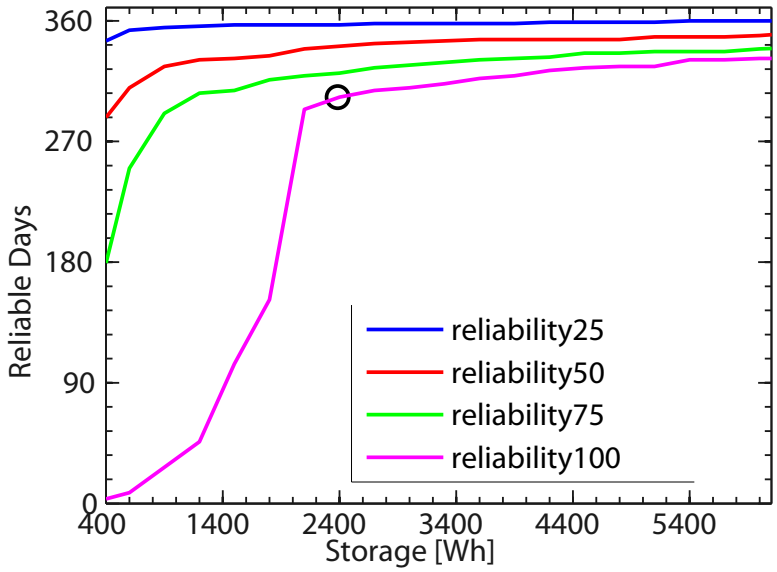

Figure 4-15: Reliability with storage variation under load B

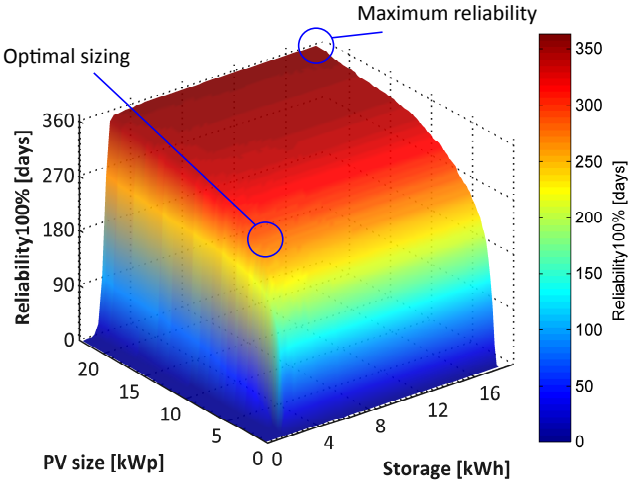

Figure 4-16: Reliability100 with storage and PV variation under load A

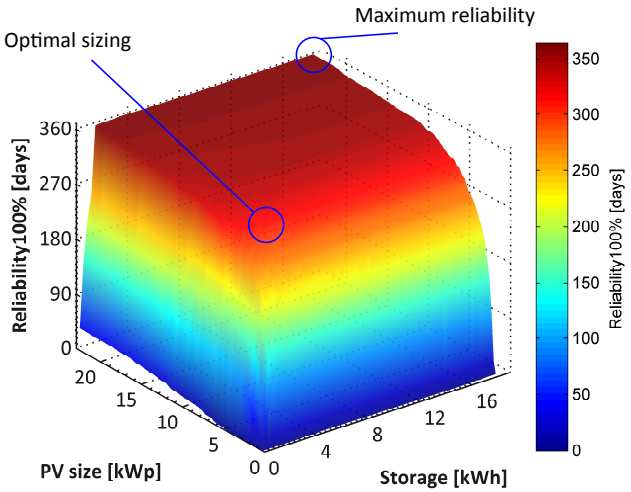

Figure 4-17: Reliability100 with storage and PV variation under load B

Optimizing for maximum reliability - Load B

In light of these results for the various system sizes, an optimized size is chosen below having a PV size of 12 modules (i.e. $12 * 240\ W_p = 2.88\ kW_p$) and 2.4 KWh of battery storage. A much more detailed analysis of the optimized system is then performed.

4-5-5 Optimized model - no BTMS

After the optimization of the storage sizing, we will now see the performance of the model under the different load conditions. No active BTMS is considered in these results.

Delivered load

Figure 4-18 and Figure 4-19 show the percentage of daily load being successfully delivered throughout the year. The load demand is being completely met in summer due to the high irradiance levels. In the winter months, the PV system clearly does not generate enough power to meet the load demands.

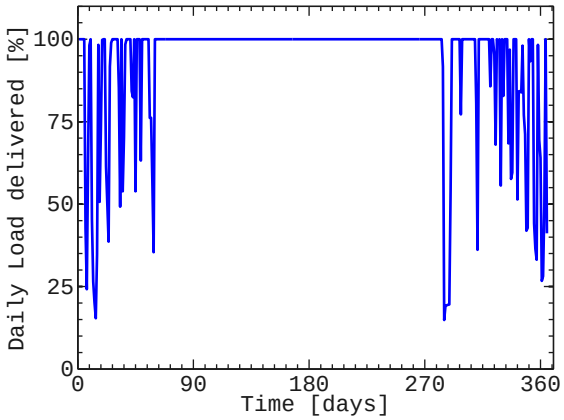

Figure 4-18: Normalized load energy delivered by the charging station under load A

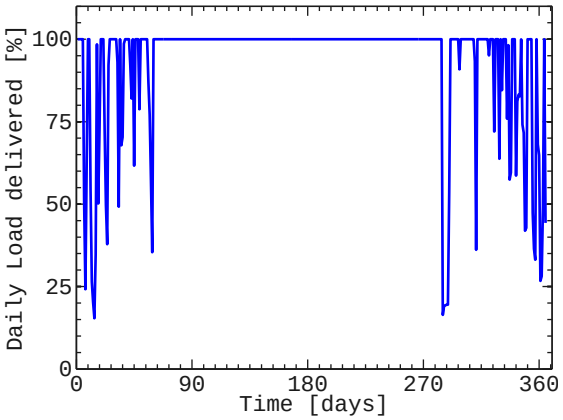

Figure 4-19: Normalized load energy delivered by the charging station under load B

SOC variations

The daily levels of the SOC [5]of the battery system are now looked at over the entire year.

As can be seen from Figure 4-20 and Figure 4-21, the SOC tends to reach its limits in the winter months (the limits have been set to 20%, as discussed in section 4-2-6). The summer months are better, where the battery does not seem to be discharged beyond a certain point at most times. Again, this is because of the surplus energy that the system enjoys in the summer months as opposed to the winter months.

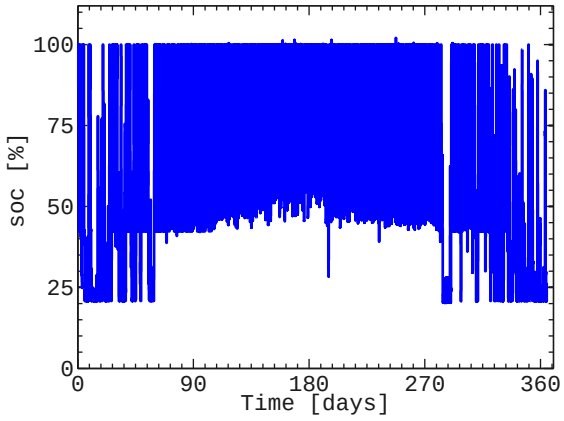

Figure 4-20: SOC variation over the year 2011 under load A

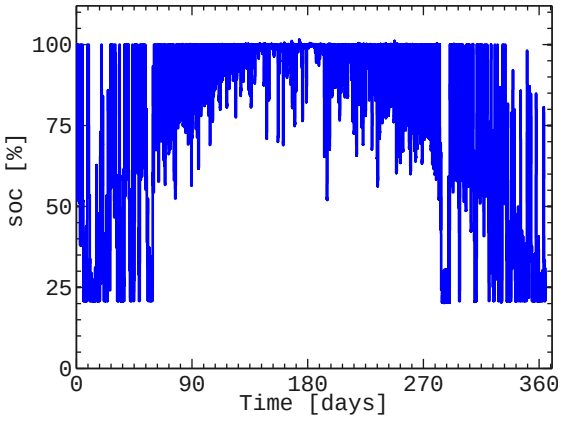

Figure 4-21: SOC variation over the year 2011 under load B

[5]There are various types of SOC definitions - rated, measured and practical. Check appendix A-3 for details. The SOC mentioned here is the measured SOC.

Energy Dump

Figure 4-22 and Figure 4-23 show the energy being dumped throughout the year for load profiles A and B respectively. The energy being dumped is quite large in the summer due to the surplus PV energy delivered by the PV modules.
Being an autonomous system, the only way to make use of this energy is to employ a seasonal storage. Otherwise, this energy is just wasted. But seasonal storage comes with its own set of costs. A possible option is to feed the excess energy into the utility grid. Chapter 5 explores the option of grid connectivity in greater depth.

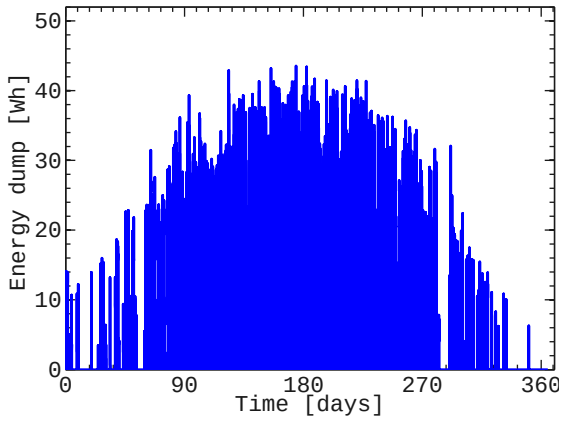

Figure 4-22: Surplus energy dumped away by the charging station under load A

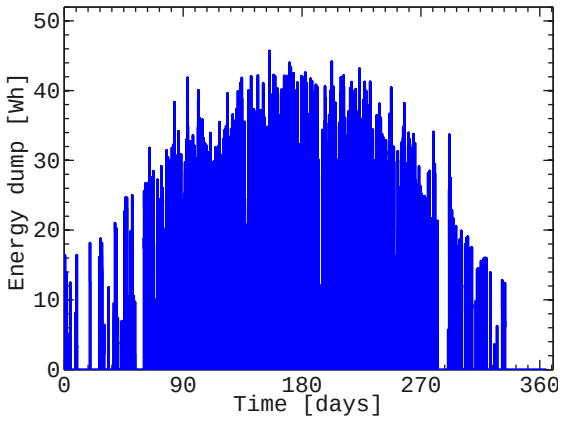

Figure 4-23: Surplus energy dumped away by the charging station under load B

Another look at the amount of energy being dumped can be seen from Figure 4-24 and Figure 4-25, which compare the monthly yield to the monthly dump levels. Although the system fares well in the summer to meet the load requirements, the system also clearly wastes a lot of energy in the form of the dump when it produces surplus power. As shown in Figure 4-12, the system only dumps energy when the battery is full as well as the load is met. As both of these requirements are not met in the winter months(Figure 4-18 and Figure 4-20), the dumped energy also goes down.

Some applications of this excess energy can be thought of, like creating an infotainment spot with Wi-Fi access, public transport help, small advertisement billboards with back-light, etc. Perhaps a small storage could be dedicated for such ancillary services.

Monthly Reliability

Finally, let us look at the monthly performance of the system under different load profiles. A simple monthly reliability has been defined in the following manner:

$$\text{Monthly Reliability} = \frac{\text{Total energy delivered to the load in the month}}{\text{Total energy expected by the load in the month}} * 100 \quad (4\text{-}10)$$

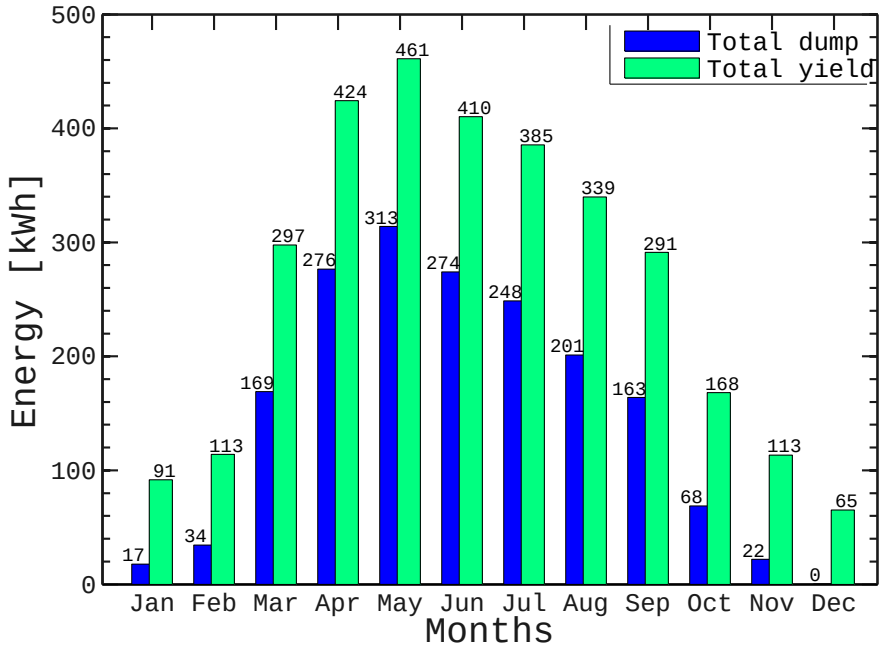

Figure 4-24: Monthly dump measured against monthly yield for load A

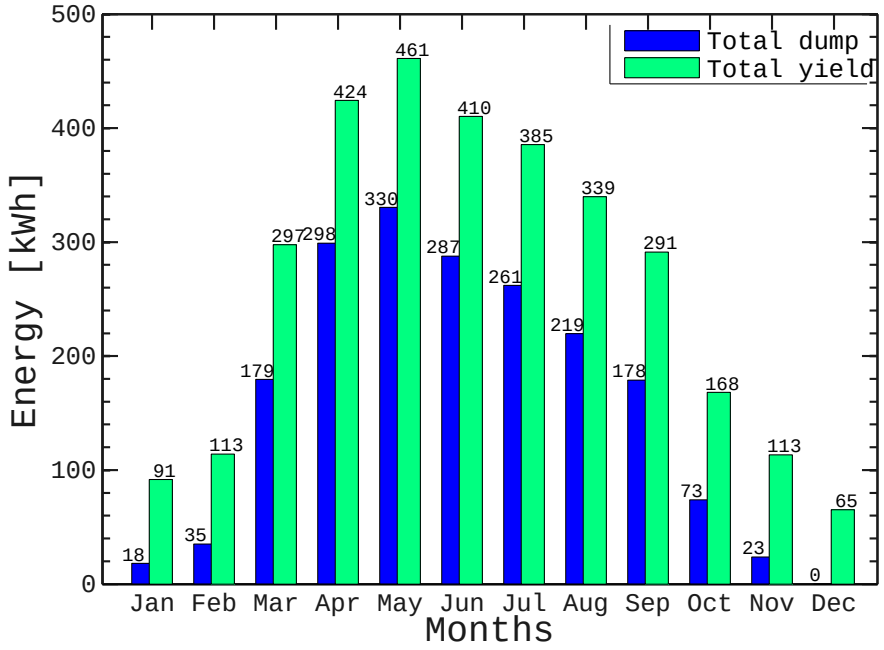

Figure 4-25: Monthly dump measured against monthly yield for load B

It can be seen in Figure 4-26 and Figure 4-27 that the system does extremely well from March to September. The winter months witness much lesser reliability, as expected due to poor irradiance levels and the lack of seasonal storage. A larger size of the system can ensure an even higher system reliability in winter. However, it must be noted that the high system reliability comes at a cost. This is because the dumped energy also increases in the summer if the system is sized so as to maximise winter reliability. The current system configuration is already losing a lot of energy in the summer in the form of dump, as shown in Figure 4-24 and Figure 4-25.

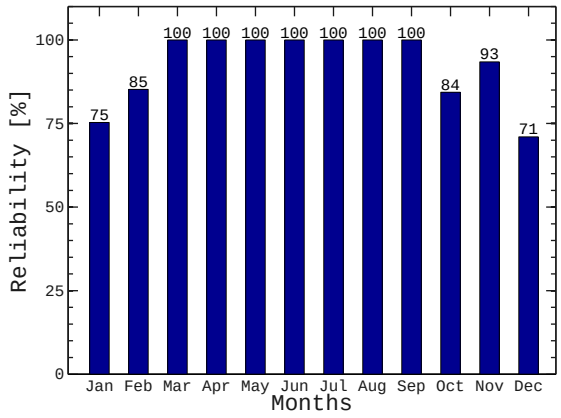

Figure 4-26: Monthly system reliability - load A

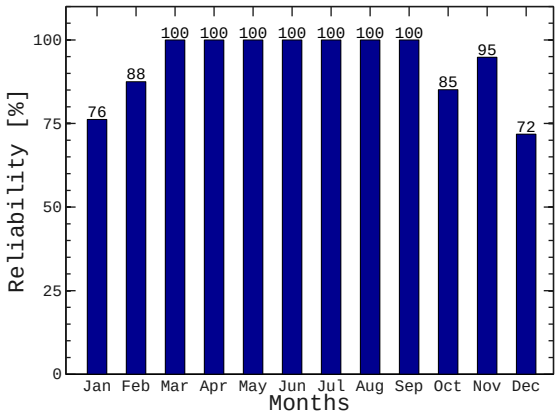

Figure 4-27: Monthly system reliability - load B

4-5-6 System performance under active BTMS

This is the situation when the autonomous system implements an active self thermal regulation system for the battery (BTMS). The results from this scenario show less system reliability, as expected. A lot of energy is spent in simply keeping the battery system warm in the colder months.
The key results like monthly reliability and the monthly yield-dump profiles are shown in the following plots. The only solace is that the amount of energy being dumped is lesser compared to the system without BTMS because some of that energy is used to regulate the battery temperature. But the BTMS does not stop there, it eats up into the load energy as well, and affects the reliability plots as shown in Figure 4-28 and Figure 4-29.

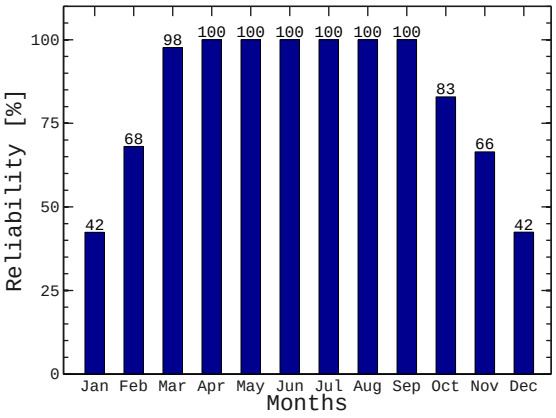

Figure 4-28: Monthly reliability with BTMS, load A

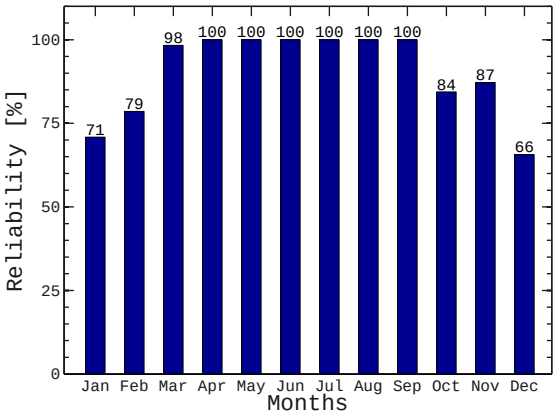

Figure 4-29: Monthly reliability with BTMS, load B

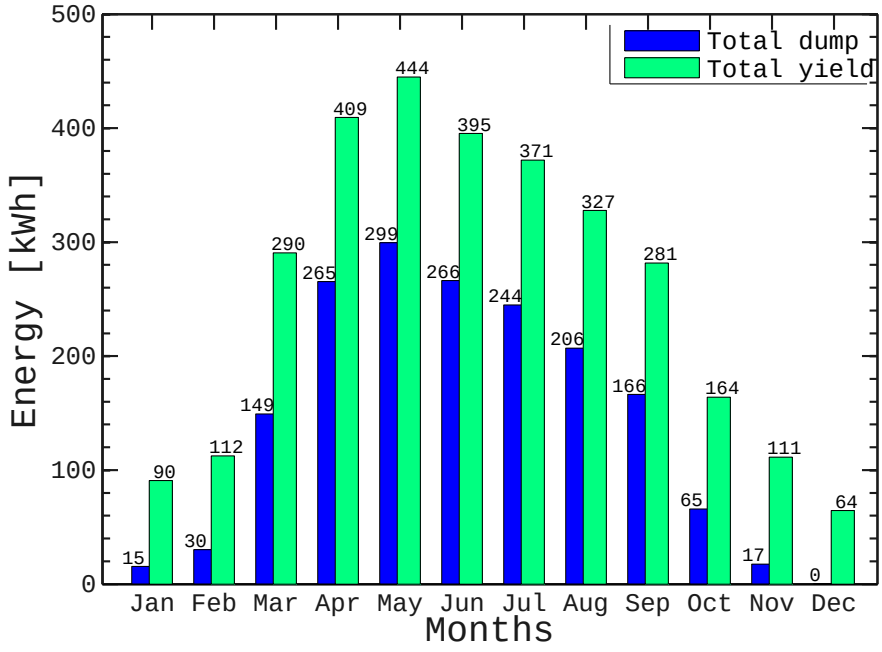

Figure 4-30: Monthly dump with BTMS, load A

4-5-7 Energy distribution

As the system described has several system components and multiple phenomena dictating the power flow at each instant, it is interesting to study the final energy distribution in the system under various conditions. To this end, some of the important energy values have been tabulated below. To put these numbers in perspective, the year under

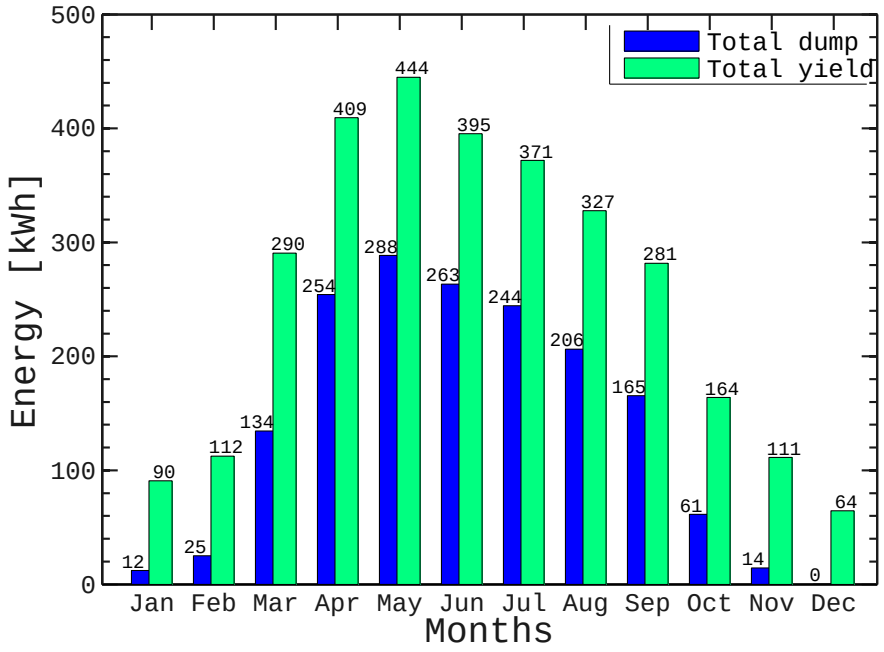

Figure 4-31: Monthly dump with BTMS, load B

consideration in the system modeling enjoyed a total PV yield of *3.16 MWh*, and the total annual load energy demanded was *918.8 kWh*.

Table 4-4: Total energy distribution in the system.

	Load delivered (kWh)	Energy dumped (MWh)	Battery losses (kWh)	Electronic component losses (kWh)	Cable losses (kWh)
Load A - no BTMS	850.2	1.79	154.65	302.20	63.25
Load B - no BTMS	854.8	1.9	42.45	302.20	63.25
Load A - with BTMS	766.8	1.73	300.45	302.20	63.25
Load B - with BTMS	831.9	1.67	295.35	302.20	63.25

Note: The cables losses have been assumed to be 2% of the PV power at each instant. The power electronics (inverter and charge controller)have been assumed to be 90% efficient.

Battery Utilization Factor (BUF)

Having taken all the non-idealities of the battery into consideration, a battery utilization factor is now defined. BUF is defined as the proportion of actual utilization of the battery to the otherwise 100% utilization of an ideal battery.

$$\text{BUF} = \frac{\text{Observed battery utilization considering all non-idealities}}{\text{Expected 100\% utilization for an ideal battery}} \tag{4-11}$$

Translating it to the case at hand, we get:

$$\text{BUF} = \frac{\text{Total battery activity - battery losses}}{\text{Total battery activity}} \tag{4-12}$$

where: battery losses = The battery losses as found out in Table 4-4;
Total battery activity = total energy flowing through the battery while (dis)charging throughout the period of observation, assuming an ideal battery.

From the system modeling for 2011:
Total battery activity for load A (no BTMS) = 486 kWh.
Total battery activity for load B (no BTMS) = 206 kWh.

Thus the BUF values have been calculated as:
BUF(Load A) = 68.17%.
BUF(Load B) = 79.39%.

It must be noted that the BUF is heavily dependant on the choice of load profiles. This is because the load activity is primarily responsible for the discharging activity of the battery throughout its lifetime. Also, the irradiance levels and the PV output largely dictates the charging activity of the battery. Therefore, BUF is concluded to be not the ideal indicator to judge the practical battery performance.

4-6 Conclusions

Load profile The two load profiles give varying results in the autonomous system scenario. Load profile A is a little more pessimistic with a full charge demanded on every bike albeit having lesser number of e-bikes. Load profile B is more realistically distributed, and seems to be catered to a little more easily by the charging station as the monthly reliability plots show marginal increase in reliability for load B(refer Figure 4-26 and Figure 4-27).

Storage As seen in the figures showing system reliability, the storage size fails to contribute to system reliability beyond a limit. For a given PV size, there is an optimal storage size that has to be determined first.
The BTMS for the storage is a major overhead that tends to pull down the system reliability. To avoid this, excellent active as well as passive thermal regulation scheme needs to be devised, in a much greater depth than covered in this report. BTMS is the unavoidable price to pay for not having the battery storage indoors, as recommended by all the manufacturers.

Dump There is a remarkable amount of energy being dumped in the summer months. Again, this is unavoidable without some sort of seasonal storage, which a limited battery fails to provide. Also, the idea of simply 'dumping' harnessed energy works against the philosophy of sustainability on which this thesis is based upon.

Grid connectivity An excellent alternative is a grid-connected charging station. In this way we can not only alleviate the winter woes of the system but we can also supply the grid in summer with the excess production. To reduce grid reliance, a combined storage and grid-connected topology could be used. This might help in achieving greater autonomy as well as reliability. The next chapter will deal exclusively with exploring the technical feasibility of such a system.

Chapter 5

Grid Connected System

This chapter deals with the sizing and optimizing of a charging station that is grid-connected. Different scenarios are considered and the system performance is analyzed under load profiles A and B. A new performance metric is defined that would help in determining the optimal size of the system.

5-1 System topologies

In the realm of grid-connected PV systems, two main kinds of topologies exist. The first is a purely grid-connected PV systems, and does not have any back-up or storage. The other is a grid-connected system with a limited battery-storage. Both topologies have their own advantages and disadvantages.

5-1-1 Grid-connected PV system

This is a PV system in which the generated PV power is fed to the grid via a grid-tied[1] inverter. When the system produces enough power to meet the load requirements, the excess power is fed to the grid and the load can be said to be powered by solar electricity. When the system produces insufficient power, the remainder of the load needs are met by the grid. A simple system topology of a grid-connected PV system has been shown in Figure 5-1.

The inverter shown in the figure is a grid-tied inverter. It acts as a current source and pumps AC current into the grid after inversion. It typically synchronizes with the grid to

[1]The terms grid-connected and grid-tied are synonymous and are used interchangeably throughout this chapter.

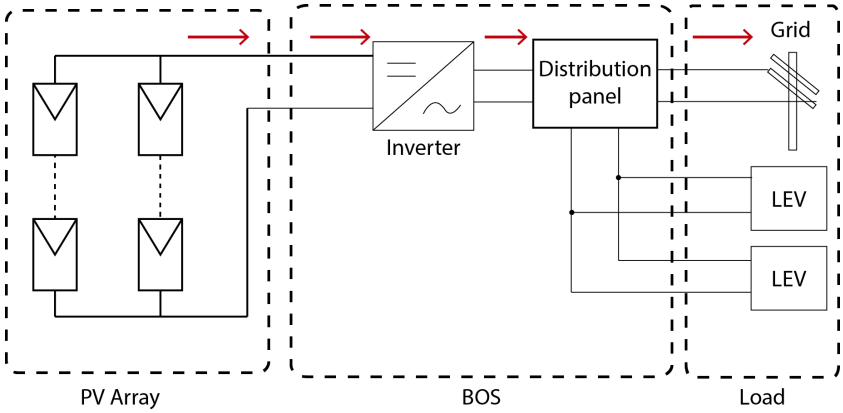

Figure 5-1: A typical grid connected PV system without battery storage

maintain a voltage and frequency in tandem with the grid. On the other hand, an off-grid inverter, like the one discussed in chapter 4 acts as a voltage source as it has to power the AC loads independently. Most grid-tied inverters come with in-built anti-islanding capabilities. This means that the inverter can identify if there are certain faults within the grid, and can disconnect the PV power from the grid under such a scenario.

Merits and demerits of a grid-tied system

Advantages of using a grid-tied PV system:

1. The system is 100% reliable (except when there is a grid failure, which is rare in the Netherlands where the proposed system is to be located) without having to oversize the system, unlike the autonomous PV system.
2. Due to the absence of a battery, there are no additional storage costs involved.
3. There is a possibility of earning credits if the utility allows the facility of net-metering, which is currently common in The Netherlands[2] [27].

Disadvantages of using a grid-tied PV system:

1. The system is completely reliant on the grid for storage.
2. The system fails to meet the load requirements if the grid fails even temporarily.
3. The implementation of this system is only feasible where integration with the grid is easily possible.

[2]Net metering is an electricity policy under which consumers earn retail credit for the electricity they generate and feed to the grid.

5-1-2 Grid-connected PV system with battery storage

This type of system is the same as the grid-connected system explained above, except that there is an additional storage in place. This storage is typically in the form of a battery. Conventionally, the role of the storage is simply to act as a backup in case the utility grid fails. However, in this chapter we shall examine a different use of the same setup of such a system. The battery in the system discussed in this chapter will not only serve as a backup in case of grid failure, but will also be able to make the system less reliant on the grid as compared to a completely grid-connected system. A typical grid-connected PV system with battery storage is shown in Figure 5-2.

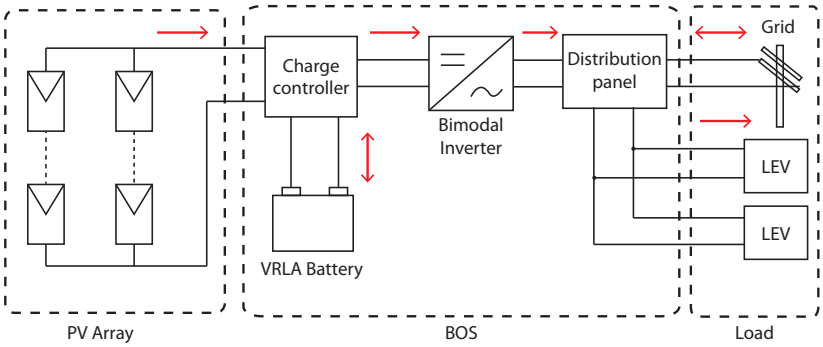

Figure 5-2: A typical grid connected PV system with battery storage

The main difference between this system and the purely grid-connected one is the use of the special inverter. This inverter is sometimes referred to as a bimodal inverter. It has the properties of both the off-grid inverter and the grid-tied inverter. It can serve as an off-grid inverter while being connected to the charge controller and the AC load. In this case it works as a voltage source. When the battery is charged and the load is met, it serves as a grid-tied inverter feeding the excess power into the grid. In this case it works as a current source. Thus the inverter is more complex, but can toggle between both the modes of operation in a sequential manner. There are complex power management systems that are already designed and discussed in literature to meet such bimodal power requirements[28].

Merits and demerits of a grid-connected system with battery storage

Advantages of using a grid-tied PV system with battery storage:

1. The system enjoys a higher degree of autonomy from the grid as compared to a purely grid-tied system.
2. The system can continue to meet the load demand even if the grid fails temporarily.
3. The system can guarantee a 100% reliability in meeting the load requirements.

Disadvantages of using a grid-tied PV system with battery storage:

1. There are added costs due to storage and its maintenance.
2. The system is less autonomous compared to a fully autonomous PV system.
3. The power electronics required in the system are more involved and the system installation is non-trivial.

Choice of the system model

As discussed in section 5-1-2, the battery need not be looked upon as merely a back up in case of grid failure. It can also assume the role of a daily storage. The system model described in this chapter will seek to explore the possibilities of meeting load requirements using a grid-connected PV system with battery storage.

5-2 System modeling

PV module

The PV module considered for the system modeling is, like in the autonomous system, the Sanyo Heterojunction with Intrinsic Thin-layer (HIT) module. The HIT module is chosen because of its high Module Ideality Factor (MIF) value that ensures maximal yield per area (refer section 3-4). The important specifications at Standard Testing Conditions (STC) or Nominal Operating Cell Temperature (NOCT) of the PV module have been re-tabulated below.

Table 5-1: Characteristics of Sanyo HIT 240 W_p PV module

Name	Sanyo HIT N240 SE10
Brand	Sanyo
Type	HIT
Pmax STC(W)	240
NOCT ($^\circ C$)	44
Width (m)	1.58
Height (m)	0.798
Area (m^2)	1.26084
Efficiency nom STC (%)	19
Voc STC (V)	52.4
Isc STC (A)	5.85
Temp coeff Pmmp (%/$^\circ C$)	-0.3
Temp coeff Voc (%/$^\circ C$)	-0.25
Temp coeff Isc (%/$^\circ C$)	0.0301

5-2-1 Power electronics

As the system being modeled is a hybrid system with a grid connection as well as battery storage, both the charge controller and a bimodal inverter will be required in the system. The inverter is assumed to have an in-built Maximum Power Point Tracking (MPPT) mechanism that ensures that the PV modules always functions at the maximum power point. This will ensure maximum yield at different irradiance levels. However, the system incurs additional losses due to the power electronic components, which are together assumed to be 90% efficient.

5-2-2 Energy Balance

Like the system model described for the autonomous charging station, the grid connected system is modeled in this chapter chiefly using energy balance.

Equation (5-1) to (5-4) capture the essence of energy balance happening in the system. In general, the system model samples the load at intervals of 1 minute, and follows an algorithm to control the power flow in the system. This is explained in greater detail in section (5-2-3). Equation (5-1) considers the case of a surplus of PV power production when the excess power is used to charge the battery storage, while equation (5-2) represents the scenario of deficit in PV power where the battery covers the load. If the battery cannot cover the load fully, then the grid begins to assist. Also, if the battery is full charged then the system feeds a portion of the PV energy output to the grid(Equation (5-4)).

$$\begin{aligned} E_{Load} &= E_{PV} - E_{Battery} - E_{Losses} \\ &\text{(if } E_{PV} \text{ - } E_{Losses} > E_{Load}\text{, Battery SOC} \leq 100\%\text{)} \end{aligned} \tag{5-1}$$

$$E_{Load} = E_{PV} + E_{Battery} - E_{Losses} + E_{Grid} \quad \text{(if } E_{PV} - E_{Losses} < E_{Load}\text{)} \tag{5-2}$$

$$E_{Load} = E_{PV} - E_{Losses} \quad \text{(if } E_{PV} - E_{Losses} = E_{Load}\text{)} \tag{5-3}$$

$$\begin{aligned} E_{Load} &= E_{PV} - E_{Battery} - E_{Losses} - E_{Grid} \\ &\text{(if } E_{PV} - E_{Losses} > E_{Load} \text{ and Battery SOC} = 100\%\text{)} \end{aligned} \tag{5-4}$$

where
E_{Load} = Energy supplied to the load,
E_{PV} = Energy generated by the PV array,
$\pm\ E_{Battery}$ = The energy flowing from or to the battery,
E_{Losses} = All the losses happening in the system bundled together, like cable losses and component inefficiencies,
$\pm\ E_{Grid}$ = The energy being dumped when there is a surplus production and the battery is full.

The system model considered in this chapter does not feature an active Battery Thermal Management System (BTMS). It is assumed that the passive thermal regulation is good enough during winter along with the self-heat that the battery generates. The thermal regulation during summer is believed to be done through the use of coolants as in most standard battery systems.

5-2-3 Control strategy

The basic control strategy has been outlined in Figure 5-3. At every time step (1 minute) in the model, the surplus energy is evaluated as $Surplus = PV - Losses - Load$. There are two main cases considered in the control flow - if surplus is negative or non-negative.

If surplus energy < 0 In this case the system is producing less than the load requirements. So the battery is first asked to complement the energy supply to the load. If the battery reaches its safety limit (20% SOC) then it stops discharging. If the load is still not completely met, the system turns to the grid to meet its power needs. In any case the system is 100% reliable as the load demand is always satisfied.

If surplus energy ≥ 0 In this case the system is self sufficient and is not reliant on the grid to meet its energy needs. The excess of energy produced is first used to fully charge the battery. If there is more energy left, this energy is then fed to the grid. A suitable net metering policy in place can help in earning credits for feeding the grid.

C-rate The model imposes the charging and discharging rate of the storage device. The maximum C-rate allowed by the model is C_{10}, which is more conservative than the C-rate limit defined for the autonomous system model of chapter 4. This is because stricter limits on the C-rate would compromise the ability of the storage device to cater to the loads at times of high power demand. While in autonomous system a harsher C-rate compromises the system reliability, a grid-connected system does not suffer from that problem. When the battery cannot supply to the load, the grid easily can. Therefore, the system model forces a C-rate limit of C_{10}, which is typically the upper limit in most PV system designs.

A high value of C-rate is typically not preferred. This is because a higher C-rate would impact the life time of the battery and also impair the efficiency of the battery. A C-rate of C_10 was used in the off-grid system simply to increase the reliability at certain points of time. In the grid-connected case, however, if the battery is limited by its C-rate, the grid can step in to fulfill load requirements.

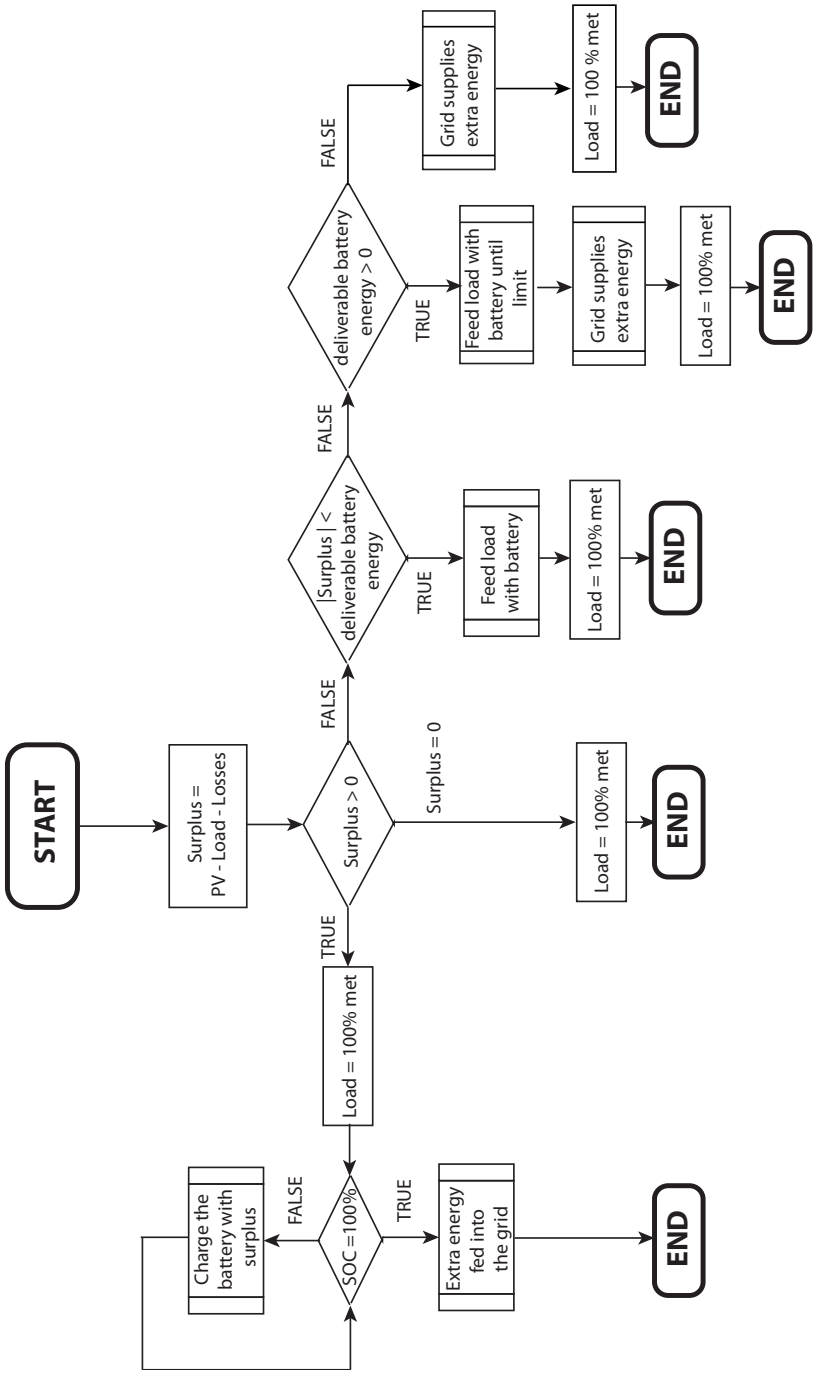

Figure 5-3: Control strategy for the grid-connected system model. (No active BTMS.)

Storage - an added benefit

The appendage of storage in the system can also be justified with the use of a robust control strategy. Currently, it is assumed that the utility does not offer a time-of-use pricing[3]. If there is a time-of-use pricing in place, the control strategy can be easily adapted to make full use of the battery as a short term storage to optimize the grid-feeding process. Thus, the battery serves a much greater purpose than merely acting as a backup in case of grid failure.

5-2-4 Measuring system performance

In the case of autonomous systems, a clear indicator of system performance was the reliability, i.e. how reliable is the system in meeting the load demands over a certain span of time. In the case of the grid-connected system, however, the reliability is always guaranteed because of a stable grid in the picture. Thus some new performance indicators need to be defined.

Electrical autarky

The term autarky indicates a condition of self-sufficiency. In the specific case of our grid-connected system, we use the term autarky as a measure of the independence of the system from the grid. Thus we define the term electrical autarky as the percentage of electrical energy used by the system that is self generated over a given time frame. Equation 5-5 shows how the electrical autarky is calculated.

$$\text{Electrical autarky} = \frac{\text{Consumed self generated electrical energy}}{\text{Total load demand}} \times 100 \tag{5-5}$$

where:
Consumed self-generated energy = Total delivered load energy - total energy imported from the grid.

Thus, an electrical autarky of 0% means that the load did not meet its requirements from the PV energy at all and that the grid supplied all of the demanded energy. Conversely, a 100% electrical autarky means that the system is completely independent of the grid. In general, a high degree of autarky is preferred.

Maximizing the electrical autarky of the system is not enough; a 100% electrically autarkic system simply means that it is an autonomous system akin to the one in chapter 4, bringing along its own share of problems with the excess energy and system oversizing. Thus electrical autarky needs to be optimized and not necessarily maximized.

[3]Time-of-use pricing refers to the system where electricity is differentially priced by the utility at different times of the day based on the demand and supply at those times.

Effective Autarky Ratio (EAR)

If the electrical autarky is increased unchecked, the system also increases the amount of excess energy it dumps into the grid. The quantity excess energy is defined for a given time frame and expressed as a percentage in Equation (5-6).

$$\text{Excess energy} = \frac{\text{Total energy exported to grid}}{\text{Total PV yield}} \times 100 \tag{5-6}$$

In order to optimize the system sizing, it is beneficial to have a lower value of the excess energy. Therefore, while the electrical autarky needs to be maximized, the excess energy has to be minimized.
Thus the need for a new indicator is realized. Consequently, a new indicator called Effective Autarky Ratio (EAR) is defined. The effective autarky ratio is the ratio of the electrical autarky and the excess energy of the system over a period of time. The EAR calculation is shown in the (5-7).

$$\text{EAR} = \frac{\text{Electrical autarky}}{\text{Excess energy}} \tag{5-7}$$

It might appear that the EAR could go to infinity if the excess energy estimated by the model is 0. But the excess energy can never be 0 because the model assumes a 100% battery State of Charge (SOC) in the beginning of the simulation year. This means that there is at least some amount of excess energy in the beginning when there is no load, the battery is full and there is PV power being produced. Therefore, the EAR can never go to infinity but take very high values for low system sizes. But these values are discarded because very low system sizes also lead to decreased electrical autarky levels. Thus the optimal system size is the one that maximizes the EAR without compromising on the electrical autarky of the system. This is the guiding indicator in deciding the optimal size of the system as discussed in the following section.

5-2-5 System optimization

The system is analyzed over a range of possible sizes of the PV and the storage system. The autarky, excess energy and EAR values have been calculated for each of the system sizing combinations.

Electrical autarky

The electrical autarky over the period of one year has been determined through system simulation, and plotted in Figure 5-4 and Figure 5-5 as a function of both the PV size and storage size. The plots drawn are contours such that each contour represents a specific level of autarky for various possible system configurations. The contours show that the autarky levels increase for increasing system sizes. Also, a certain autarky level can be

targeted with different sizing combinations. However, the apexes of these hyperbolic curves represent the optimal sizes for the each autarky levels (refer Figure 5-4).

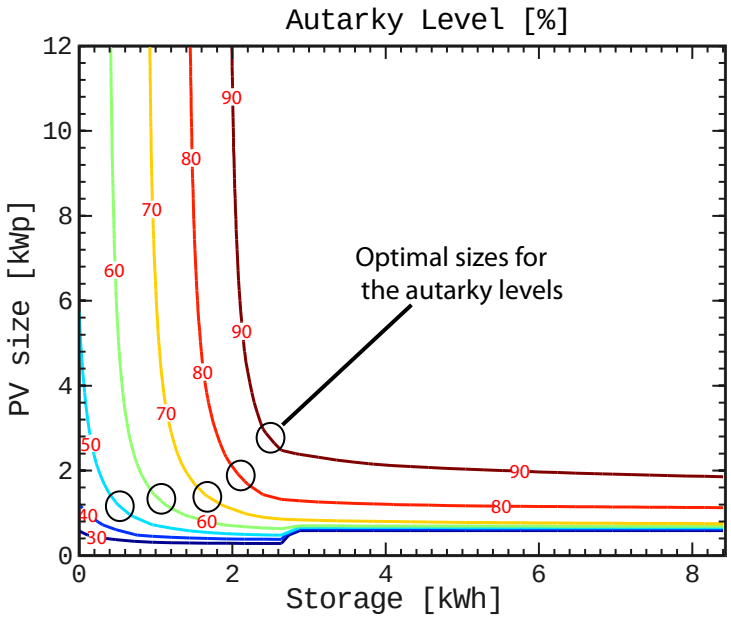

Figure 5-4: Electrical autarky levels - Load A

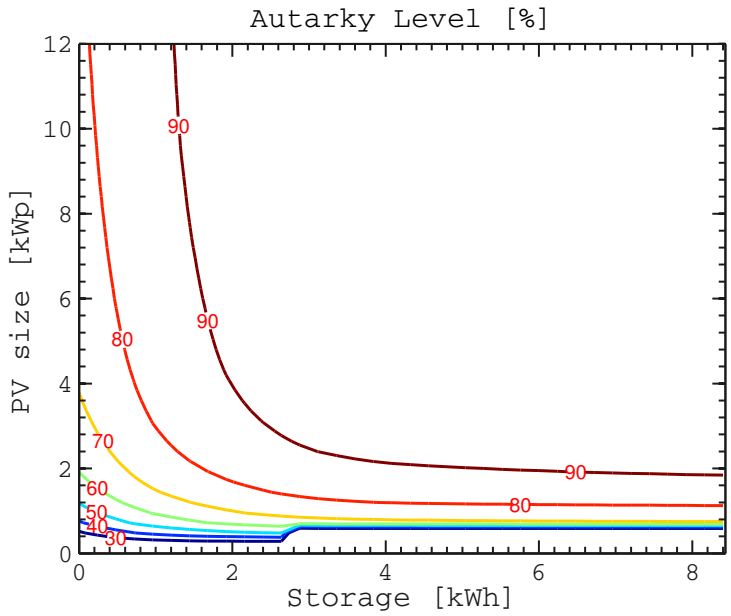

Figure 5-5: Electrical autarky levels - Load B

Excess energy

The excess energy levels over the period of one year have been simulated and plotted in Figure 5-6 and Figure 5-7 as a function of both the PV size and storage size. It is seen that the excess energy uniformly increases with increase in PV sizing. For a given PV size, the increase in storage size has little effect on the excess energy levels beyond a point.

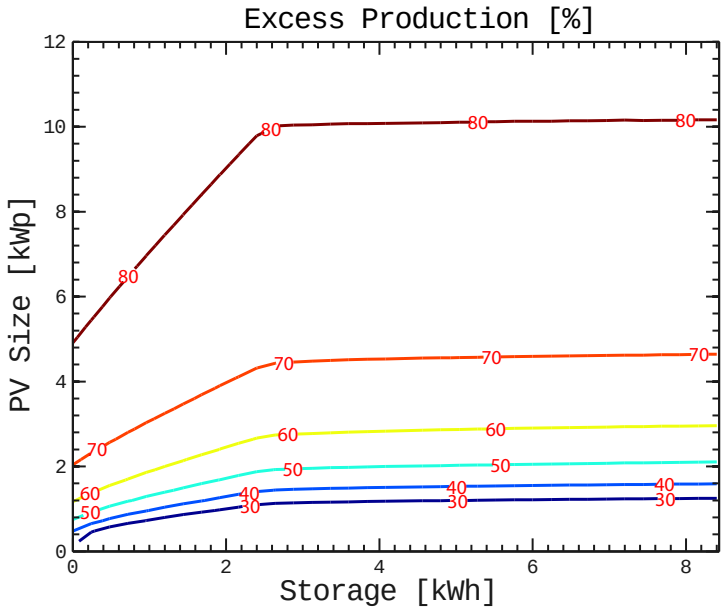

Figure 5-6: Excess energy levels - Load A

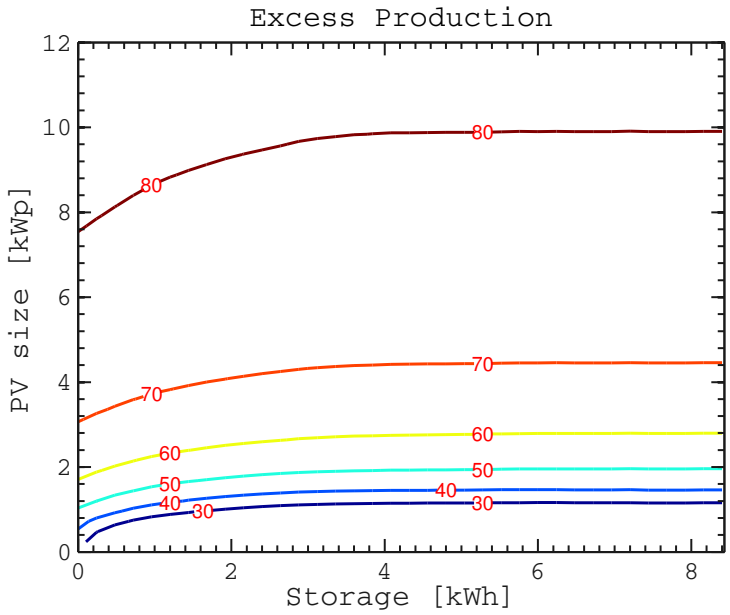

Figure 5-7: Excess energy levels - Load B

Load profile B is seen to have smoother contours for similar excess energy levels. This is because load profile B is more spread out throughout the day, and thus the storage has to work lesser in smoothing out the intermittency of the PV power. Thus adding more storage does not help in significantly curtailing the excess power fed to the grid.

EAR

The EAR numbers have been evaluated and drawn in Figure 5-8 and Figure 5-9. Again, it is seen that the storage has little effect on the EAR beyond a point. These graphs help in determining the optimal system size as shown below.

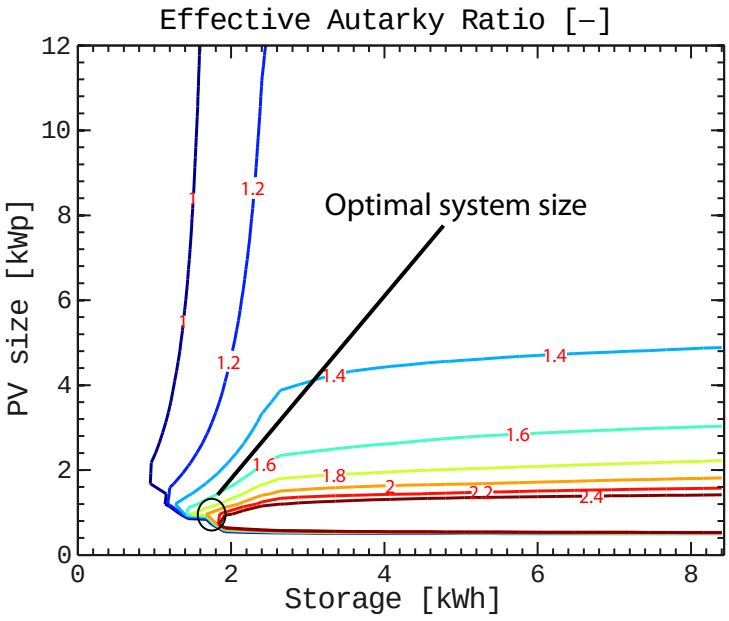

Figure 5-8: Effective Autarky Ratio (EAR) - Load A

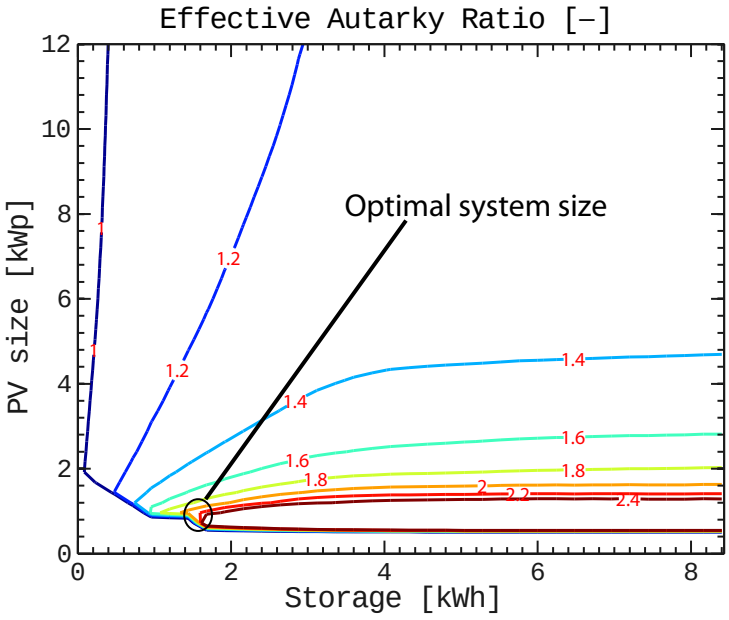

Figure 5-9: Effective Autarky Ratio (EAR) - Load B

Optimal size For the optimal size of the system, certain criteria are defined, like the EAR should be high, the electrical autarky should be at least 50%; system size, especially

storage, should be as low as possible. The extra restriction on storage is due to the fact that battery storage is usually the weak link in the PV system, needing to be replaced at least twice over the lifetime of the PV modules. From the extensive analysis of the electrical autarky, excess energy levels, and EAR values, the following system size was chosen as the optimal one for both the load profiles.
PV size = 0.96 kWp;
Storage size = 1.68 kWh.
The above PV size can be achieved with as low as *4* Sanyo HIT modules. This sizing is valid for both the load profiles as both the load profiles have the same energy requirements, but different distributions. This optimal sizing translates to the following values(refer Table 5-2) for the system metrics over the period of one year.

Table 5-2: System metrics for the optimized sizing.

	Electrical Autarky (%)	**Excess energy** (%)	**EAR**(%)
Load A	63	31.8	2
Load B	67	29.6	2.2

5-2-6 Optimized system

With the optimized system size, the system is again analyzed to examine the specific behavior of the system components and the performance indicators.

Reliability

As the system is grid connected, the grid acts as a reliable seasonal storage. Whenever the PV and the battery system fail in delivering the promised load, the grid provides the necessary energy. Thus the system reliability is 100% throughout the year.

SOC variations

The battery SOC for the system under both the loads is now analyzed. Figure 5-10 and Figure 5-11 capture the SOC variations over the period of one year. It can be seen that the battery SOC levels reach their limits in winter. Nonetheless the grid feeds the load at all such times. The system tends to maintain a higher average SOC level in the summer under load B as compared to load A. This can be attributed to the difference in the nature of the two load profiles.

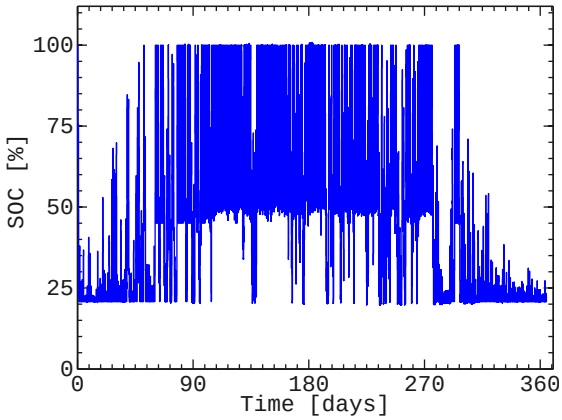

Figure 5-10: SOC variation under load A

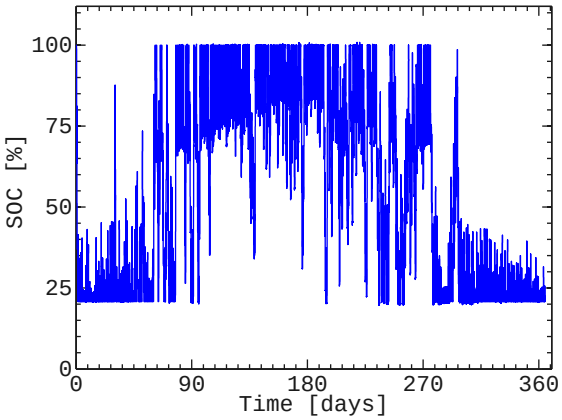

Figure 5-11: SOC variation under load B

Feeding the grid

It is seen how the monthly excess energy levels change over the year. Figure 5-12 and Figure 5-13 capture the monthly excess energy fed to the grid. The excess levels are fairly high in summer and are much lower in the winter. The system shows largely a similar behavior in the monthly energy fed to the grid. Monthly excess energy levels under load A are slightly higher in summer months and lower in winter months than the excess energy levels under load B. Again, this slight difference can be traced back to the nature of the load, where load B is more evenly distributed throughout the day for the same total energy levels.

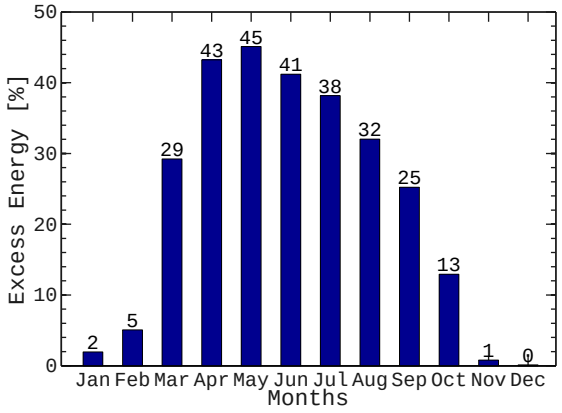

Figure 5-12: Monthly excess energy under load A

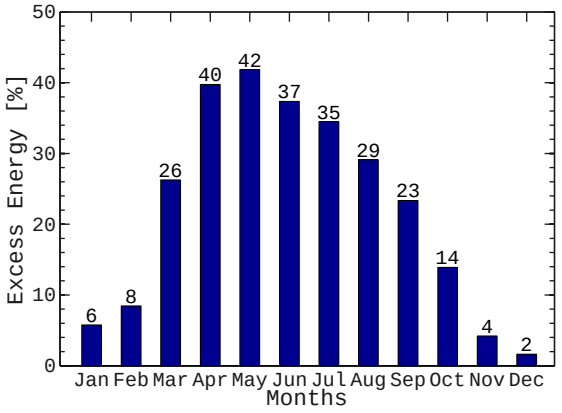

Figure 5-13: Monthly excess energy under load B

Auxiliary features Now that the reliability of the system is 100%, and there is also a net surplus of PV production, some auxiliary services could also be offered at the power

station under the grid connected scenario. For instance, the charging station could also be equipped with a Wi-Fi hotspot. Another helpful service could be a back-lit map and public transport-route info provided at the charging station. Perhaps the most revenue earning example could be small billboards for advertisement that are lit up at night at the charging station.

Monthly electrical autarky

For the optimized system, the electrical autarky levels throughout the year are now analyzed. Figure 5-14 and Figure 5-15 capture the monthly electrical autarky levels of the system under load A and load B respectively. The autarky levels are clearly lower in the winter. This is because the PV modules do not provide sufficient power to the load, and as a result the system becomes exceedingly grid reliant.
The system under load B displays slightly better autarky levels than under load A. Again, this can be attributed to the difference in the two load profiles. Load B, being more distributed throughout the day, is more easily catered to by the PV power, while load A has higher but concentrated demands during the day.

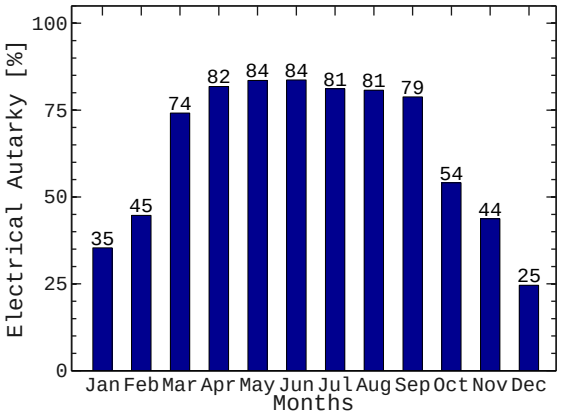

Figure 5-14: Monthly electrical autarky levels under load A

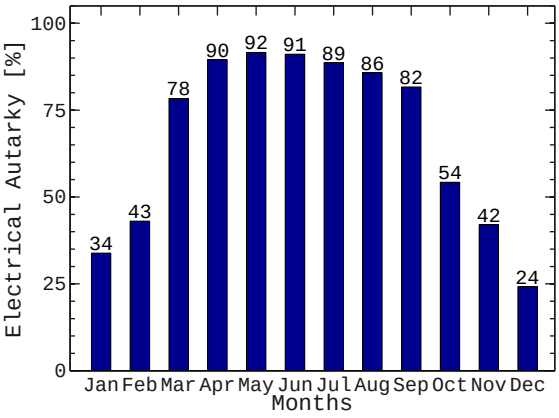

Figure 5-15: Monthly electrical autarky levels under load B

5-2-7 Energy distribution

It is interesting to examine the total annual distribution of energy to get a measure of the system losses and the total exchange of energy with the grid.

It can be seen from Table 5-3 that there is a net positive amount of energy being exported to the grid on an annual basis. This quantity is marginal for both the loads, and this is because minimal interaction with the grid has been the backbone of the system optimization in this chapter. The optimal Effective Autarky Ratio (EAR) value ensures that the system is autarkic to a higher degree without having to dump a large amount

Table 5-3: Energy distribution in the grid connected charging station

	PV yield (kWh)	Cable losses (kWh)	Power electronic losses (kWh)	Load delivered (kWh)	Exported to grid (kWh)	Imported from grid (kWh)	Battery losses (kWh)
Load A	1054	21.1	100.71	919.8	335.81	331.85	8.43
Load B	1054	21.1	100.71	919.8	312.46	302.75	2.68

Note: The cables losses have been assumed to be 2% of the PV power at each instant. The power electronics (inverter and charge controller)have been assumed to be 90% efficient.

of net excess of energy into the grid. It is also observed that the battery losses have been significantly reduced as compared to the autonomous system. This can be mainly attributed to the reduced storage size and the associated reduction in inefficiencies.

Also, it must be noted that the total load delivered is the same as the total load demanded. Therefore, the system reliability is 100% throughout the year.

5-3 Pilot charging station

Now that the charging station size has been optimized, its various characteristics have been summarized in Table 5-4. For the sizing of the power electronics, refer to the appendix section A-4.

Table 5-4: Pilot charging station - specifications.

Parameter	**Value**
PV size (W_p)	960
PV Area (m^2)	5.04
PV Array topology	2 x 2
Battery size (kWh)	1.68
Battery voltage (V)	48
Inverter size (W)	960
Charge Controller size	48V, 500W x2
Total charging sockets	10

5-4 Conclusions

Reliability Compared to an autonomous PV system, a grid-connected system is always assured of meeting its load requirements. This is because the grid acts like an infinite source and backup in case there is not enough solar power being generated. Thus, the reliability of the grid-connected PV system discussed in this chapter is 100%.

Use of storage Most conventional grid-tied PV systems do not use storage. Most grid connected systems with battery storage work merely as backup in case of grid failure. In this chapter, we have seen a more active battery storage that complements the PV production and the grid in meeting the load requirements. The battery serves as a good daily storage, while the grid acts as good seasonal storage.

Electrical autarky and Effective Autarky Ratio (EAR) It was seen how maximizing the electrical autarky is not enough; it needs to be optimized so as to also keep the grid-feeding in check. The optimal sizing of the system was more easily achieved after defining the Effective Autarky Ratio (EAR). In general, a maximal annual EAR for the least size is a good indicator to zero down on the ideal system size.

Technical feasibility The detailed work in this chapter proves beyond doubt the technical feasibility of a grid-connected system with a battery storage (hybrid system). The proposed system is not only 100% reliable but is also optimally grid reliant. However, it remains to be seen if such a system is financially viable and is carbon negative over its lifetime. These aspects are covered in great detail in the next chapter.

Choice of system topology Given the advantages of a hybrid system over both grid-connected system and off-grid system as discussed in this chapter, the hybrid system topology is chosen for the charging station design.

Chapter 6

Lifetime, Costs and Environmental Analysis

So far the technical feasibility of a charging station under different system topologies has been ascertained. But the system also needs to be cost-effective, durable, and environmentally friendly.

In this chapter, predictive models to estimate the lifetime of the PV module and battery are developed and discussed. A concise economic analysis is covered that affirms the financial viability of the system. A basic environmental analysis also quantifies the extent to which such a system can be net energy positive over its lifetime. The chapter deals with analyzing these aspects for the grid-connected PV system topology for the charging station[1].

6-1 Lifetime Estimation

The system models in chapters 4 and 5 do not cover the calendar effects on the system components. Calendar effects imply that the component performs worse as the years progress until the yield of the system is severely impacted and the particular component has to be replaced or repaired.

In this section the two most important system components - PV module and battery - are analyzed and their effectiveness is measured throughout their lifetime. While the calendar effects on the PV module output are analyzed, the battery lifetimes are also

[1] because the grid connected topology was found to be more reliable than the autonomous one, and hence is the system of choice. Unless otherwise mentioned, all analyses pertain to a grid-connected system with battery storage.

estimated under different load scenarios. An accurate calculation of the PV and battery lifetimes would also impact the financial analysis because the system yield would change with degradation of the PV modules, and the battery system would have to be replaced.

6-1-1 PV module lifetime

The Sanyo Heterojunction with Intrinsic Thin-layer (HIT) module datasheet specifies that the module produces at least 90% of the rated power for 10 years, and at least 80% of the rated power for 25 years [29]. Thus, a second order degradation model was developed for the PV module using interpolation as shown in Figure 6-1. The first year is assumed to be at 100% of rated power[2].

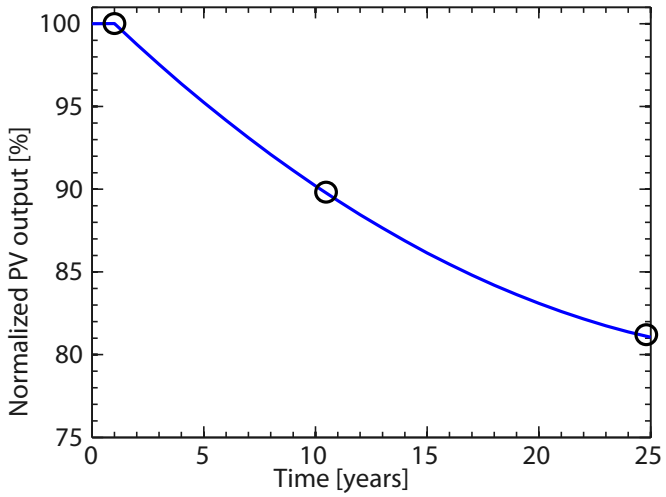

Figure 6-1: Normalized PV production over 25 years.

It can be seen that the PV module is not going to be the bottleneck of the system, and can continue working for at least 25 years, and possibly many more.

6-1-2 Battery lifetime

Estimating the cycle-life of the battery is much more difficult. This is because of multiple reasons:

- Though the manufacturer specifies how the number of cycles change with varying temperature, Depth of Discharge (DOD) and C-rate (while the other parameters are constant, refer section 4-2) the actual usage of the batteries experiences a range of combinations of all those factors.

[2]This rated power is assumed to be at Standard Testing Conditions (STC). Obviously, the temperature and irradiance will still play a role in the actual power output.

- The actual application of batteries hardly ever sees a complete charge-discharge cycle in the PV system. In reality, the battery use consists of several 'micro-cycles', wherein the battery charges and discharges for short spans of time.
- The actual lifetime degradation due to the battery chemistry is difficult to accurately estimate. The most realistic way of life estimation is to monitor battery parameters and to check electrolyte levels real time.

Battery lifetime estimation model

In general, cycle lifetime for a battery is defined as the number of (dis)charging cycles until the actual remaining capacity drops below 80% of the nominal capacity [24]. For a lead acid battery (also the battery choice for the system in this thesis), the cycle lifetime depends on DOD and temperature as shown in Figure 6-2.

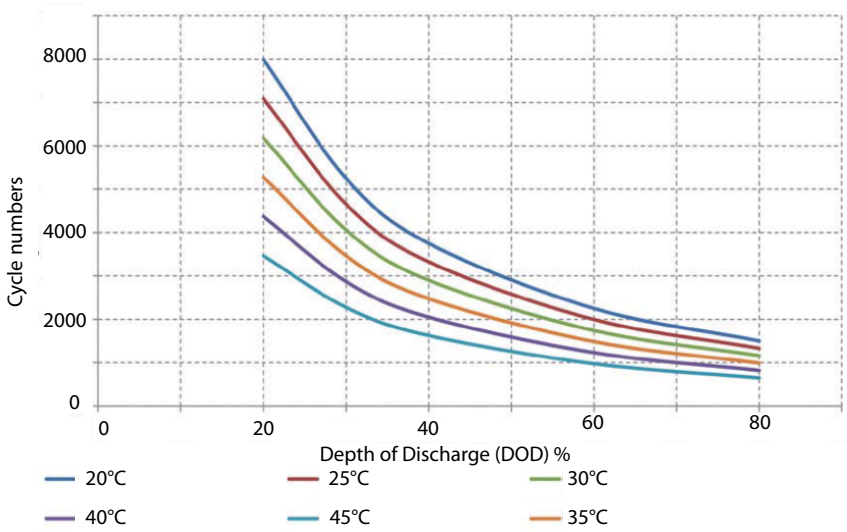

Figure 6-2: Cycle life Vs DOD at different temperatures (*source: [24]*).

This graph (Figure 6-2) helped in estimating the cycle numbers available for a given average temperature and average depth of discharge as shown in the following section.

Scope of the battery lifetime estimation model While the model estimates the lifetime of the battery, it does not take into account the calendar effects. Aging of the battery could be because of several reasons like anodic corrosion, positive active mass degradation, irreversible formation of lead sulphate, loss of water and short circuits. The rate at which aging occurs has a strong correlation with the usage patterns of the battery [30]. It is difficult to determine the exact cause that would lead to degradation and eventual end of the service life.

Hence the model only aims at determining the active lifetime of the battery given the DOD, temperature and (dis)charging rates during operation.

Cycle life estimation From the system model described in sections 4-5 and 5-2, average values for the State of Charge (SOC) and the temperature that the battery experienced over the year are derived.

As seen in Table 6-1, there is an average battery SOC of **48%** or DOD of **52%** under load A. The battery performs a little better under load B with an average SOC of **52%**. Combining the SOC and temperature information with the manufacturer's data (Figure 6-2), the expected cycle life is obtained for the battery under the two load conditions.

Table 6-1: Lifetime estimation of the VRLA battery

	Average battery temperature (°C)	**Average SOC (%)**	**Cycle life (number)**	**Lifetime (years)**
Load A	13	48	3500	13
Load B	13	52	3900	14.5

Average lifetime from cycle life Given the total number of cycles for the battery, the average number of cycles was determined for the battery per year. This was done by aggregating the effect of all the 'micro-cycles' that the battery undergoes in the year. The calculations are demonstrated in equations 6-1 through 6-3.

$$E_C = \sum_{t=1}^{365*24*60} E_{B_i} \tag{6-1}$$

where
E_C = Total battery charging energy over the year;
E_{B_i} = Energy added to the battery in minute i.

$$\text{Total charge cycles per year} = \frac{E_C}{(1 - \overline{SOC}/100) * E_{B_{rated}}} \tag{6-2}$$

where
$\overline{SOC}$ = Mean SOC value throughout the year;
$E_{B_{rated}}$ = Rated battery capacity.

$$\text{Lifetime (years)} = \frac{\text{Cycle life(number)}}{\text{Total charge cycles per year}} \tag{6-3}$$

Thus, the lifetimes of the battery under the two load profiles have been evaluated and tabulated in Table 6-1.

6-1-3 Balance of System (BOS) lifetime

The cables, racks, and other mounting paraphernalia are certainly not the bottleneck in the lifetime of the system. However, power electronic components have a much lesser average lifetime. Thus, the inverter would need to be replaced in the system lifetime.

Inverters need to be handled carefully during their lifetime. If a good quality inverter is kept well protected from the weather elements and is suitably ventilated, then the lifetime can be optimized to as much as 10 years[31].

A good quality charge controller generally fares better than the inverter in terms of lifetime, but a lot depends on the quality of the product and the appropriate usage. The financial model (section 6-2) assumes a lifetime of 10 years for the inverter and 12.5 years for the charge controller.

6-2 Financial Analysis

Once a project has been designed for technical specifications and functionality, the natural next step is to examine the financial implications of implementing the project as a pilot, and thereafter on a larger scale. A lot of niche technological applications tend to provide for highly challenging business cases. Especially when it comes to the energy sector, government incentives, regulatory and tax policies and legal frameworks can impact project costs too. The purpose for doing the financial analysis is discussed below.

Purpose : Every project starts at the design phase, where a business concept is developed to sell a product/service and generate revenues. In our case, the electricity generated at the solar-powered charging station is the final consumable, which is sold to Light Electric Vehicle (LEV) users. In order to create the infrastructure for the project, certain costs need to be provided for. Thus, the final revenues that the project generates must be more than the costs to ensure profitability. This feasibility is examined below through various financial tools.

6-2-1 Levelized Cost of Electricity (LCOE)

In this section, the financial feasibility of the charging station is analyzed using the **LCOE** model. LCOE allocates the costs of an energy plant across its useful life, to give an effective price per unit of energy (kWh). It is similar to averaging the up-front costs across production over a long period of time [32]. It provides a cost/kWh value, which is convenient to compare with what consumers pay to their utilities, and can also be used to compare lifetime costs of various sources of energy. An illustration of the LCOE model is shown in Figure 6-3.

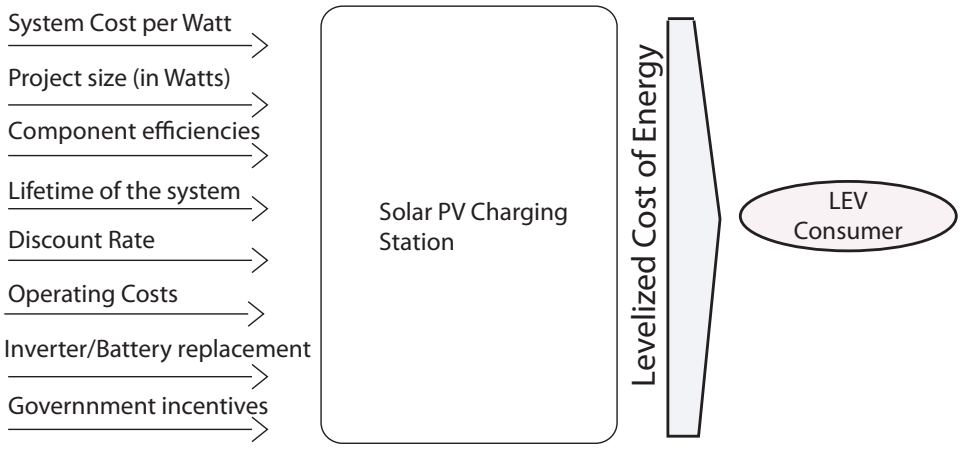

Figure 6-3: LCOE model components.

Components of the LCOE analysis :

- **System size**: This tells us the total generating capacity of the solar PV modules in Watts.
- **System costs**: This covers the initial investment in setting up the charging infrastructure. This includes costs of PV modules, Storage, cables, inverters, land and labour. This varies widely with the scale of the project from €$3.8/W_p$ for small projects (sub kW) to €$2.7/W_p$ for large projects (several kW).
- **Productive life**: This tells us the total life of the charging station. Normally, solar projects are very durable and can last up to 20-30 years.
- **De-rating**: The energy that is generated by the PV modules and that which is finally available for use varies depending on the component losses of the system. This is captured by the de-rating and can range from 75-90% of the generated power.
- **Discount rate**: It is the rate at which future revenues are discounted for the present value, and it hopes to capture the total returns on investment the project can generate. It also signifies the opportunity cost of the funds used. A discount rate of 4% has been assumed for this analysis, which is in the range of the typical discount rates for developing countries [33].
- **Incentives**: It denotes the government tax breaks provided to investors in the renewable energy sector. It is currently pegged at 36% in the Netherlands [34].
- **System degradation**: It captures the degradation of performance of the various components of the charging system. It ranges from 0.5% to 1% of total system

yield per annum. In this case, this is already accounted for in the lifetime analysis of the PV module.

- **Operation and maintenance costs**: The routine cleaning and maintenance costs are accounted for in this category. They are typically 0.5% per annum.
- **Inverter and battery replacement**: These two components have a smaller lifetime compared to the PV module. Hence they need to be replaced intermittently, depending on usage and quality. These costs are also considered in the LCOE model.

The values the above parameters take in the LCOE model for this charging station have been tabulated in Table 6-2, along with the LCOE estimated by the model.

Table 6-2: LCOE model parameters.

	Off grid		**Grid connected**	
Parameter	**Load A**	**Load B**	**Pilot case**	**Large scale**
Project size (W)	2,880	2,880	960	10,000
Cost/watt	€3.70	€3.70	€4.00	€3.00
Investment Tax Credit	36%	36%	36%	36%
Watt-hours/Watt-peak	295	297	1,095	1,095
De-rating	85%	85%	85%	85%
Discount rate	4.0%	4.0%	4.0%	4.0%
Productive years	25	25	25	25
Degradation	0.50%	0.50%	0.50%	0.50%
Operations cost	0.50%	0.50%	0.50%	0.50%
Battery Replacement Year	5x	13	13	13
Battery replacement cost (€/Wh)	0.15	0.15	0.15	0.15
Inverter replacement year	10	10	10	10
Inverter replacement cost (€/W)	0.70	0.70	1.00	0.80
Levelized cost of electricity	**€0.940**	**€0.867**	**€0.257**	**€0.197**

Table 6-2 captures the LCOE values for both the grid connected and the autonomous configurations. It is interesting to note that the LCOE analysis is not differentiated for the two load profiles in the grid-connected scenario. This is because the two load profiles consume the same amount of energy, and nearly all the energy being produced is being used by the loads in the grid-connected scenario. On the other hand, the amount of useful energy (the rest simply being dumped) varies for the different load profiles in the autonomous charging system.

For the autonomous charging station, the LCOE have been found to be **€0.94/kWh** and **€0.867/kWh** respectively for load profiles A and B without active Battery Thermal Management System (BTMS) involved. As expected, the energy being dumped costs the autonomous system dearly.

The grid-connected topology fares much better in comparison. For the pilot case of a $960W_p$ rated charging station, the **LCOE** is found to be **€0.257/kWh**. Currently, in the Netherlands, the grid produced electricity is available at **€0.22/kWh**.

Since we have modeled a very small pilot system with limited capacity, the costs are slightly higher. As long as the project is implemented on a small scale, government subsidies, and additional sources of revenues (like commercial advertisements) etc. may have to be used to bolster the profitability. However, as the capacity and scale are expanded, the costs can come down to as low as **€2.7**/W_p due to the impact of economies of scale [35].

Thus, a community based approach of implementation would benefit the project and improve the cost effectiveness for the end consumers, thereby triggering a shift from grid based charging to solar charging. Another salient feature of a solar powered charging station is that the only fuel used is solar irradiation. Thus, the costs are inflation independent, and end up saving a lot of costs in the long run despite the seemingly high initial investment.

6-2-2 Net Present Value (NPV) and Payback period

After having determined the levelized cost of production of energy, the next step is to find out if the LEV charging station is a viable project to invest in based on its revenue generating potential. This section details the Net Present Value (NPV) of the cash flow generated by the charging station, the Internal Rate of Return (IRR) of the project, and the Payback period for the initial investment. NPV, IRR and Payback period are financial metrics that are used across industries to determine the financial robustness of new projects.

The analysis has been done on a single pilot Solar based LEV charging station, with a capacity to charge up to 30 e-bikes per day. It is a grid-connected application with continuous power supply. 2 days have been set apart for annual maintenance purposes. The revenue model used assumes that consumers will pay on a per-charge basis, via a payment system that uses the same technology as a parking meter. An additional setup cost of €1/W_p is added to account for the investment in payment infrastructure for the consumers. The discount rate has been taken as 4%, the same as used in the LCOE calculations. The underlying parameters in the financial analysis have been tabulated in Table 6-3.

Net Present Value (NPV)

The LCOE calculations for the pilot charging station gave a value of €0.25/kWh. However, as mentioned in the previous section, this is not a grid-competitive rate to sell power at. Thus, it is assumed that our pilot plant has additional sources of revenue in the form of commercial advertisements and government incentives in its nascent stages. This has

Table 6-3: Parameters for evaluating the NPV and payback period.

Parameters	**Scenario 1**	**Scenario 2**	**Scenario 3**
Number of Bikes Charged per day	30	30	30
Number of Opertaional Days	363	363	363
Total Charging Station Capacity (W_p)	960	960	960
Setup cost per unit (€/W_p)	4	4	4
Payment Infrastructure cost (€/W_p)	1	1	1
Total Setup Cost (€)	4800	4800	4800
Discount Rate (%)	4	4	4
Annual Maintenance Cost (% of Setup cost)	0.5	0.5	0.5
Total Battery replacement cost (€)	250	250	250
Total inverter replacement cost (€)	1000	1000	1000
Annual Income from Ads and Subsidies (€)	400	600	1000

also been incorporated into the model and helps us bring down the price of power to €0.20/kWh, thus making it a competitive offering.

The NPV for any project is evaluated based on equation 6-4. Three different scenarios have been considered for the additional revenue earned, based on which the NPV varies. The different scenarios are:

1. Scenario 1: An additional revenue of €400/year is generated.
2. Scenario 2: An additional revenue of €600/year is generated.
3. Scenario 3: An additional revenue of €1000/year is generated.

$$NPV = -C_0 + \sum_{t=1}^{N} \frac{C_t}{(1+r)^t} \tag{6-4}$$

where: C_0 = Initial investment,
t = year number,
N = system lifetime,
r = discount rate,
C_t = Net Cash flow in year t.

Based on equation (6-4), the NPV values for the 3 scenarios have been evaluated and tabulated in Table 6-4. Scenario 3 shows the highest NPV of **€12230** due to the extra revenue assumed in the scenario.

Internal Rate of Return (IRR)

The Internal Rate of Return (IRR) of a project is the rate of discount, which when applied to the project cash flow leads to an NPV of 0. The IRR has been iteratively

evaluated based on the equation (6-5).

$$\text{Initial investment} = \sum_{t=1}^{N} \frac{C_t}{(1+IRR)^t} \tag{6-5}$$

where: t = year number,
N = system lifetime,
IRR = Internal Rate of Return,
C_t = Net Cashflow in year t.

Table 6-4 captures the IRR values of the 3 different scenarios. Scenario 3 shows the highest IRR of **31%**.

Payback period

The Payback period of a project is defined as the time in years, when the project recovers its initial investment, and starts generating a net positive cash flow. The graph shown in Figure 6-4 illustrates the payback period for the LEV solar charging station in the 3 estimates of additional revenue.

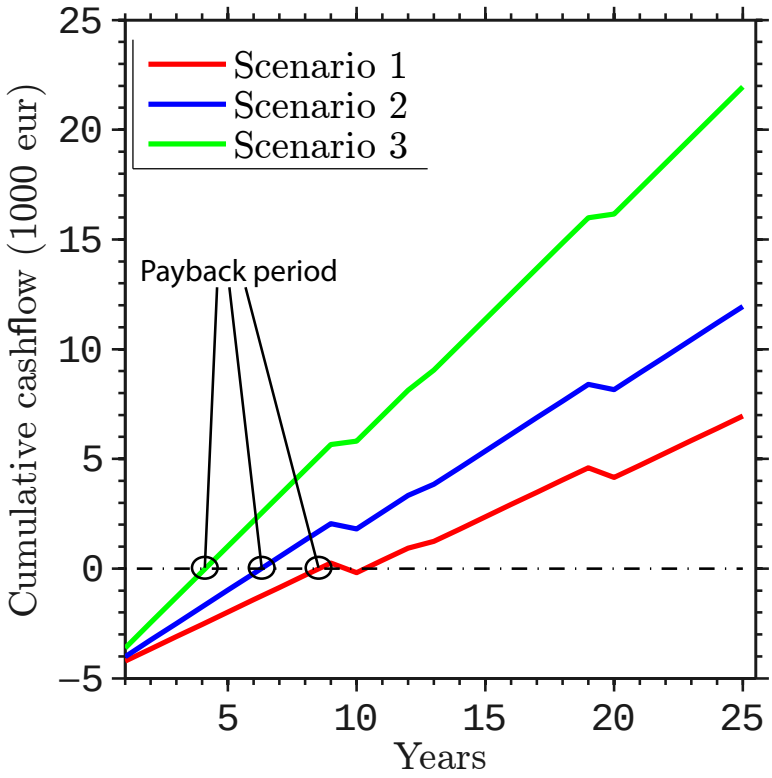

Figure 6-4: Cumulative cash flow and payback period.

Table 6-4: Financial metrics for the pilot charging station.

Metric	Scenario 1	Scenario 2	Scenario 3
NPV (€)	2858	5982	12230
Payback period (years)	8.5	6.5	4
IRR (%)	10	17	31

Significance of the financial metrics NPV determines the profitability of a project or an investment, hence higher the NPV, the more viable a project is over its entire life. Assuming all other factors are same among 2 projects, it is the IRR that is used to determine which project to invest in. It is also called the economic rate of return. It is the rate of growth that the project is expected to show, and hence,a higher IRR is a sign of a financially robust project.

6-3 Environmental Analysis

While the proponents of solar energy are touting PV to be the panacea for the global energy crisis, there are skeptics who claim PV does more harm to the environment than good in its lifetime. This section aims at analyzing the overall environmental impact of the PV module. It should be noted that the scope of the environmental analysis in this section is limited mainly to energy analysis. The adverse impact of individual chemicals and manufacturing processes are beyond the scope of this chapter.

6-3-1 Energy Analysis of PV systems

Firstly, the total amount of energy invested in the manufacture of the PV system components need to be taken into account. There are several works in literature which have done an in-depth study on the energy cycle of PV technologies ([20], [18]). Most of the values for the energy analysis in this section have been adapted from the works of E. Alsema [18].

PV modules Manufacturing silicon based PV modules, especially crystalline silicon (c-Si) is currently a very energy intensive process. The energy requirements to manufacture present day polycrystalline silicon PV module is around **32 MJ/Wp** without frame, and **35 MJ/Wp** with aluminum frame. This number increases by around **7 MJ/Wp** for monocrystalline silicon. It is assumed that the HIT module consumes energy for its production mid-way between the energy required for thin-film amorphous and monocrystalline silicon production. This is found to be comparable to the energy required for the production of the polycrystalline modules [20]. Therefore, the energy value for polycrystalline modules has been used in the energy estimation for production of the system without any loss of generality.

Battery Manufacturing lead acid batteries is also quite energy intensive. Even after assuming a high recycling rate of scrap batteries, present day lead acid batteries consume about **11 MJ/Ah** of battery capacity.

Other BOS The power electronics and cabling are estimated to require around **1.6 MJ/Wp**. For mounting the PV panels, the support structure, as analyzed in a recent study of Dutch roof installation system, are estimated to consume around **240 MJ/**m^2.

Thus, the total energy needs of the PV system can now be estimated. Table 6-5 captures the various energy values of the PV system components, including the total system energy requirement. Approximately 10.5 MWh of energy was spent in building this system.

Table 6-5: Energy analysis of the charging station

System component	Energy per unit	Component size	Total energy (MJ)	Total Energy (kWh)
PV modules with frame	35 (MJ/Wp)	960 Wp	33600	9333
Battery	11 (MJ/Ah)	140 Ah	1540	428
Power electronics and cables	1.6 MJ/Wp	1000 Wp	1600	444
Support structure	240 MJ/m^2	5.04 m^2	1210	336
Total Energy			**37950**	**10542**

6-3-2 Energy Payback Time (EPBT)

Having calculated the total energy that went into manufacturing the PV system components, it is interesting to see if the PV system is a net positive producer of energy in its lifetime. Energy Payback Time (EPBT) is defined as the ratio of the total energy input during the system life cycle and the yearly energy generation during the system usage [18].

$$\text{EPBT} = \frac{\text{Total Energy input during the system life cycle}}{\text{Yearly energy generation by the system}} \tag{6-6}$$

Using equation (6-3-2) the EPBT is evaluated for the charging station in the hybrid system topology, and found to be ***10.5 years.*** This is a very conservative estimate as compared to the usual values of 4 to 7 years as estimated for low irradiance locations [18]. This is because the estimate discussed here takes into account the extra losses due to the temperature and irradiance fluctuations. Also, the input energy estimates for the entire system is fairly conservative.

6-3-3 Energy Yield Ratio (EYR)

Energy Yield Ratio (EYR) is defined as the ratio of the amount of energy yield of a system throughout its lifetime to the amount of energy invested in its manufacture.

$$\text{EYR} = \frac{\text{Total energy yield}}{\text{Total invested energy}} \quad \text{throughout the lifetime.} \tag{6-7}$$

There is a common misconception that more energy is invested in manufacturing the PV modules than they would ever yield throughout their lifetime. This is certainly untrue. In fact, depending on the geographical location where the modules are being used in their lifetime (equatorial regions will naturally enjoy a higher PV yield), the Energy payback ratio for a PV module can be as high as 14 for a single PV module[36]. In comparison, the EYR for conventional coal-fired generation has been estimated to be anywhere between 2.5 and 5.1[37].

For the charging station being designed, the EYR is found using equation (6-7) to be ***2.5***. Similar to the EPBT, this is a lower than the values usually reported in literature.

This can be attributed to the fact that the energy analysis has been very conservative in accounting for all the energy spent in the manufacturing of every system component. The system yield taken has also been very conservative. Usually in these analyses the calendar effects are not considered, but degradation has been taken into account in this report. In reality, the lifetime might well be over 25 years, which might improve these metrics even more. The most hampering factor in the low value of these metrics is the extremely low irradiance level in the Netherlands.

Table 6-6: Summary of energy analysis of the system

EPBT	10.5
EYR	2.5

6-4 Conclusions

Lifetime of the system The charging system is expected to have a lifetime of at least 25 years. This is mainly because the PV module can generate power efficiently for at least 25 years. The power electronic components would need to be replaced at least once and maximum twice in the lifetime of the system. The batteries, depending on the load requirements and the kind of usage, will need one replacement during the system lifetime.

Financial analysis An in-depth financial analysis was carried out for the grid-connected charing system with storage. The LCOE was found to be **€0.257/kWh** for the pilot charging station, which is comparable to the grid price of electricity at **€0.22/kWh**. It is estimated that the LCOE will drop down to **€0.197/kWh** with increase in system size. Also, with additional revenues generated, the pilot charging station can payback its investment costs in **4** to **8.5** years, depending on the amount of additional revenues generated.

Environmental analysis Although the production of PV system components is quite energy intensive, it was seen that the PV system is net energy positive over its life time.

A conservative estimate pegs the Energy Payback Time (EPBT) at **10.5** years and the Energy Yield Ratio (EYR) at **2.5**. As manufacturing technologies develop, these numbers are poised to read better.

Chapter 7

Conclusions and Recommendations

In this thesis a solar based charging station was designed and optimized for size under several constraints. Two different system topologies were looked at - standalone system, and grid-connected system with storage. A thorough technical feasibility of the two systems under two different load profiles were carried out. Lifetimes were estimated for the battery storage under the two load profiles. Calendar effects were considered for the PV module so as to determine the exact yield over its lifetime. A brief environmental and economic analysis followed that further outlined the feasibility of the system at a pilot scale.

The questions which formed the basis of this thesis work are presented here again:

1. How much of solar energy can be harnessed through existing photovoltaic (PV) technologies for a Light Electric Vehicle (LEV) charging station based in the Netherlands?
   (a) How much of solar energy is available throughout the year in the Netherlands?
   (b) Given the intermittent nature of the weather conditions, how much of electrical power can be generated by a PV module throughout the year?
2. Is it possible to rely entirely on the solar power through the year to meet the daily charging requirements?
   (a) How does an autonomous PV system fare in terms of meeting the energy demand for LEV charging throughout the year? How can the performance of an autonomous PV system be reliably measured?
   (b) Can the reliance on the utility grid be minimized for a grid-connected charging station? How can the performance of a grid-connected system be reliably measured?

3. Does it make economical and environmental sense to move to a solar based solution for charging Light Electric Vehicles (LEVs)?
   (a) Is it financially viable to invest in a solar based charging station, as opposed to simply charging the LEVs from the grid?
   (b) Does a solar charging station payback the energy it used up in its production?

7-1 Conclusions

1.(a) *How much of solar energy is available throughout the year in the Netherlands?*
There is an average annual irradiation of **1.05** MWh/m^2 on the flat horizontal ground in the Netherlands. This translates to a daily average irradiation of around **2.8 - 2.9** kWh/m^2 as analyzed over 4 years of irradiation data. These values increase by an average of 15% if the PV modules are inclined at an optimal **tilt angle** of **38**° with an **azimuth** of **0**°. The annual irradiation can be thus maximized to about **1.2** MWh/m^2 with an optimized orientation.

1.(b) *Given the intermittent nature of the weather conditions, how much of electrical power can be generated by a PV module throughout the year?*
A PV model was generated to accurately estimate the yield of a PV system under the varying conditions of temperature and irradiance. The PV yield increases with increase in irradiance, but drops with a rise in temperature. Several modules were analyzed under the model and a **Module Ideality Factor (MIF)** was defined. This factor indicates the effective yield achievable under temperature and irradiance effects. The highest MIF number was found for the Sanyo HIT module as **89%.** The Sanyo module was also the choice for all the system modeling and simulations. The use of the MIF value will help the architects of PV systems design size their systems much more accurately.

1. *How much of solar energy can be harnessed through existing PV technologies for a LEV charging station based in the Netherlands?*
With the optimal choice of the Sanyo HIT modules, around **208** kWh/m^2 of solar energy can be effectively harnessed. This is the true yield taking into account the temperature and irradiance effects, as estimated by the PV model. This value is reflective of the weather conditions for a representative year in the Netherlands.

2.(a) *How does an autonomous PV system fare in terms of meeting the energy demand for LEV charging throughout the year? How can the performance of an autonomous PV system be reliably measured?*
An autonomous PV system with battery storage was analyzed for performance throughout the year. The system can technically meet the load requirements, but at the cost of producing excess energy in peak summer.
Performance indicators called **reliability** and **dump energy** were defined. Reliability is

the measure of the percentage of load demand being completely met by the autonomous system. Dump energy is the surplus energy that the PV modules yield during the day, especially in the summer months. Thus, in the absence of seasonal storage, it is impossible to provide 100% reliability without dumping excess energy during abundant sunshine.

2.(b) *Can the reliance on the utility grid be minimized for a grid-connected charging station? How can the performance of a grid-connected system be reliably measured?*
A grid-connected charging station model was created and analyzed for performance over the year. The system is more promising showing a 100% reliability at all times. Two performance indicators were defined - **electrical autarky** and **Effective Autarky Ratio (EAR)**. The system size was optimized to provide a high EAR, and high for the least size. The final system size has an electrical autarky of around **67%**, and an EAR of **2.2** under load B with **100% reliability**. Under load A the system size has an **electrical autarky** of around **63%** and an **EAR** of **2** with **100% reliability**.

2. *Is it possible to rely entirely on the solar power through the year to meet the daily charging requirements?*
Yes, it is indeed possible to rely on solar power through the year for a charging station. Although, in the context of energy balance, the grid-connected system topology should be used. The PV system would then feed a marginal net excess to the grid, thus still being net energy positive while meeting load demands.

3.(a) *Is it financially viable to invest in a solar based charging station, as opposed to simply charging the LEVs from the grid?*
For the pilot sized system, the **Levelized Cost of Electricity (LCOE)** is estimated to be around **€0.257/kWh** , slightly higher than the current grid price of electricity. However, additional revenue could be generated through auxiliary services like advertisements, Wi-Fi, etc. Also, government subsidies would play a big role in driving the costs down further.
At pilot scale, with additional revenue, the payback period can be between **4 and 8.5** years, depending on the amount of additional revenues generated. The Net Present Value (NPV) analysis shows a best case NPV of **€12230** and an Internal Rate of Return (IRR) of 31%. At large scales, the **LCOE** can go down to **€0.197/kWh**.

3.(b) *Does a solar charging station payback the energy it used up in its production?*
The solar charging station takes around **10 years** to payback all the energy used in the production of all its components. In fact, in its lifetime, it pays back over **2.5 times** the energy went into producing the system components. However this is a conservative estimate due to the practical considerations like temperature effects and calendar effects. With progress in technology, less energy intensive manufacturing could ensure a much lower Energy Payback Time (EPBT) and a much higher Energy Yield Ratio (EYR) in the future.

3. *Does it make economical and environmental sense to move to a solar based solution for charging LEVs?*
Indeed, it makes perfect environmental and economical sense to move to a solar based solution for charging LEVs, especially on a large scale.

In conclusion, a comprehensive feasibility study was carried out in this report for the design of a solar based charging station for LEVs. The data and the numbers used in this thesis are almost all taken from datasheets of the latest commercial products in existence today. Thus, the calculations of the various models described in this report have practical significance in the Netherlands, and Western European regions with similar climactic conditions in general. Also, as the PV and storage technologies evolve rapidly, the author hopes that such charging stations would provide a better ***'sun mileage'***[1] to these LEVs.

7-2 Recommendations

This thesis report, albeit comprehensive, had to define a restricted scope to meet the various goals in the limited time available. Nonetheless some more aspects could be considered in the design of such a charging station that could cater to both present and future needs of LEVs and Electrical Vehicles (EVs) in general.

7-2-1 Scalability

The size of the pilot charging station considered in this thesis is small(sub kW_p), owing to conservative load profiles that cater to e-bikes with partial or no charge. Currently the system under load profile B can charge 30 e-bikes with partial battery charge and under load profile A can charge 10 e-bikes with no battery charge. Depending on the location of implementation, this number can easily be increased to at least 5 times.

Some of the biggest benefits from scaling would be decreased costs, leading to a lower LCOE. Other benefits include becoming a net producer of power that can feed the national grid, or even the local microgrid.

7-2-2 Load profiles

Although a generic load profile has been analyzed in the form of load profile B that emulates the average bike usage data for the whole of the Netherlands, more accurate load profiles need to be used to model the system. Accurate load profiles would not only show daily variation within a week, but would also show seasonal variation. Such load profiles would also assuage the charging station's commitment to meet the load demands in severe winter.

[1] Sun mileage is the amount of distance covered by an Electrical Vehicle (EV) that has been charged using solar energy.

7-2-3 Charging methodology

In terms of sheer volume, the LEVs enjoy a much larger number than the conventional EVs. However, conventional EV design is much more complex, and the product is logically priced much higher. Thus, the revenues in the EV segment far outweigh the LEV segment. There is a solid structure in the EV research which has lead to the development of charging standards around the world. Europe, the United States and Japan have well defined charging standards that the EV manufacturers take note of. Such a standard system is lacking in the LEV space.

Currently almost all LEV manufacturers prefer to have their own charger with their own interface, power ratings, charging rate, etc. A universal set of charging standards is lacking and this could be explored further. Such standards can have benefits like fast charging and the use of off-board chargers in the LEV space too.

Fast charging

Most fast charging stations for conventional EVs are based on DC charging and stick to stringent standards as defined in the region. If a charging standard is defined for the LEVs, then fast charging can be an option at the charging station too. But that would mean off-board chargers, which would deem the manufacturer's current set of regular chargers unusable for fast charging. Thus a normalized charging interface will also be required across the LEVs. Nonetheless, the system capabilities required for fast charging can be looked into more detail.

7-2-4 Implementation

Given the comprehensive and practical nature of the results and values that have been obtained in this report, it is a natural next step to think of implementing such a charging station dedicated for LEVs. The author will be happy to see many such charging stations in the near future.

Appendix A

Appendices

A-1 PV datasheet

The relevant pages of the Sanyo Heterojunction with Intrinsic Thin-layer (HIT) PV module datasheet are attached here.

HIT® photovoltaic module

SANYO

EN

HIT-N240SE10
HIT-N235SE10
HIT-N230SE10

R&D technology adaptation

Improvement of the cell efficiency to reduce
- Carrier recombination loss
- Optical absorption loss
- Resistance loss

Three tabs application
- Reducing electrical loss between the cell fingers and tabs
- Making the tab width thinner to expand the light receiving surface

New tab design

Anti-reflection glass

Light capturing technology
- Reducing reflection and scattering of incoming light
- Improving generated electricity levels in morning and evening times

19.0*%
190 W/m²

* For HIT-N240SE10

HIT cell technology

The SANYO HIT(Heterojunction with Intrinsic Thin layer) solar cell is made of a thin mono crystalline silicon wafer surrounded by ultra-thin amorphous silicon layers. This product provides the industry's leading performance and value using state-of-the-art manufacturing techniques.

Environmentally-Friendly Solar Cell

More Clean Energy
HIT can generate more clean Energy than other conventional crystalline solar cells.

Special Features

SANYO HIT solar modules are 100% emission free, have no moving parts and produce no noise.The dimensions of the HIT modules allow space-saving installation and achievement of maximum output power possible on given roof area.

High performance at high temperatures

Even at high temperatures, the HIT solar cell can maintain higher efficiency than a conventional crystalline silicon solar cell.

HIT® Solar Cell Structure

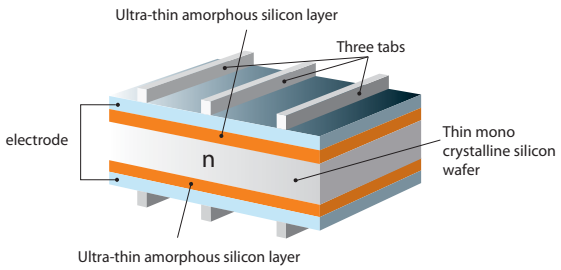

Changes in generated power daytime

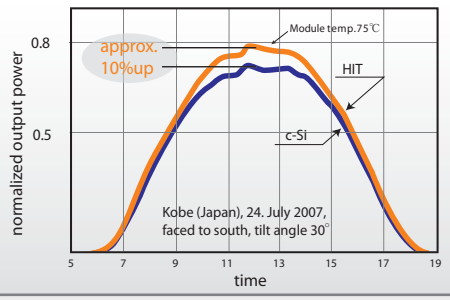

HIT® Photovoltaic Module

The HIT cell and module have very high conversion efficiency in mass production.

Model	Cell Efficiency	Module Efficiency	Output / m²
HIT-N240SE10	21.6%	19.0%	190 W/m²
HIT-N235SE10	21.1%	18.6%	186 W/m²
HIT-N230SE10	20.7%	18.2%	182 W/m²

HIT® Photovoltaic Module

Electrical and Mechanical Characteristics

HIT-N240SE10, HIT-N235SE10, HIT-N230SE10

EN

Electrical data (at STC)

	Models HIT-NxxxSE10		
	240	235	230
Maximum power (Pmax) [W]	240	235	230
Max. power voltage (Vmp) [V]	43.7	43.0	42.3
Max. power current (Imp) [A]	5.51	5.48	5.45
Open circuit voltage (Voc) [V]	52.4	51.8	51.2
Short circuit current (Isc) [A]	5.85	5.84	5.83
Maximum over current rating [A]	15		
Output power tolerance [%]	+10/-5*		
Maximum system voltage [V]	1000		

Note: Standard Test Conditions: Air mass 1.5, Irradiance = 1000W/m², cell temperature = 25°C
* All modules measured by SANYO facility have output with positive tolerance

Temperature characteristics	240	235	230
Temperature (NOCT) [°C]	44.0	44.0	44.0
Temperature coefficient of Pmax [%/°C]	-0.30	-0.30	-0.30
Temperature coefficient of Voc [V/°C]	-0.131	-0.130	-0.128
Temperature coefficient of Isc [mA/°C]	1.76	1.75	1.75

At NOCT	240	235	230
Maximum power (Pmax) [W]	182	179	175
Max. power voltage (Vmp) [V]	41.1	40.5	39.9
Max. power current (Imp) [A]	4.44	4.41	4.38
Open circuit voltage (Voc) [V]	49.4	48.9	48.3
Short circuit current (Isc) [A]	4.71	4.70	4.70

Note: Nominal Operating Cell Temperature : Air mass 1.5 spectrum, Irradiance = 800W/m², Air temperature = 20°C , wind speed 1 m/s

At low irradiance	240	235	230
Maximum power (Pmax) [W]	45.9	44.7	43.8
Max. power voltage (Vmp) [V]	41.7	41.0	40.6
Max. power current (Imp) [A]	1.10	1.09	1.08
Open circuit voltage (Voc) [V]	49.0	48.4	47.8
Short circuit current (Isc) [A]	1.17	1.17	1.17

Note: Low irradiance: Air mass 1.5 spectrum, Irradiance = 200W/m², cell temperature = 25°C

Dependence on irradiance

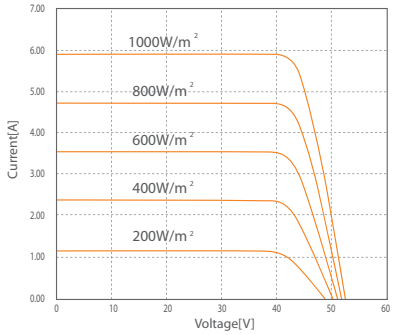

Reference data for model HIT-N240E10
(Cell temperature: 25°C)

Dimensions and weight

unit: mm

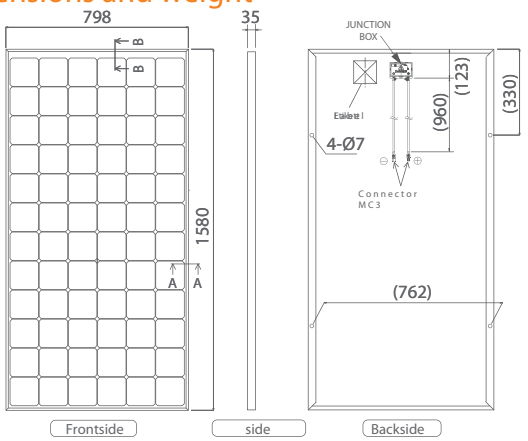

Section A-A Section B-B

Weight: 15 Kg
Weight/m²: 11,9 Kg/m²

Guarantee

Power output: 10 years (90% of Pmin) 25 years (80% of Pmin)
Product workmanship: 10 years
(Based on guarantee document)

Materials

Cell material: 5 inch HIT cells
Glass material: AR coated tempered glass
Frame materials: Black anodized aluminium
Connectors type: MC3

Certificates

www.tuv.com TÜVRheinland ID: 0000023431
- Safety tested, IEC 61730
- Periodic Inspection

IEC 61730
IEC 61215

CE

APPROVED PRODUCT
MCS
BRE GLOBAL LISTED
Certificate No. MCS PV0034
Photovoltaic System

Electrical Protection Class II

Member of

PV CYCLE

Please consult your local dealer for more information.

⚠ CAUTION! Please read the installation manual carefully before using the products.

Due to our policy of continual improvement the products covered by this brochure may be changed without notice.

SANYO Component Europe GmbH
Solar Division
Stahlgruberring 4
81829 Munich, Germany
Tel.+49-(0)89-460095-0
Fax.+49-(0)89-460095-170
http://www.sanyo-solar.eu/en
email: info.solar@sanyo-solar.eu

SANYO

SANYO Electric Co.,Ltd.
Solar Division
http://www.sanyo.com/solar/

05/11

A-2 Solar battery datasheet

The relevant pages of the Hoppeke Valve Regulated Lead Acid (VRLA) Solar Battery datasheet are attached here.

7.9 Temperature influence on battery performance and lifetime

7.9.1 Temperature influence on battery capacity

Battery capacity depends significantly on ambient temperature. Lead acid batteries loose capacity with decreasing temperature and vice versa, as shown in *fig. 7–6*. This should be considered when sizing the battery.

Temperature range for OPzS solar.power batterie:

Possible temperature range: -20 °C to 45 °C
Recommend temperature range: 10 °C to 30 °C

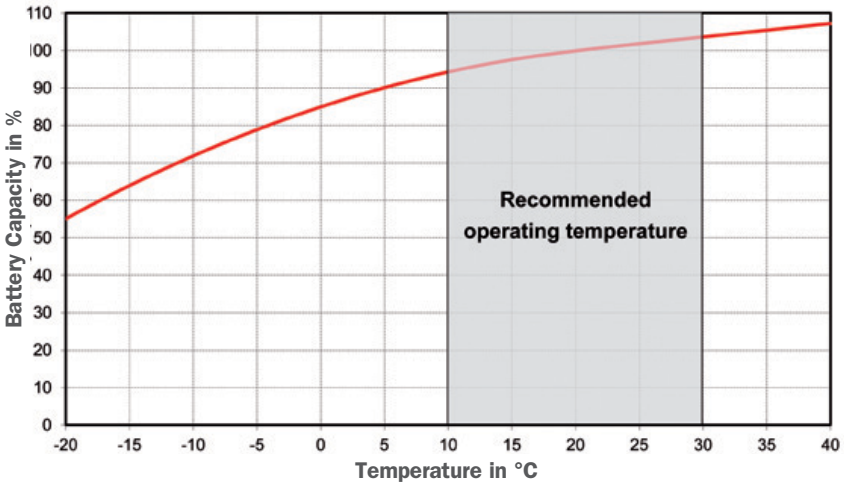

Fig. 7–6: OPzS solar.power: Dependency of battery capacity on temperature

7.9.2 Temperature influence on battery lifetime

As corrosion processes in lead acid batteries are significantly depending on battery temperature, the battery design lifetime is directly related to the ambient temperature.
As rule of thumb it can be stated that the speed of corrosion doubles per 10 K increase (rule by Arrhenius). Thus battery service life will be halved in case the temperature rises by 10 K.
The following graph (refer to *fig. 7–7*) shows this relationship. The diagram depicts operation in float charge mode. Additionally, the cycling lifetime has to be taken into account.

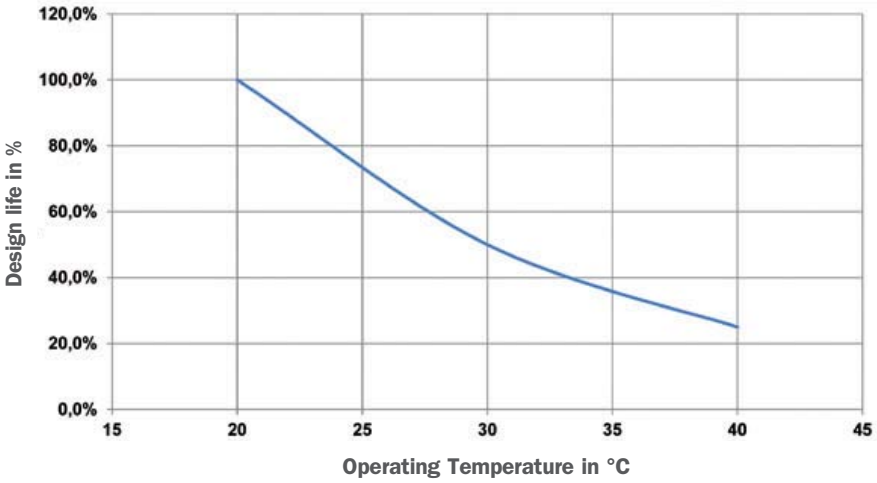

Fig. 7–7: Design life of OPzS solar.power cell as a function of ambient temperature (standby application in float charge operation with 2.23 V/cell)

7.10 Influence of cycling on battery behavior

7.10.1 Cycle life time depending on depth of discharge (DoD)

Cycle lifetime is defined as number of discharging and charging cycles until the actual remaining battery capacity drops below 80% of the nominal capacity (C_{10}). The cycle lifetime of a lead acid battery is directly depending on the regular depth of discharge (DoD) during these cycles.
Depending on different types of batteries and the design of the plates and electrodes, the cycle lifetime may vary significantly.
The following chart (*fig. 7–8*) shows the cycling behavior of a HOPPECKE OPzS solar.power under ideal operating conditions. The cycle life refers to one discharge per day. Cycle life cannot exceed stated service life under float charge conditions.

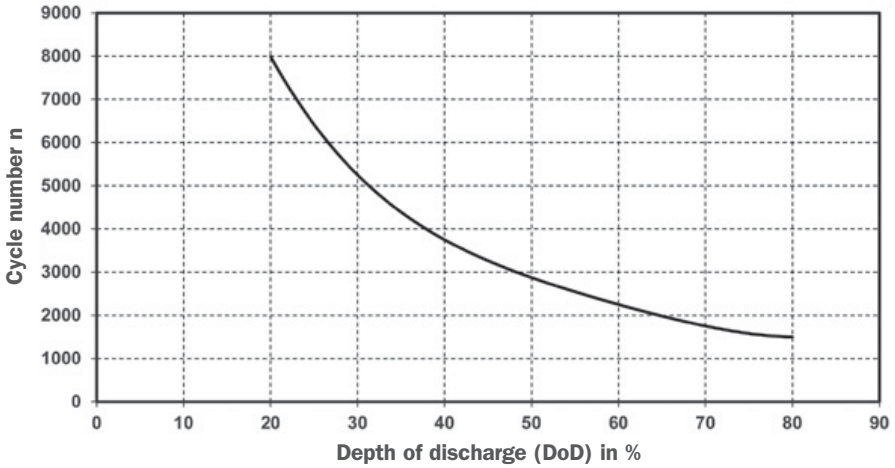

Fig. 7–8: Cycle lifetime of OPzS solar.power as a function of DoD (at 20 °C)

7.10.2 Cycle life time depending on ambient temperature

Since design life mainly depends on temperature, the cycle lifetime is affected by temperature as well. *Fig. 7–9* depicts this relation for a regular battery depth of discharge of 80%.

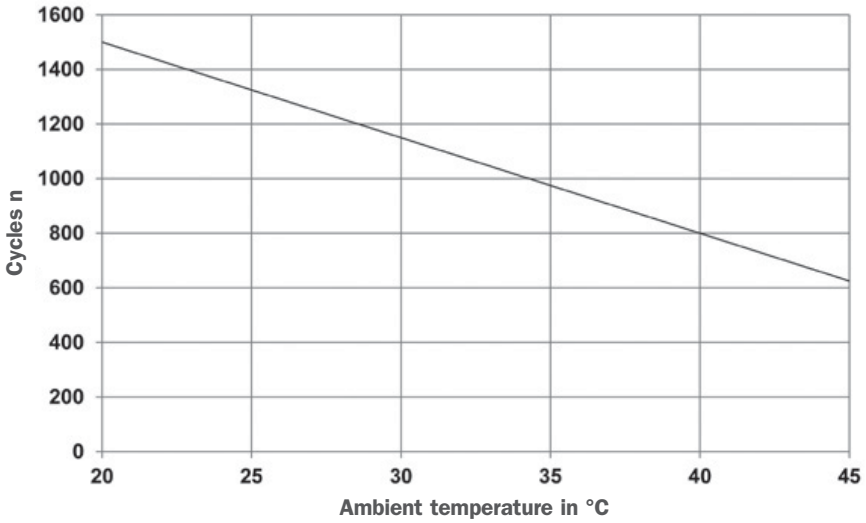

Fig. 7–9: Cycle lifetime of OPzS solar.power as a function of ambient temperature

The following figure (refer to *fig. 7–10*) depicts dependency of cycle life on depth of discharge and temperature.

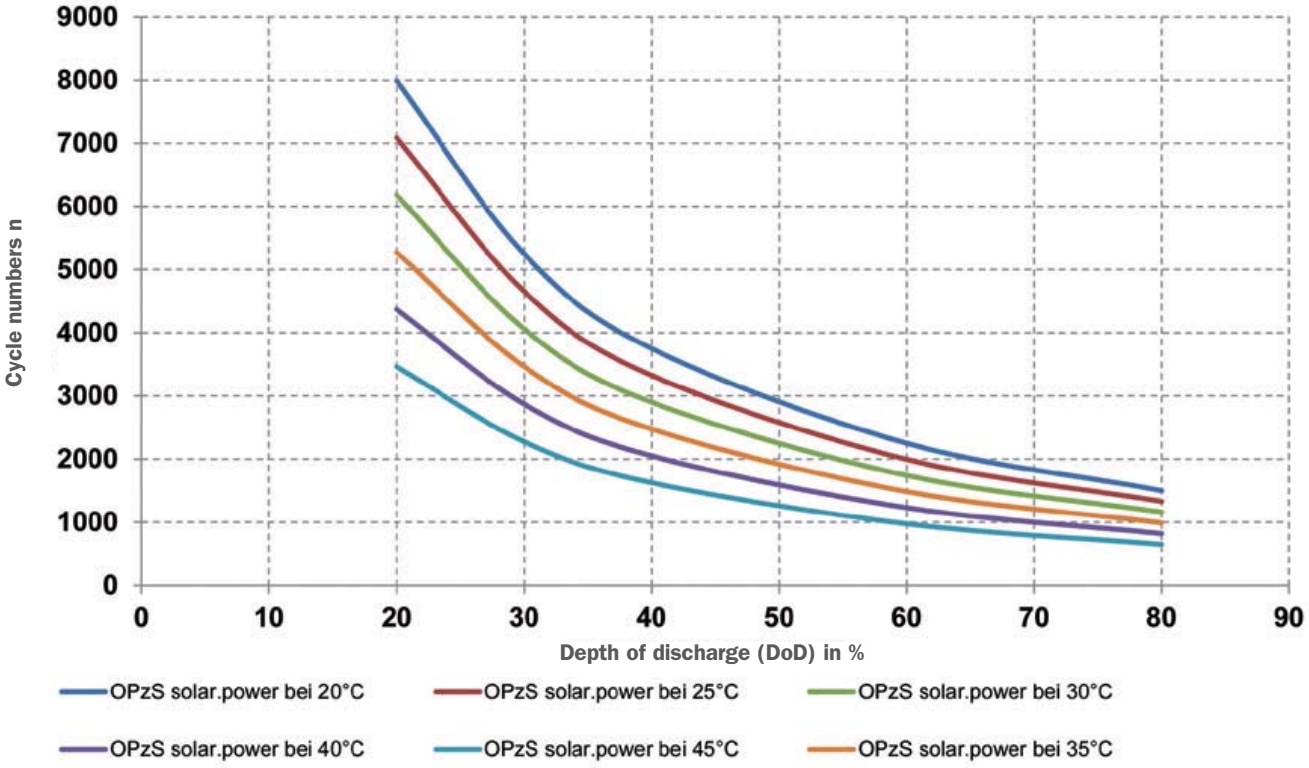

Fig. 7–10: Cycle lifetime of OPzS solar power depending on DoD and temperature

7.10.3 Electrolyte freezing point depending on depth of discharge (DoD)

The freezing point of the electrolyte (sulfuric acid) rises with increasing depth of discharge.
In case the battery is exposed to cold ambient temperatures (< -5°C) the maximum depth of discharge has to be decreased in order to avoid electrolyte freezing and potential damages of the cell jar. *Fig. 7–11* shows an example for this relation. Example: If depth of discharge is below 60% the operating temperature must not be below -18.4 °C.

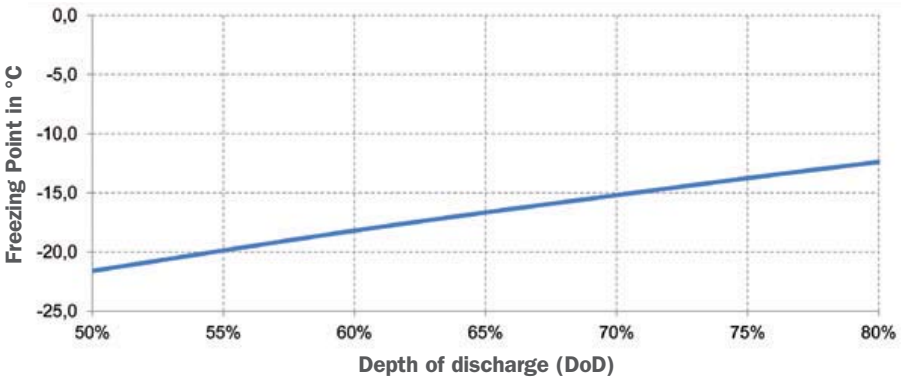

Fig. 7–11: Electrolyte freezing point as a function of depth of discharge (DoD)

7.11 Remarks to warranty management

Above mentioned information about battery performance and lifetime, particularly concerning the charging procedure and the influence of temperature and cycling, affect terms of warranty as well.
In case of a warranty claim the customer/battery operator needs to prove the compliance of above mentioned parameters with the allowed/recommended limits. Corresponding measurement logs have to be sent to the battery manufacturer. These protocols shall clearly demonstrate that the lifetime of the affected battery has not been shortened by the application and associated parameters.
The expected service life mentioned by the battery manufacturer is valid for operation under optimal conditions only. Therefore, it is not possible to solely derive warranty claims from information on the expected service life provided by the manufacturer.

For special demanding operational conditions as well as for solar and off-grid applications the expected battery service lifetime is heavily influenced by above mentioned operational conditions. In order to decide whether a battery failure was caused by manufacturing defects or operational conditions, above mentioned parameters need to be monitored and registered on a regular basis. These data have to be forwarded to the manufacturer for further analysis.

HOPPECKE recommends the usage of a battery monitoring system for monitoring and logging of critical data. Please contact your local HOPPECKE representative for information on HOPPECKE battery monitoring equipment and accessories.

7.12 Recharge-time diagrams

The following diagrams depict approximately necessary recharge times with IU-characteristic as a result of the maximum possible charging current and the actual depth of discharge (DoD) at begin of the recharge phase.

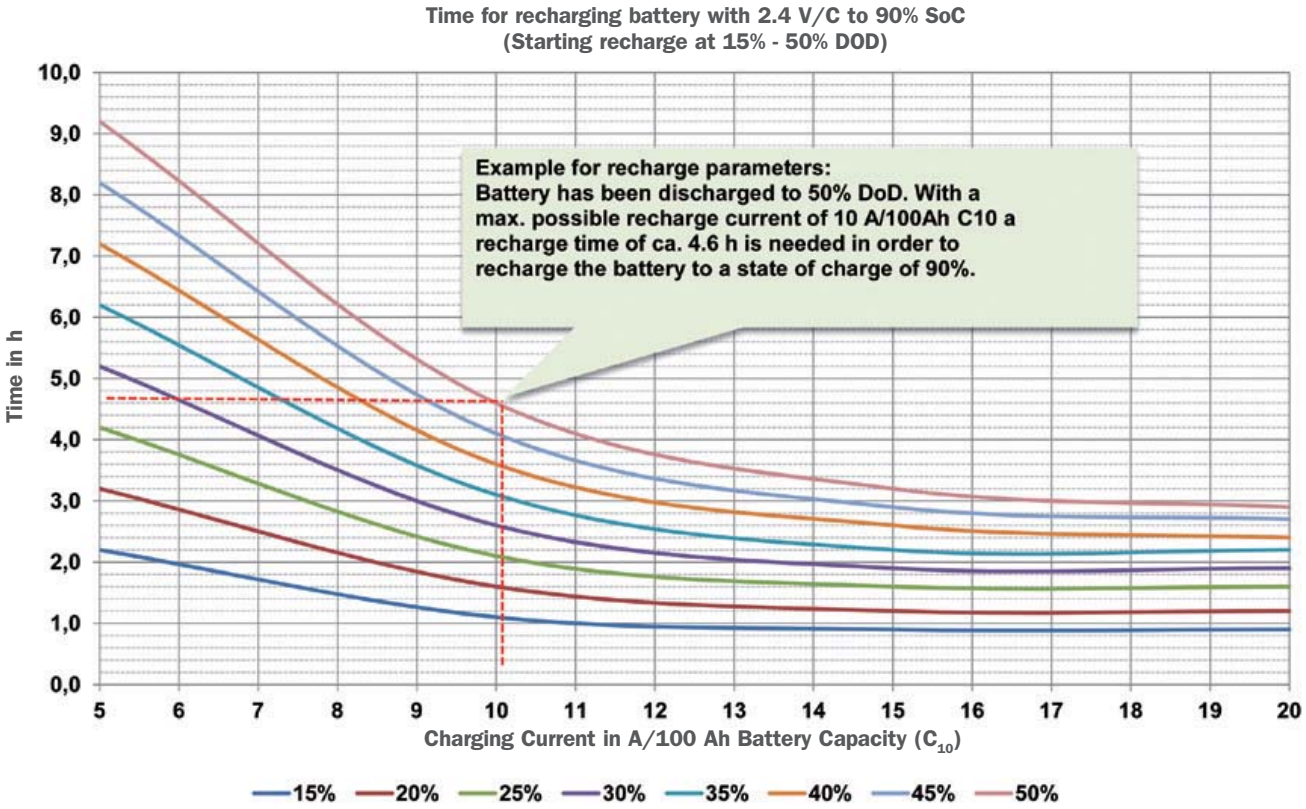

Fig. 7–12: Time of recharge depending on depth of discharge (start of charge between 15% and 50% DoD)

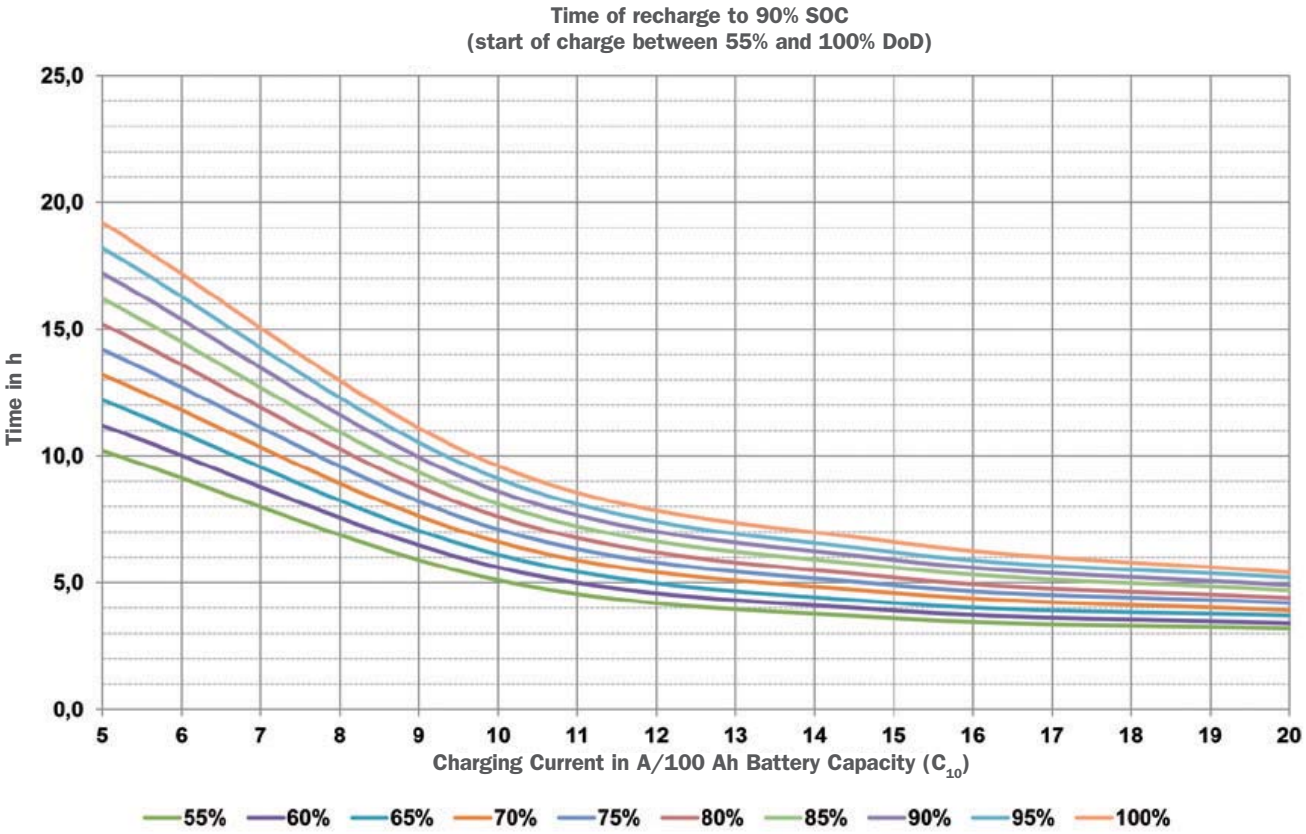

Fig. 7–13: Time of recharge depending on depth of discharge (start of charge between 55% and 100% DoD)

A-3 Battery State of Charge (SOC)

A cycle in battery terms refers to a discharge followed by a recharge. Although a nominal full cycle implies a 100% discharge of the battery, this is seldom the case. This not only because most system architects would avoid such a design where a battery is fully discharged, but also because the practical capacity and the rated capacity are slightly different. This can be seen clearly in Figure A-1 [38].

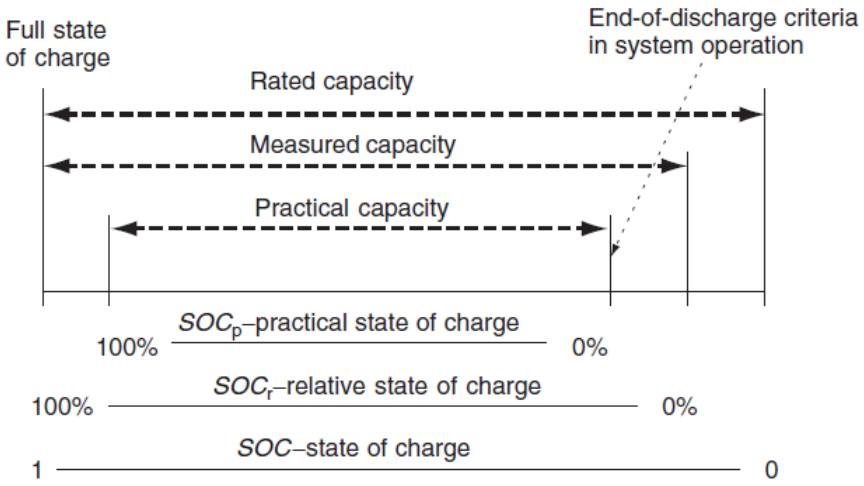

Figure A-1: Different battery capacities and states of charge.

A-4 Electrical considerations

The electrical considerations mainly pertain to the choice of sizing for the array and the power electronic components like the charge controller and the inverter. In this section, the optimal configuration for each of these devices is explored, along with the ideal topology for the arrays. Also, the total amount of power outlets (sockets) will be defined. The electrical implementation aspects considered in this section are relevant to the grid-connected hybrid setup only, as it was found to be the topology of choice in Chapter 5.

A-4-1 Simultaneous charging limit

The daily load profile in Figure 4-11 shows a peak of **504 W** in the middle of the day. As the e-bike chargers are rated at around **50 W**, this implies a maximum of **10 e-bikes** being connected to the charging station at any given time. So a total of **10** alternating current (AC) power sockets need to be provided for charging.

A-4-2 Array sizing

The total number of PV modules required is 4, as shown in Chapter 5 for optimal sizing. Each Sanyo HIT module is rated for **240 W**. For ease of power management, it is decided to have 2 strings of 2 modules (in series) each. Each string would have its own battery bank, Maximum Power Point Tracking (MPPT) charge controller and inverter. Thus each string would be individually dedicated to 5 power sockets at all times.

Given that each string would be operating at its MPPT, each string's output under Standard Testing Conditions (STC) would be 480 W. From the datasheet of the Sanyo HIT module (section A-1), the electrical parameters at MPPT have been stated as shown in Table A-1.

Table A-1: Electrical parameters at MPPT for Sanyo HIT module

	Module	**String**
V_{mpp}	43.7 V	87.4 V
I_{mpp}	5.51 A	5.51 A
P_{mpp}	240 W	480 W

A-4-3 Charge Controller

These days, a charge controller is used not only to regulate the power flow to and from the battery, but also to optimize the power being generated from thee PV modules. The use of the charge controller undoubtedly increases the longevity of the solar battery. The various functions of the charge controller have already been mentioned in the section 4-1-2.

Sizing the charge controller

Most common charge controllers are rated for 12 V, 24 V or 48 V depending on the battery size used in the system. Typical ampere ratings run from 1-60 A, and typical voltage ratings run from 6-60 V.

For safety reasons, the charge controller is typically chosen at least 25% above the maximum current of the array. Thus, the ideal charge controller should be rated for at least an input current $1.25 * I_{mpp} = 6.9\ A$. MPPT charge controllers have an input voltage rating of around **100 V** (e.g. Steca Solarix MPPT 2010 charge controller, also shown in Figure A-2).

Each battery bank is assumed to have 48 V of rated voltage. Thus the charge controller requirement will be to have a voltage rating of **48 V** at its output. The output current can be found as $I = 480W/48V = 10\ A$. Assuming a safety limit of 25%, the output rated current should be **12.5 A**.

Figure A-2: Steca charge controller with MPPT mechanism.

Additional benefit of MPPT charge controllers

As MPPT charge controllers allow for much higher voltages of the PV array as compared to the battery and the load, the current flowing through the cables to the rest of the system is reduced. This means that the diameter of the wire being used reduces proportionately. This leads to significant reduction in wiring costs.

A-4-4 Inverter

The basic functions of an inverter have already been covered in section 4-1-2. Inverters could be broadly classified into 3 categories: off-grid, grid-tied and bimodal. Off-grid inverters are voltage source inverters that need to be suitably powered sources of constant voltage for the loads being supplied to by the system. Grid-tied inverters act as a current source inverters that supply to the grid. Bimodal inverters combine both these features. They have to supply to the grid as a current source, and also to the load when disconnected from the grid as a voltage source. Bimodal inverter is the inverter of choice for the proposed pilot charging station given the hybrid nature of the system.

Inverter sizing

Off-grid inverters are usually sized based on the load requirements. Grid-tied inverters, on the other hand, are sized based on the rated PV power. The maximum rated load peaks at **504 W**, while the rated PV array size is **960 W**. So the upper bound of 960 W is taken into account.

As the irradiance levels can occasionally touch $1000W/m^2$, it is advisable to have the inverter:PV size as **1:1**. In the past it was normal to have this ratio as 0.8:1 as the resolution of the data being used by designer was hourly [20].

The inverter sizing factor c_{inv} is defined as :

$$c_{inv} = \frac{P_{PV}}{P_{INV-AC}} \tag{A-1}$$

This sizing factor describes the level of utilization of the inverter.

Power selection The best efficiency for the inverters in literature have been observed roughly for a c_{inv} of 0.9 [20]. c_{inv} values of 1.1 or higher lead to additional losses due to the inverter cutting off at high irradiance values. However, this study [20] did not take into account the losses incurred in the cables and the mis-tracking by the inverters. Thus, there is a margin to reduce the c_{inv}. This can also be attributed to the fact that there are losses occurring in the system after the PV generation stage. In the case of the pilot charging system, this can be the cable, charge controller and battery losses. Thus, it's sensible to marginally under-size the inverter (relative to the c_{inv} of 0.9).

As a result, a c_{inv} of **1** is chosen. This translates to an inverter sizing of P_{INV-AC} = **960 W.** It should be noted that the same power could be met with two inverters stacked together, in which case each inverter would have to be rated at **480 W**.

Voltage range selection For the worst case scenario, a temperature of -10°C is considered, which is the typical bottom limit of the Dutch winter temperature. At very low temperatures, the V_{OC} of the modules is high. The inverter should be able to withstand this level of V_{OC} for the entire string. For the Sanyo HIT module, the $V_{OC(-10°C,1kW/m^2)}$ is calculated as $V_{OC(STC)}$ + 4.59 V = 52.4 V + 4.59 V = 56.99 V.
Thus, $V_{max(INV)} = 2 \times V_{OC(-10°C,1kW/m^2)}$ = **114 V.**

Similarly, a lower limit of the inverter input voltage can be derived from the temperature limit of 70°C - the highest attainable cell temperature[1] in the Dutch summer (the irradiance effect on the V_{OC} is considered negligible).

$$V_{min(INV)} = 2 \times V_{OC(70°C,1kW/m^2)} = \mathbf{93\ V}. \tag{A-2}$$

Thus, the input ratings of the inverter should allow for nominal operation between **93 V** and **114 V**.

[1]The cell temperature should not be confused with the ambient temperature.

A-5 Levelized Cost of Electricity (LCOE)

This section delves deeper into the LCOE calculations that were done in section 6-2. The LCOE model does not account for the fluctuation of energy prices, since those are determined by supply and demand forces. Instead, it helps compare the cost of production of different sources of energy on a weighted average basis.

The fundamental premise of the LCOE method lies in determining the Net Present Value (NPV) of all the energy produced by a power plant in its lifetime, and the total cost borne to do so. It essentially amortizes the total cost of the plant across the term of its useful life.

For a PV system, this depends a lot on local conditions of the system's location. Therefore, in calculating the power output of the LEV charging station being designed, the data for solar irradiation has been analyzed to great depth in Chapter 2 and an accurate PV yield is determined at the module level in Chapter 3. This is specific to the Netherlands, and ensures that the calculations are accurate enough for the system based in Delft.

In the Netherlands, renewable energy projects receive tax breaks of up to 36% of the project costs [34]. This has also been incorporated in the calculation. The lifetime considered is 25 Years. The following equation was used in calculating LCOE [39].

$$LCOE = \frac{I_0 + \sum_{t=1}^{N} \frac{A_t}{(1+i)^t}}{\sum_{t=1}^{N} \frac{M_{et}}{(1+i)^t}} \tag{A-3}$$

where:
N = system lifetime in years.
t = year number.
A_0: denotes the annual total costs. These are the variable costs associated with the project. In our calculation the following components have been included in this cost:

1. Cost of Operations and Maintenance - statistically approximated as 0.5% of Capital Expenditure.
2. Cost of Battery and Inverter Replacement - on actuals.

I_0: denotes the initial investment amount. This is the Fixed Cost associated with the project. This includes the total Capital Expenditure (CapEx) calculated on a per W_p basis (rated power) with the following components.

1. Cost of PV Modules,
2. Cost of Battery and Inverter,

3. Labor for installation and

4. Wiring, racks and other miscellaneous mounting expenditures.

Total CapEx = System cost (€/W_p) × System Size (W_p).
M_{et} : Electricity production in year t. This is the most accurate PV yield that accounts for irradiance and temperature effects on the output of the PV panel. Also, it takes into account the optimal tilt and azimuth for the PV modules as placed in Delft. The system is then de-rated to account for the inefficiencies of the individual system components.

i: is the discount rate. It is calculated based on financing conditions and project risk in a particular country. Since the Netherlands is a developed country, a discount rate of 4% is applied [33].

The above calculation for the LCOE is further split up into the following steps:

Step 1 **Total Annual yield**
This has been calculated based on the accurate yield estimation from Chapter 3. Also the component inefficiencies are taken into account.

Step 2 **Discounting annual yield**
The annual yields throughout the system lifetime are discounted for each year based on the NPV formula:

$$Y_t = \frac{M_{et}}{(1+i)^t} \tag{A-4}$$

where:
Y_t = Discounted yield from year t.
i = rate of discount.
t = year number.
N = total system lifetime.
M_{et} = System yield in year t.

Step 3 **Total lifetime yield**
This is the sum total of the discounted yields:
Total lifetime yield = $\sum_{t=1}^{N} Y_t$

Step 4 **CapEx adjustment**
The CapEx is first adjusted for the tax incentives.
Adjusted CapEx = CapEx × $(1 - T)$, where T is the tax incentive.

Step 5 **Discounting annual costs**
The total costs are summed for each year and then discounted based on the NPV formula:

$$Cd_t = \frac{C_t}{(1+i)^t} \tag{A-5}$$

where:
Cd_t = Discounted cost from year t.
C_t = Annual costs in year t.
i = Discount rate.
t = year number.

Step 6 **Total lifetime costs**
The discounted costs are summed up for all the years.
Total lifetime costs = Adjusted CapEx + $\sum_{t=1}^{N} Cd_t$.

Step 7 **LCOE computation**

$$\text{LCOE} = \frac{\text{Total lifetime costs}}{\text{Total lifetime yield}} \tag{A-6}$$

Bibliography

[1] Economist, "The end of the Oil Age," *The Economist*, 23-October-2003.

[2] "GHG Emissions for Major Economies," urlhttp://www.c2es.org/facts-figures/international-emissions/annual-ghg, 2010, [Online; accessed 7 - July - 2013].

[3] International Energy Agency, "Energy Technology Perspectives 2012 - Pathways to a Clean Energy System," urlhttp://www.iea.org/Textbase/npsum/ETP2012SUM.pdf, 2012, [Online; accessed 28-June-2013].

[4] ——, "EV City Casebook - A Look At The Global Electric Vehicle Movement," urlhttp://www.iea.org/evi/evcitycasebook.pdf, 2012, [Online; accessed 28-June-2013].

[5] N. S. for Nature and Environment, "Action Plan for Electric Transport En route to one million electric cars in 2020," 2012.

[6] O. van Vliet, A. S. Brouwer, T. Kuramochi, M. van den Broek, and A. Faaij, "Energy use, cost and CO2 emissions of electric cars," *Journal of Power Sources*, vol. 196, no. 4, pp. 2298–2310, Feb. 2011. [Online]. Available: http://linkinghub.elsevier.com/retrieve/pii/S037877531001726X

[7] E. Loveday, "Hire Electric installs Washington's largest solar-powered charging station," http://green.autoblog.com/2010/12/02/hire-electric-washingtons-largest-solar-charger/, 2010, [Online; accessed 30-June-2013].

[8] ResearchMoz.us, "Light Electric Vehicles, Mobility Vehicles, E-Motorcycles and Micro-EVs (Quadricycles) 2013-2023: Market Analysis, Size, Share, Trends and Forecast Research Report," url-

http://www.prweb.com/releases/2013/6/prweb10863042.htm, 25-June-2013, [Online; accessed 30-June-2013].

[9] D. J. C. MacKay, *Sustainable Energy — Without the Hot Air*. Cambridge, UK: UIT Cambridge, Nov. 2008. [Online]. Available: http://www.inference.phy.cam.ac.uk/sustainable/book/tex/sewtha.pdf

[10] Gazelle, "Gazelle e-bike Plus Innergy Series - User Manual," 2012.

[11] de onderzoekers van de Fietsbalans, "Fietsen in cijfers," http://www.fietsersbond.nl/de-feiten/fietsen-cijfers#vragen, 2011, [Online; accessed 27-June-2013].

[12] www.justebikes.co.uk, "E-bike sales grow to take 42% of revenue in Holland," http://www.justebikes.co.uk/news/general/e-bike-sales-grow-to-take-42-of-revenue-in-holland/, 2013, [Online; accessed 27-June-2013].

[13] J. W. van Schaik, "One Million e-Bikes on Dutch Roads," http://www.bike-eu.com/Sales-Trends/Market-trends/2012/11/One-Million-e-Bikes-on-Dutch-Roads-1115062W/, 2012, [Online; accessed 27-June-2013].

[14] A. Luque and S. Hegedus, *Energy Collected and Delivered by PV Modules*. John Wiley & Sons, Ltd, 2011, pp. 984–1042. [Online]. Available: http://dx.doi.org/10.1002/9780470974704.ch22

[15] ——, *Handbook of photovoltaic science and engineering*. Wiley. com, 2011.

[16] S. E. Handbook, "Solar Irradiance Calculator, Solar Electricity Handbook," http://solarelectricityhandbook.com/solar-irradiance.html, 2013, [Online; accessed 29-June-2013].

[17] G. Nieuwint, "A model to convert global horizontal irradiance to that on an inclined plane," June 2013, part of the Master of Science thesis: The design of a self-sufficient street light system.

[18] A. McEvoy, T. Markvart, and L. Castaner, *Practical Handbook of Photovoltaics: Fundamentals and Applications: Fundamentals and Applications*. Elsevier, 2003.

[19] P. Trinuruk, C. Sorapipatana, and D. Chenvidhya, "Estimating operating cell temperature of {BIPV} modules in thailand," *Renewable Energy*, vol. 34, no. 11, pp. 2515 – 2523, 2009. [Online]. Available: http://www.sciencedirect.com/science/article/pii/S0960148109000962

[20] D. G. fur Sonnenenergie, *Planning and Installing Photovoltaic Systems: A Guide for Installers, Architects and Engineers*. Taylor & Francis, 2008. [Online]. Available: http://books.google.nl/books?id=fMo3jJZDkpUC

[21] M. Durr, A. Cruden, S. Gair, and J. McDonald, "Dynamic model of a lead acid battery for use in a domestic fuel cell system," *Journal of Power Sources*, vol. 161, no. 2, pp. 1400 – 1411, 2006. [Online]. Available: http://www.sciencedirect.com/science/article/pii/S0378775306000401

[22] M. Root, *The TAB battery book*. McGraw-Hill, New York, 2010.

[23] J. Stevens and G. Corey, "A study of lead-acid battery efficiency near top-of-charge and the impact on pv system design," in *Photovoltaic Specialists Conference, 1996., Conference Record of the Twenty Fifth IEEE*, 1996, pp. 1485–1488.

[24] Hoppecke, "Installation , commissioning and operating instructions for vented stationary lead-acid batteries," 2013.

[25] A. A. Pesaran and M. Keyser, "Thermal Characteristics of Selected EV and HEV Batteries," *Annual Battery Conference: Advances and Applications*, pp. 1–7, Jan. 2001.

[26] J. Valenciano, M. Fernandez, F. Trinidad, and L. Sanz, "Lead-acid batteries for micro- and mild-hybrid applications," *Journal of Power Sources*, vol. 187, no. 2, pp. 599 – 604, 2009. [Online]. Available: http://www.sciencedirect.com/science/article/pii/S0378775308021812

[27] R. A. Van der Veen and L. J. De Vries, "The impact of microgeneration upon the dutch balancing market," *Energy policy*, vol. 37, no. 7, pp. 2788–2797, 2009.

[28] D. Velasco de la Fuente, C. Rodriťguez, G. Garcerať, E. Figueres, and R. Gonzalez, "Photovoltaic power system with battery backup with grid-connection and islanded operation capabilities," *Industrial Electronics, IEEE Transactions on*, vol. 60, no. 4, pp. 1571–1581, 2013.

[29] Sanyo, "Sanyo HIT-N240SE10 datasheet," *Sanyo PV datasheet*, pp. 1–2, 2013.

[30] P. Ruetschi, "Aging mechanisms and service life of lead-acid batteries," *Journal of Power Sources*, vol. 127, no. 1-2, pp. 33 – 44, 2004, <ce:title>Eighth Ulmer Electrochemische Tage</ce:title>. [Online]. Available: http://www.sciencedirect.com/science/article/pii/S0378775303009340

[31] J. D. Mondol, Y. G. Yohanis, and B. Norton, "Optimising the economic viability of grid-connected photovoltaic systems," *Applied Energy*, vol. 86, no. 7Ű8, pp. 985 – 999, 2009. [Online]. Available: http://www.sciencedirect.com/science/article/pii/S0306261908002493

[32] P. Grana, "Demystifying LCOE," http://www.renewableenergyworld.com/rea/blog/post/2010/08/demystifying-lcoe, 2010, [Online; accessed 30-June-2013].

[33] K. Blok, *Introduction to energy analysis*. Techne Press, 2007.

[34] KPMG, "Taxes and incentives for renewable energy." June-2012. [Online]. Available: http://www.kpmg.com/Global/en/IssuesAndInsights/ArticlesPublications/Documents/taxes-incentives-renewable-energy-2012.pdf

[35] U. Wang, "The Cost of Going Solar and How To Do the Math," http://gigaom.com/2010/08/20/the-cost-of-going-solar-and-how-to-do-the-math/, 2010, [Online; accessed 30-June-2013].

[36] B. S. Richards and M. E. Watt, "Permanently dispelling a myth of photovoltaics via the adoption of a new net energy indicator," *Renewable and Sustainable Energy Reviews*, vol. 11, no. 1, pp. 162–172, 2007. [Online]. Available: http://www.sciencedirect.com/science/article/B6VMY-4F9SVYF-1/2/7a5b3593c81816f888c3580e11b6d552

[37] P. L. Spath, M. K. Mann, and D. R. Kerr, "Life cycle assessment of coal-fired power production," National Renewable Energy Lab., Golden, CO (US), Tech. Rep., 1999.

[38] A. Luque and S. Hegedus, *Electrochemical Storage for Photovoltaics*. John Wiley & Sons, Ltd, 2011, pp. 896–953. [Online]. Available: http://dx.doi.org/10.1002/9780470974704.ch20

[39] C. Kost, D. T. Schlegl, J. Thomsen, S. Nold, and J. Mayer, "Study - levelized cost of electricity renewable energies," *Renewable Energy Innovation Policy - FRAUNHOFER INSTITUTE FOR SOLAR ENERGY SYSTEMS ISE*, 2012. [Online]. Available: http://www.ise.fraunhofer.de/en/publications/veroeffentlichungen-pdf-dateien-en/studien-und-konzeptpapiere/study-levelized-cost-of-electricity-renewable-energies.pdf

Glossary

List of Acronyms

STC	Standard Testing Conditions
PV	photovoltaic
NOCT	Nominal Operating Cell Temperature
KNMI	Koninklijk Nederlands Meteorologisch Instituut
MATLAB	Matrix Laboratory
MPPT	Maximum Power Point Tracking
LEVs	Light Electric Vehicles
LEV	Light Electric Vehicle
EV	Electrical Vehicle
EVs	Electrical Vehicles
BTMS	Battery Thermal Management System
VRLA	Valve Regulated Lead Acid
SOC	State of Charge
DOD	Depth of Discharge
SOH	State of Health
BOS	Balance of System
RE	Renewable Energy

EYR	Energy Yield Ratio
BSRN	Baseline Surface Radiation Network
POA	Plane of Array
c-Si	crystalline silicon
FF	Fill Factor
MIF	Module Ideality Factor
BUF	Battery Utilization Factor
DC	direct current
AC	alternating current
HIT	Heterojunction with Intrinsic Thin-layer
GHGs	Green House Gases
GHG	Green House Gas
IEA	International Energy Agency
BEV	Battery Electric Vehicle
BEVs	Battery Electric Vehicles
EAR	Effective Autarky Ratio
EPBT	Energy Payback Time
LCOE	Levelized Cost of Electricity
NPV	Net Present Value
IRR	Internal Rate of Return
CapEx	Capital Expenditure